Special Core Analysis of Low Reservoir Quality Chalk

Master Thesis In Reservoir Physics

By

Mari Høyvik

Department of Physics and Technology

University of Bergen

November 2016

Abstract

This experimental work investigates Low Reservoir Quality Chalk (LRQC) reservoir properties using outcrop samples from six zones. The thesis is part of Joint Chalk Research Programme, Phase 7 (JCR 7), a large interdisciplinary consortium that focus on chalk research. The work have two main parts: Part A measures porosity, permeability and study flow, oil storage- and oil recovery potential for LRQC; Part B evaluates the use of a new method to measure relative permeability and capillary pressure using spontaneous imbibition with controlled boundary conditions.

Porosity and permeability are two important properties that define the quality of a reservoir. Porosity was measured, with gas or brine, for 24 core plugs and ranges between φ=14.2-26.0%. Absolute permeability, measured with constant rate injection of brine, gas or oil, ranges between K=0.002-0.820 mD. Permeability varied with injected fluid, and gas porosity and permeability were on average higher than measured with brine. Local heterogeneities within core plugs identified with CT imaging significantly influenced the measured reservoir properties.

Oil recovery potential and multiphase flow properties were measured on 12 LRQC core plugs. The initial water saturation, established using constant differential pressure during oil injection in cores initially 100% water saturated, varied between S_{iw}=32.9-38.1%. Oil recovery during forced or spontaneous imbibition was on average 36.5% OOIP.

Relative permeability and capillary pressure for five LRQC core plugs were determined experimentally based on a methodology using spontaneous imbibition. A special boundary condition and theory proposed by (Haugen et al., 2014) was applied for the first time to LRQC core plugs to estimate relative permeability and capillary pressure. Relative permeability to water ranged between $k_{r,w}$=0.055-0.366, whereas capillary pressure ranged between $P_{c,f}$ = 8.4-47.3 kPa.

Acknowledgements

First of all I would like to thank my main supervisor, Associate Professor Martin Fernø and co-supervisor, Dr. Marianne Steinsbø at the Department of Physics and Technology, University of Bergen. Thank you for valuable guidance and support writing this thesis. In addition, I would like to thank Professor Arne Graue for running the group at the Department of Physics and Technology and for the opportunity to travel abroad on conferences for educational purpose.

I would also like to thank researcher Niels Bo Jensen at the Department of Earth Science, UoB for geological guidance and good help. Numerous individuals provided assistance throughout the semester and I would like to thank the staff associated with the reservoir physics group for their expertise and knowledge.

Thanks to all my friends and fellow students at UoB who have been with me on this five year long journey, especially Silje Lande. Thank you all for fun times, good conversations and interesting discussions.

Finally, I would like to thank my parents, Bente and Ketil, and my boyfriend, Sondre for support and motivation during my study and writing this thesis.

Bergen, November 2016
Mari Høyvik

Table of Contents

Introduction

Today the oil-and-gas industry is challenged with a low oil price, and many companies are forced to cut their costs. Nevertheless, the industry still search for new oil and gas reservoirs and improved production methods, because the need for fossil fuels worldwide due to growing economic and population. The global energy demand is expected to increase by 25% from 2014 to 2040 (ExxonMobilCorporation, 2014). Renewable energy is expected to play a larger part in the energy mix in the near future, but fossil fuels will still be among the main energy resources for many years to come.

Over the past 30 years, much effort has been put in research on improving hydrocarbon recovery from chalk reservoirs. According to (Jos Maas, 2014), significant volumes of hydrocarbons is trapped in Low Reservoir Quality Chalk (LRQC), representing a huge economical potential. To be able to produce this hydrocarbon, the work in understanding and predict oil production from low permeable chalk reservoirs is central. Chalk is known as a micro pore reservoir, meaning particles of calcite broken up in pieces from coccoliths. Chalk usually have high porosity, but the permeability are normally in the milli-darcy range (Hardman, 1982). LRQC has low values for both porosity and permeability, causing low oil mobility and possible challenges during production. So far, not many laboratory tests have been performed on LRQC due to the difficulties in achieve reliable data.

The study of reservoir properties of LRQC is of interest due to possible large in situ volumes of hydrocarbons in these reservoirs. Pressure depletion is a cheap and easy way to produce oil, but recovery is generally lower than 15 % of the oil originally in place (OOIP). Secondary recovery methods that injected fluids into the reservoir can be used to maintain reservoir pressure and increase recovery compared with pressure depletion. Injection of water into low permeable, fractured chalk is observed as an effective method to improve oil recovery, especially if the formation is water-wet (Thomas et al., 1991). Spontaneous imbibition is driven by surface energy and occur due to capillary forces between immiscible fluids in a porous medium (Morrow and Mason, 2001). The experimental work in this thesis is divided into two main parts. **Part A** measures porosity, permeability and flow, storage and oil recovery potential for Low Reservoir Quality Chalk. According to (Graue, 1993), low permeable chalk reservoirs in the North Sea are heavily fractured. CT images of each zone were in addition studied in part A to evaluate possible heterogeneities and fractures. **Part B** utilize a newly proposed imbibition test (Haugen et al., 2014) to estimate capillary pressure and relative permeability in chalk and sandstone based on the *two-ends-open free spontaneous imbibition* (TEOFSI) boundary condition by (Dong and Zhou, 1998). In this thesis, the methodology was for the first time performed on LRQC core plugs to evaluate its potential in low-permeable formations.

Part I – Introduction & Theory

1 Basic reservoir and core analysis parameters

1.1 Porosity

The term "Porosity" describes the voids or spaces between rock grains that can store and transport fluids. Porosity determines the hydrocarbon content in a certain rock and is an important reservoir parameter. Effective porosity defines pores connected together, whereas residual porosity refers to pores that are disconnected. Effective and residual porosity together, defines total porosity (Lien, 2004). Porosity is history dependent; meaning the sedimentary rocks earlier impact of mechanical and chemical diagenesis during their burial process, has a huge effect on the outcome of the rocks porosity. For example might a slower mechanical diagenesis give earlier accumulation of hydrocarbons within the rock. Porosity decrease with depth and is directly connected to permeability (Zolotukhin and Ursin, 2000). Porosity is defined as the ratio between the pore volume (V_p) and the total volume of the rock (V_b) (Selley and Sonnenberg, 2014).

$$\varphi = \frac{V_p}{V_b} = \frac{\frac{W_{sat} - W_{dry}}{\rho}}{\pi r^2 l} * 100\ \% \tag{1}$$

where V_b is the total volume of rock, V_p is the pore volume, W_{dry} and W_{sat} are the weight of the core plug before and after saturation [g], ρ is the density of the brine [g/ml], and r and l are the radius and length of a cylindrical core plug, respectively [cm]

The pore volume, V_p may be estimated in the laboratory with gas using ideal gas law

$$pV = nRT \tag{2}$$

where p [pa] is the pressure of the gas, V [m^3] is the volume of the gas, n [moles] is the amount of substances of gas, R [0.08206 L*atm/(mol*K)] is the ideal gas constant and T [K] is temperature. With constant temperature (T) and volume (V), the law can be used to compare the same substances under two different sets of conditions, expressed as

$$p_1 V_1 = p_2 V_2. \tag{3}$$

The equation shows that, as volume increase, the pressure of the gas decreases in proportion. In case of a vacuum condition, Boyle's law can be expressed as follows

$$\mathrm{p_{ref}V_{ref}} + \mathrm{p_{core}(V_P + V_{dv})} = \mathrm{p_{tot}(V_{ref} + V_P + V_{dv})} \tag{4}$$

where P_{ref} is the pressure in the reference volume, V_{ref} is the reference volume, P_{tot} is the final pressure, V_p is the bulk volume and V_{DV} is the tubing volume.

1.2 Permeability and the influence of different fluids

Fluid transportation through reservoir rocks is complex and cannot be described by one theory alone. Permeability *K* of a porous medium is its capability to transmit fluids through its network of interconnected pores. It is one of the most significant properties to evaluate in a reservoir, and directly connected to porosity (Zolotukhin and Ursin, 2000).

1.2.1 Absolute permeability

One single fluid present and flowing through the media is known as the absolute permeability. The original work was carried out by Henry Darcy (1856), which said; "Permeability is a primary mechanism that comes from pure mechanical nature and is a result of the forces that are acting on the fluids". For a horizontal, laminar flow, Darcy's law can be expressed as

$$Q = \frac{KA}{\mu}\frac{(P_b - P_a)}{L} \tag{5}$$

where Q [m^3/s] is the volume flow rate, K [m^2] is the absolute permeability, A [m^2] is the cross sectional area of the medium, μ [Pa·s] is the viscosity of the fluid, L [m] is the length of the medium and $(P_b - P_a)$ [Pa] is the pressure drop across the medium. The unit for permeability is Darcy [D] and is defined as when a fluid with 1 cP viscosity flows at a velocity of 1 cm/s for a pressure drop of 1 atm/cm (Selley and Sonnenberg, 2014). Darcy's law is only valid when there is no chemical or physical reaction between the fluid and the medium.

1.2.2 Effective and relative permeability.

In a petroleum reservoir, there is usually more than one phase present in the medium, such as initial water, oil or gas. The permeability gets more complex with several fluids present, and the term effective permeability, K_{eff} comes to use. K_{eff} relates to the fluids relative saturations, flow rate, pressure gradient and fluid properties. With more than one fluid present, the permeability of each immiscible fluid will be lower than the absolute permeability, because one fluid will restrict flow of the other (Zolotukhin and Ursin, 2000).

For fluid i (i=w, o, g), the effective permeability can be defined as

$$u_i = \frac{K_{eff,i}}{\mu_i} \tag{6}$$

where u_i is the velocity of the fluid i, $K_{eff,i}$ is the effective permeability of fluid i, μ_i is the viscosity of fluid i. This applies for an incompressible fluid with a horizontal flow.

The relative permeability is a critical parameter for evaluation of fluid mobility and reservoir performances. Its defined as the ratio between the effective permeability of the phase and the absolute permeability of the media. Relative permeability, in addition to porosity and permeability is significantly dependent on pore geometry, wettability, fluid saturation, saturation history, reservoir temperature, reservoir pressure, overburden pressure and rock types (Guo et al., 2012). For fluid i (i=w, o, g) the relative permeability can be expressed as

$$K_{ri} = \frac{K_i}{K} \tag{7}$$

where K_{ri} is the relative permeability of fluid i and a dimensionless property, K_i is the effective permeability and K is the absolute permeability.

The relative permeability curves are usually plotted against the saturation of the wetting phase. The relative permeability of the wetting phase increase as the wetting phase saturation increase, due to the wetting phase becoming more mobile. At the same time, the relative permeability of the non-wetting phase decreases. Figure 1 illustrates the relative permeability to oil and water for one Low Reservoir Quality Chalk core plug measured in this thesis. The area between the dashed lines (S_w=0.32-0.58) is the mobile area and the amount of fluid able to flow. S_{iw} is initial water saturation (trapped water) *while* S_{or} is residual oil saturation (trapped oil). Results of relative permeability calculations and measurements are discussed in more detail in the Results section later.

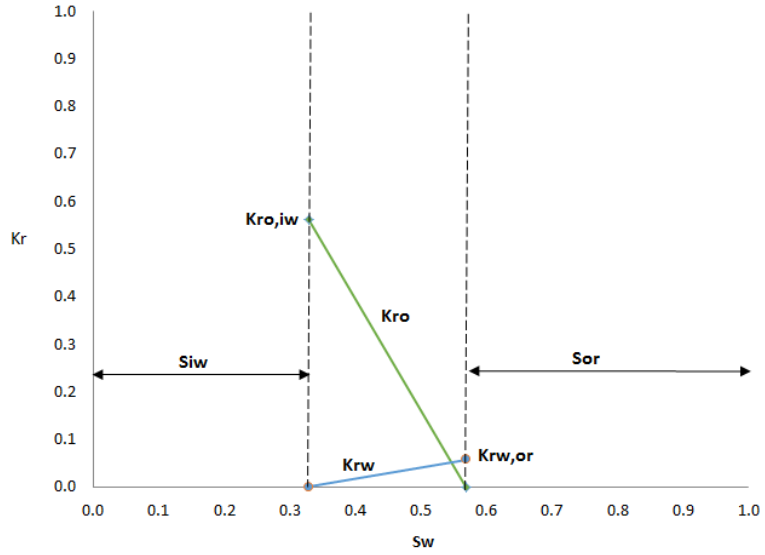

Figure 1 – Relative permeability curve of one Low Reservoir Quality Chalk core plug. Relative permeability is shown for oil (green line) and water (blue line) versus water saturation. The area in between the dashed lines (S_w=0.32-0.58) is the mobile area. S_{iw} is initial water saturation (trapped water), 32% of total pore volume. S_{or} is residual oil saturation (trapped oil), 42 % of total pore volume. $K_{ro,iw}$ is the relative permeability endpoint for oil after water imbibition and $K_{rw,or}$ is the relative permeability endpoint for water after oil drainage.

According to (Ewy et al., 2013), the effect of overburden pressure on relative permeability for LRQC, may be significant. Therefore, measurements should be performed at representative pressure conditions. Relative permeability measurements of LRQC therefore require special attention and its notoriously difficult in laboratory procedures to obtain representative data (Jos Maas, 2014). In low permeable rock, it can be an experimental challenge to obtain low $S_{wi,}$ and its accuracy becomes important due to its dependence to LRQC wettability and relative permeability, as discussed in the Result section later.

1.2.3 Gas permeability measurements

Gas is a highly compressible fluid. Darcy's law can therefore not be used directly and needs a modification. (Klinkenberg, 1941) discovered that when small gas molecules are exposed to low mean pressures, their mutual collision reduces. This allows them to move through the pore channel with minimum frictional interaction with the walls, also known as the slippage effect. «Based on the fundamental assumption that, as long as the rate of flow is proportional to the pressure gradient, the permeability constant of a porous medium is a property of the medium, and is independent of the fluid used in its determination» (Klinkenberg, 1941). As a result, the flow velocity at the walls is non-zero together with a high gas velocity in general. Gas permeability is then caused to have a higher value than the liquid permeability (Zolotukhin and Ursin, 2000). This phenomenon is known as the Klinkenberg effect, and is used by altering Darcy's law by adding another term;

$$K_{eff,i} = K(1 + \frac{b}{P_m}) \tag{8}$$

where $k_{eff,i}$ [m^2] is the effective gas permeability, K [D] is the absolute (liquid) permeability, b [Pa] is the Klinkenberg factor which depends on the type of gas used and P_m [bar] is the mean pressure. The Klinkenberg effect becomes more noticeable with a decreasing mean pressure, lower permeability and increasing mean free path. This is for when lighter gases are used.

1.4 Wettability definitions and its effect on recovery potential

Wettability is defined as "the tendency of one fluid to spread on, or adhere to, a solid's surface in the presence of other immiscible fluids" (Craig, 1971). The understanding of wettability is crucial for oil recovery optimization, and relates strongly to relative permeability and capillary pressure. In a rock/oil/brine system, the rock has either a preference for water or oil, preferred to as water-wet or oil-wet (Anderson, 1986a); (Abdallah et al., 1986). The wettability determination for LRQC is important due to reservoir performance understanding and is one of the key parameters when it comes to spontaneous imbibition (Anderson, 1986b).

To define wettability, Amott (1959) presented a method using spontaneous- and forced imbibition and drainage to describe the displacement properties in a system. Ratios between spontaneous displacement volumes and total displacement volumes are used as wettability

indices. The two Amott indices are often combined to give the Amott-Harvey Index. The index is a number between -1 and 1, defining porous mediums wettability. The Amott-Harvey method is determined by measuring four different saturations, S_{wirr}, S_{spw}, S_{spo} and S_{or}. Spontaneous imbibition after primary drainage is represented in the S_{wirr} and S_{spw} area, at S_{spo} and S_{spw}, the capillary pressure equals zero and the latter point, S_{spw} a forced imbibition process displace the system from S_{spw} to S_{or}. At S_{or}, oil can spontaneously be injected to reach S_{spo}. A forced (secondary) drainage displacement can bring the system back to $S_{wirr.}$ (Jos Maas, 2014)

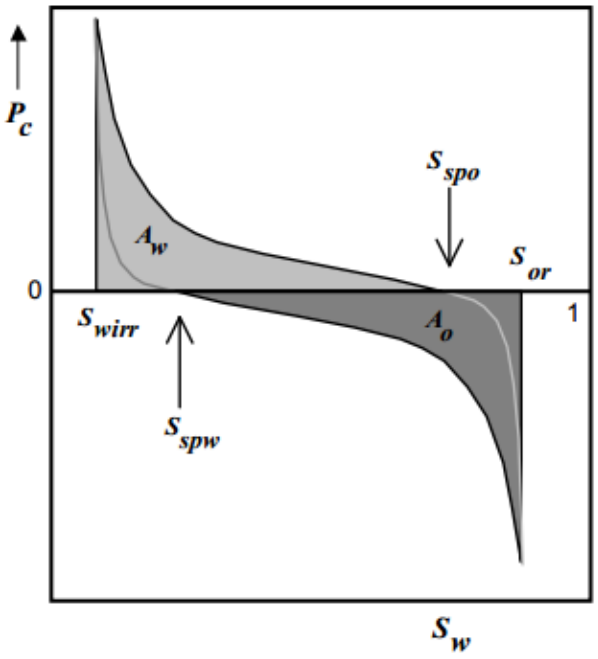

Figure 2 – Wettability index parameters used for Amott-Harvey and USBM tests. Capillary pressure is plotted against water saturation. Four displacement processes are illustrated; primary drainage, spontaneous imbibition, forced imbibition and secondary drainage. The four different saturations, S_{wirr}, S_{spw}, S_{spo} and S_{or} are used to determine the Amott Harvey Index. (Jos Maas, 2014).

The Amott-Harvey index is calculated through the water index I_w:

$$I_w = \frac{S_{spw} - S_{wirr}}{1 - S_{wirr} - S_{or}} \tag{9}$$

where S_{spw} is the water saturation for a zero capillary pressure during the imbibition process, S_{wirr} is the irreducible water saturation and S_{or} is the residual oil saturation after imbibition.

The oil index I_o:

$$I_o = \frac{S_{spo} - S_{or}}{1 - S_{wirr} - S_{or}} \tag{10}$$

where S_{spo} is the oil saturation for a zero capillary pressure during the secondary drainage process, S_{wirr} is the irreducible water saturation and S_{or} is the residual oil saturation after imbibition.

These water and oil index combined gives:

$$I_{AH} = I_w - I_o \tag{11}$$

By (Dake, 1983) the Amott-Harvey defines wettability of a rock as:

- Water-wet when the index is between +0.3 and +1.0.
- Intermediate- or mixed-wet when the index around zero.
- Oil-wet when the index is between -0.3 and -1.0.

When the wettability of a medium moves from strong towards less water-wet conditions, a reduction in recovery by spontaneous imbibition is observed and viscous forces are proved to have a bigger impact. (Jadhunandan and Morrow, 1991) The residual oil saturation seem to increase with reduction in water-wetness and the lowest saturations are obtained with wettability in the range of I_w =0.1-0.3. (Jadhunandan and Morrow, 1995)

1.5 Capillary pressure

"The molecular pressure difference across the interface of the two fluids" is the definition of capillary pressure (Lien, 2011). Spontaneous imbibition is possible due to the capillary effect and this fundamental property is therefore very important. Spontaneous imbibition requires that the porous media have a wetting preference, dividing liquids into a wetting and a non-wetting phase. The wetting preferred fluid has the strongest adhesive force and causes its interface to curve. The capillary pressure, P_c in this case can be written as the pressure of the wetting phase, P_w minus the pressure of the non-wetting phase, P_{nw}:

$$P_c = P_w - P_{nw} \tag{12}$$

In a pipe, the non-wetting phase gets squeezed though the pore throat. Here, the capillary pressure depends on the size of the pore radius (r), interfacial tension (σ) between the two fluids and the wetting angle (θ):

$$P_c = \frac{2\sigma\, cos\theta}{r} \tag{13}$$

This formula tells us that the capillary pressure is inversely proportional to the radius (r).

During a spontaneous displacing process, the non-wetting fluid will not enter the pore of the rock through the pore aperture without additional pressure. This additional pressure required is inversely related to the pore aperture diameter or radius (Jos Maas, 2014). However, even if the incoming fluid is the preferred wetting phase, a threshold pressure need to be overcome (see Figure 7). "The threshold pressure corresponds to the capillary pressure in the narrowest part of the pore. In a flooding at a low injection rate the invading fluid will enter the most narrow pores first" (Lenormand et al., 1983). The invading fluid only enters a pore if the capillary pressure is equal or greater than the threshold pressure of that pore.

2 Geological description of Low Quality Reservoir Chalk

In this chapter, a geological description of LRQC is presented. This geological description is included to help predict expectations related to density, fractures, heterogeneities and lamination within each zone. Chalk usually contains other materials in addition to pure chalk. The geological description for LRQC show a larger content of clay in some of the outcrops. The impact of more clay in chalk outcrops compared to a cleaner and more pure chalk is lower porosity, permeability and therefore lower flow potential and oil capacity.

2.1 Originality of LRQC core plugs

In total, 26 core plugs were obtained from Eastbourne, Sussex, England. The cores are from rocks of Late Cenomanian-Early Turonian age, a time characterized of important global palaeoceaographic and palaeoclimatic perturbation, including an oceanic anoxic event that affected the deeper ocean basins and resulted in an extensive deposition of organic-rich mudrocks (Schlanger and Jenkyns, 2007). These changes in the nature of alluvial deposits may be affected by global sea-level change and regional palaeogeography, and had a major impact on the depositional environment in Eastbourne and content of the outcrops collected.

Low Reservoir Quality Chalk (LRQC) core plugs used in this thesis are drilled from six large outcrops collected from two different coastal cliff sections at Gun Gardens and Pinnacle Steps near Eastbourne. A correlation of different sections, zones and positions related to the outcropped sections are illustrated in Figure 3. The geological description is performed in close collaboration with researcher Niels Bo Jensen from the Department of Earth Science, UoB, who collected the samples. This thesis is a part of a bigger project, connected to the Joint Chalk Research Programme, Phase 7 (JCR 7). The Eastbourne area has previously been thoroughly studied and described geologically by Professor Andy Gale, University of Portsmouth. Core plugs drilled from each outcrop at every location are listed in Table 1. The zones are linked by colour through the thesis for better recognition during comparison. Figure 4 and 5 are photos from the locations where Niels Bo Jensen collected the samples.

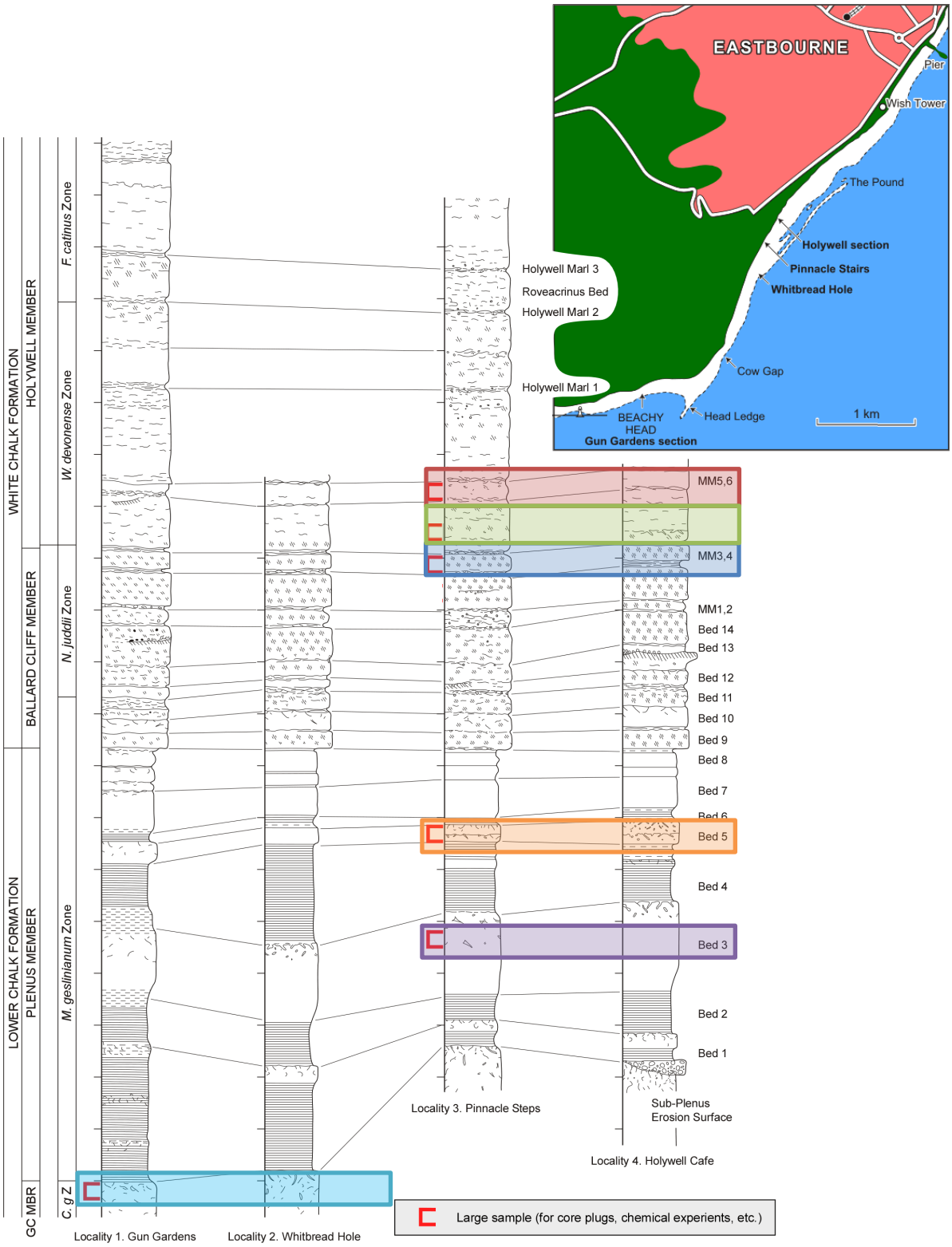

Detailed correlation of the Plenus Marl and lowest Middle Chalk (Upper Cenomanian–Lower Turonian) west of Eastbourne, Sussex. After Gale et al. (2005).

Figure 3 - Detailed correlation of the Plenus Marl and lowest Middle Chalk (Upper Cenomanian, Early Turonian) west of Eastbourne, Sussex. Map showing an overview of the Eastbourne coast and position of different locations. Samples were collected from different zones at Gun Gardens and Pinnacle Steps, and are marked with red boxes. Core plugs drilled from outcrop at each zone are listed in Table 1. (Modified from (Gale et al., 2005))

Table 1 – Overview of each core plugs former zone, location, member and formation. The identification of the core plugs referees to zone and core plug number i.e. ZIGZAG V12. Meaning, the ZIGZAG zone and vertically drilled sample no. 12. ZIGZAG H12 means a horizontally drilled sample from the same zone. Each zone is defined by one colour that will follow through the rest of the thesis when comparing zones; zone MM5-6 is red, zone MM4-5 is green, zone MM3-4 is blue, zone BED5 is orange, zone BED3 is purple and zone ZIGZAG is turquoise.

Formation	Member	Location	Outcrop sample / zone	Core sample
White chalk formation	Holywell member	Pinnacle Steps	MM5-6	V3 V4 H4 H5 H6
	Ballard cliff	Pinnacle Steps	MM4-5	V1 C2 H1 H2
		Pinnacle Steps	MM3-4	V7 V7 H7 H8 H9
Lower chalk formation	Plenus Marl	Pinnacle Steps	BED 5	H10A H10B
		Pinnacle Steps	BED 3	V14 V15 H14 H15
	Grey Chalk	Gun Gardens	ZIGZAG	V11A V11B V12 H12 H13 V11

Figure 4 – Photo of visible layers defined by different colours at Pinnacle Steps, Eastbourne England. The upper area is known as the Ballard Cliff Member, while the lower area is the Plenus Marl Member. The two grey layers express zones that contains more clay, where the top one is BED 5, according to Figure 3. Photo is taken by Niels Bo Jensen, researcher at the Department of Earth Science, UoB.

Figure 5 – Photo of the Gun Gardens location in Eastbourne England showing different layers, fractures and block that have fallen out. The photo also illustrates how far from the ocean the sections have been collected. See Figure 5 for the description of different layers visible. Photo is taken by Niels Bo Jensen, researcher at the Department of Earth Science, UoB.

Four vertical sections along the coastal cliffs west of Eastbourne are presented as a detail correlation in Figure 3. Each section are presented in the form of a 2D–sedimentary log outline with variation in composition, texture and structure of beds (Gale et al., 2005). The ZIGZAG sample was collected from the Grey Chalk member at Gun Gardens. It has up to 10 wt% clay minerals and scattered broken bivalve shells. The top of the Grey Chalk is marked by a sharp boundary to the overlying and more clay rich Plenus Marl Member, where BED3 and BED5 are collected. BED3 and BED5 are development from relatively clay-rich and laminated sediments. These sediments show a variation from zero macro fossils to more clean chalks with bioturbation, bivalve and gastropod fragments (Gale et al., 2005). The higher clay content and greater preserved lamination in BED3 and BED5 may cause lower porosity, permeability and give higher density within the two zones. The gradual cleaning-upward is

interpreted during deeper water. Here, a drop in supply of siliciclastics results in a deposition of a cleaner chalk. MM3–4, MM4–5 and MM5–6 are collected from this area, known as Ballard Cliff and Lower Holywell Members. This is all fine grained, clean chalks with less than five wt% clay. The sediments contain thinly bedded calciphere-rich nodular and weakly nodular chalks separated by thin, often wispy, flaser marls. This cleaner chalk composition suggest higher porosity and permeability values within the three MM zones.

2.2 Sea-level changes impact on Low Quality Chalk.

Relative sea-level changes had a major impact on the sedimentation in the Eastbourne area (Gale et al., 2005); Pearce et al. (2009). Depending on sea-level increase or decrease, the changes can either cause higher clay content or leave the outcrops as a cleaner chalk. Through the Grey Chalk member, the relative sea-level decreased, possibly as much as 15 meters (Figure 6) during a Highstand System Trackt (HST). HST refers to rocks deposited when relative sea-level was at its highest. Chalk is usually developed under more open ocean conditions. The depositional environment during HST is therefore to be less influence by siliciclastics and leaving a more pure chalk in the Grey Chalk member. HST reflects the possible lower clay content in the ZIGZAG zone.

Lowstand Systems Trackt, reflect a lower relative sea-level. This was developed at the beginning of the Plenus Marl Member, where BED3 and BED5 were collected. The sediment composition in the Plenus Marl member is affected by more sediments transportation further out on the coastal plain by the rivers due to LST. This sediment transportation results in a higher clay content in BED3 and BED5. A higher clay content reflects little chlorite, smaller and finer sediments in size and less purity for the two zones.

In the upper part of the Plenus Marl member, where MM3-4, MM4-5 and MM5-6 are collected is it believed that the relative sea-level starts to rise again. The shift is marked by a Transgressive Surface (TS) at the top of BED3 in Figure 6. A transgression refers to a relative rise in sea-level and is characterised by the coastline moving in a landward direction. This situation will often result in sediment starvation as sediments are then being deposited more landward. Sediments of this period of relative sea-level rise are referred to as the Transgressive Systems Tract (TST). The TST is characterised by smaller chalk cycles with minor variation in relative clay content and bioturbation, which reflects the geological description of zone MM3-4, MM4-5 and MM5-6. In Balland Cliff Member it changes again to HST. Sea-level rises, less clay is added from land and the chalk becomes more pure. The cyclic nature of deposition is evident from the changes in composition for the outcrops. From laminated clay-rich to more bioturbated and clean chalks.

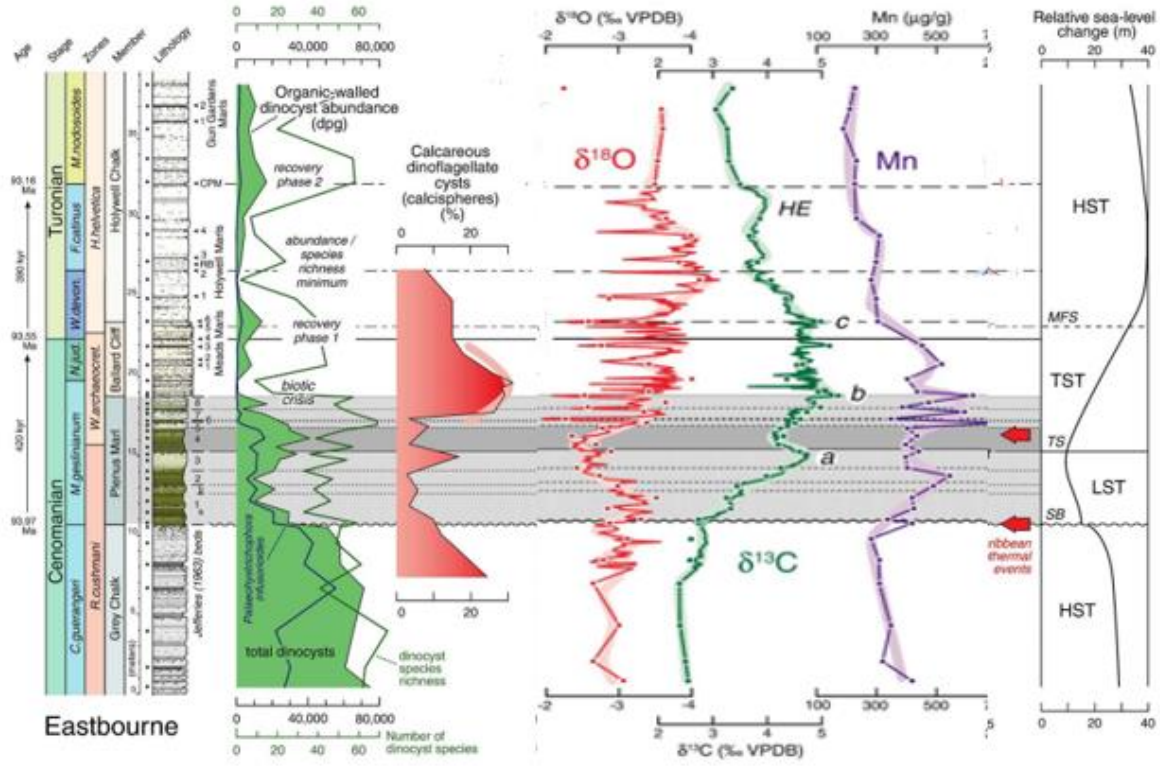

Figure 6 - Dinocyst absolute abundance profiles, palaeoenvironmental proxies, stable-isotope and elemental chemostratigraphy through the Cenomian-Turonian interval at Eastbourne. Different zones and their lithology are shown in the first column to the left and are coloured to describe rock content (green means more clay content). First green column describes number of dinocyst species and how they change over time. Second red column describes isotope data of $\delta^{18}O$ and second green column isotope $\delta^{13}C$. The isotope values are a function of Vienna Pee Dee Belemnite (VPDB) versus time. The sea-level change trough the Cenomanian-Turonian interval is illustrated to the right. The cold event is shown as a dark grey horizontal layer through all columns. Figure is modified from (Pearce et al., 2009).

CO_2 is a primary nutrient for many photosynthesising algae and bacteria in the ocean. Figure 6 (third green line from the right) shows $\delta^{13}C$ increases during Plenus Marl Member. At this time, the world oceans are recorded as very nutritious. This high organic production causes more animals to excavate and dig voids within the future rock. Porosity and void space is assumed to be higher during this time period, causing the collected outcrop from this time period to have a better position for better flow capacity and oil storage. Upwelling currents bringing nutrient-rich deep water to the surface waters is a probable cause for the exceptional high organic productivity.

The scale in Figure 6 shows continuing purity through the profile, but with natural variations. Ballard Cliff and Holywell chalk are much whiter and their lithology shows more of a pure chalk. Sediments often become finer and better sorted deeper down. However, not always correct for carbonates, because their presence may not be a result of physical transportation by current or wave process. Chalks being a special case of carbonate rocks and by nature very fine grained as they are primarily sourced from tests of nanoplanktonic coccolithophorid algae with possibilities of lower porosity and permeability. Heterogeneities within grainsize in

chalk might happen if the chalk is mixed with other carbonate secreting planktic and benthic microalgaes and possibly benthic macroorganisms (Meurant, 1972).

2.3 Image technique for evaluation of characteristics and heterogeneities

Computed Tomography (CT) is an image technique that uses several X-ray images from different angels, to create cross sectional (tomographic) images. A CT image can visualize the inside of a porous medium by measuring differences as a fraction of X-rays that passes through the core plug.

Two-dimensional images were evaluated in the computer program ImageJ where all images can be imported as a series, to define fractures or larger pore spaces. In ImageJ, CT number was defined as -1000 for air and 1500-1800 within the porous medium. Different CT numbers within the core plug are visible as lighter and darker grey tones. Air and lighter density areas are dark/black, whereas heavier density areas are lighter/white.

3 Recovery by displacement processes for cylindrical core plugs

3.1 Steady state and unsteady state.

Steady and unsteady state describes fluid flow behaviour. Steady-state flow refers to the condition where the fluid properties at a point in the system do not change over time. The method involves injecting two or three fluids into a core sample at the same time at constant rate or pressure. The method is known to give reliable relative permeability data by extending the duration of constant rate or pressure until the equilibrium between the injected fluids can be reached. This technique gives information about saturation, flow rates and pressure gradients. Darcy's law is then used to calculate the effective permeability for each phase. The steady-state technique also involves the Hassler method, single-sample dynamic, stationary phase and Penn State (Honarpour and Mahmood, 1988).

Unsteady state methods involve replacing in-situ fluids by an injecting fluid with constant rate or pressure. This is a faster method than steady-state and can give saturation vs relative permeability data quickly. Unsteady state only uses the Buckley Leverett Equation for basis analyses with both immiscible and incompressible fluids. "Even though unsteady- state is the quickest method, more difficulties are characteristic, such as operational problems" (Honarpour and Mahmood, 1988).

3.2 Hagan-Poiseuille equation

For linear flows, the Hagan-Poiseuille Equation applies. Its a physical law that was first derived theoretically in 1839 by Gotthilf Heinrich Hagen and a year later, inferred from experimental measurements by Jean Léonard Marie Poiseuille. The Hagan-Poiseuille Equation is the initial step to derive equations that describe imbibition processes. The equation is based on defining the pressure drop from the idea that the fluid is incompressible and Newtonian and runs through a cylindrical tube with no acceleration.

$$\Delta P = \frac{8\mu LQ}{\pi r^4} \tag{14}$$

where ΔP is the pressure drop, L is the length of the pipe, Q is the volume flow rate and r is the radius of the tube. (Kirby, 2010, Lewis and Boose, 1995, Vogel, 1994)

3.3 Imbibition into saturated core plugs

During a two-phase displacement situation, important information about the rock and its characteristics can be determined. An increase in the wetting phase saturation is known as imbibition. During LRQC tests, when water is imbibed into an oil-saturated core plug until no further production it tells us something about the residual oil saturation and helps evaluate the LRQC properties as a reservoir rock. Problems connected with definitions of wettability and imbibition in oil recovery can be avoided if the imbibition until no further production can be explained as a percentage of pore volume saturation, S_{wi} (Morrow and Mason, 2001). However, the endpoint saturations are not always easy to measure, and difficulties might come in converting such laboratory data to results valid for in-situ reservoir conditions.

Spontaneous free imbibition

The process by which the wetting phase is absorbed into a porous media displacing the non-wetting phase by capillary pressure is known as spontaneous imbibition. Spontaneous imbibition was tested on LRQC using the Two-Ends Open (TEO) and All-Faces Open (AFO) boundary conditions, explained in Section 3.4. By placing a core sample in a container with free access to brine, the core will imbibe water automatically. The process is driven by surface energy without any applied pressure, explained in the experimental setup in Section 4.4.1. During spontaneous water imbibition, water displaces oil in the smaller pores first due to their higher capillary pressure, illustrated in Figure 7. This process is probably used more in daily activities than lab work, for example using a towel after a shower, or wetting a spounge to erase the board (Morrow and Mason, 2001). Capillary forces drive spontaneous imbibition, but in a reservoir, gravitational forces might also have an impact. In this thesis, the gravitational forces are neglected due to the small sized core samples. (Li et al., 2003) discusses in addition to spontaneous free imbibition, imbibition performed as dynamic forced imbibition:

Dynamic forced imbibition

By forcing the wetting phase through a porous medium and displacing the non-wetting phase, it is a process specified as dynamic forced imbibition (Morrow and Mason, 2001). In this thesis known as waterflooding. In addition to an external pressure by injection, gravity forces can also lead to waterflooding (Li et al., 2003). During waterflooding, water displaces oil in the smaller pores first due to their higher capillary pressure and then extends to the larger pores with decreasing capillary pressure. Waterflooding is a common secondary oil recovery method, especially in regions where the water is easily accessible and therefore become cost-effective. One of the most important factors that affect waterflooding is the residual oil saturation (S_{or}) and the ability to increase the oil recovery/ lower S_{or}. These factors are strongly dependent on the wetting properties of the rock. Due to the post-waterflood residual oil saturation (Morrow, 1990), which is shown as an effective process if the porous medium is weakly water-wet.

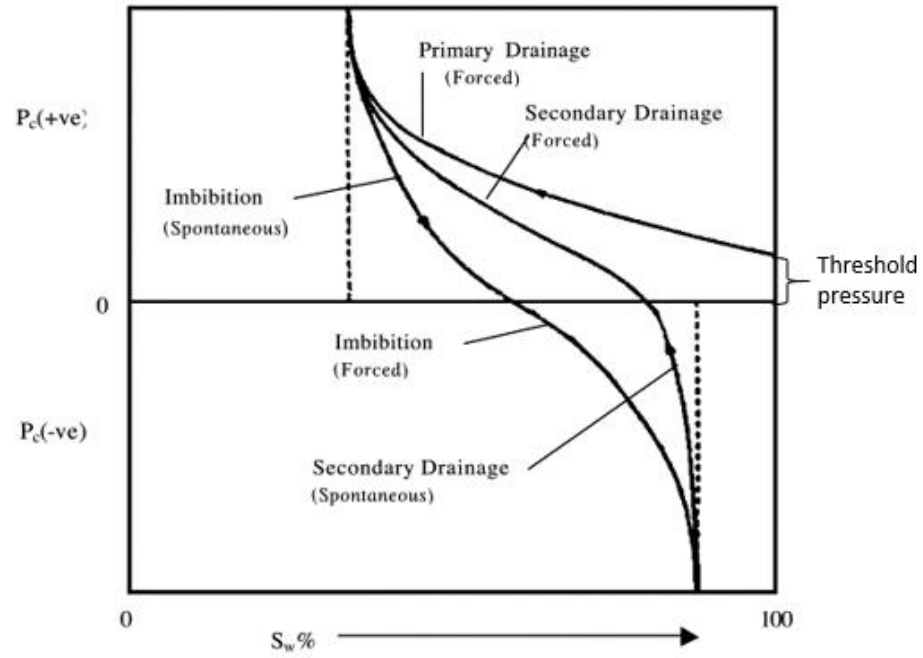

Figure 7 – Capillary pressure curves for forced and spontaneously imbibition and drainage versus water saturation. In an initially 100% water saturated core plug, primary oil drainage is the first flooding process. The displacement starts as the threshold pressure is overcome. The large pores with low capillary pressure are displaced first, and water saturation decrease quickly. Smaller and smaller pores are then displaced due to their higher capillary pressure until production end at S_{wi}, initial water saturation. A spontaneous imbibition driven by capillary pressure is then possible. Oil is displaced until zero capillary pressure and water saturation is increased. If the system is not strongly water-wet, further oil production can be conducted by forced water imbibition. Otherwise, in a strongly water-wet system, the oil production after spontaneous imbibition is zero. In a weakly water-wet system, oil can spontaneously displace the water from negative to zero capillary pressure and then be repeated by forced secondary drainage, which in this case ends at the same S_{wi} as the first (primary) drainage. Figure modified from (Morrow and Mason, 2001)

3.4 Boundary conditions during LRQC tests

In a laboratory test, a few fixed points within fluid flow can be controlled before an experiment. One of these is the boundary condition that decides the possible flow directions. Continuum equations depend upon these boundary conditions and they are therefore an important factor (Mason and Morrow, 2013). In a cylindrical core plug, different faces can be sealed leaving four main possibilities, examples shown in Figure 8:

- All-Faces Open (AFO)
- One-End Open (OEO)
- Two-Ends Open (TEO)
- Two-Ends Closed (TEC)

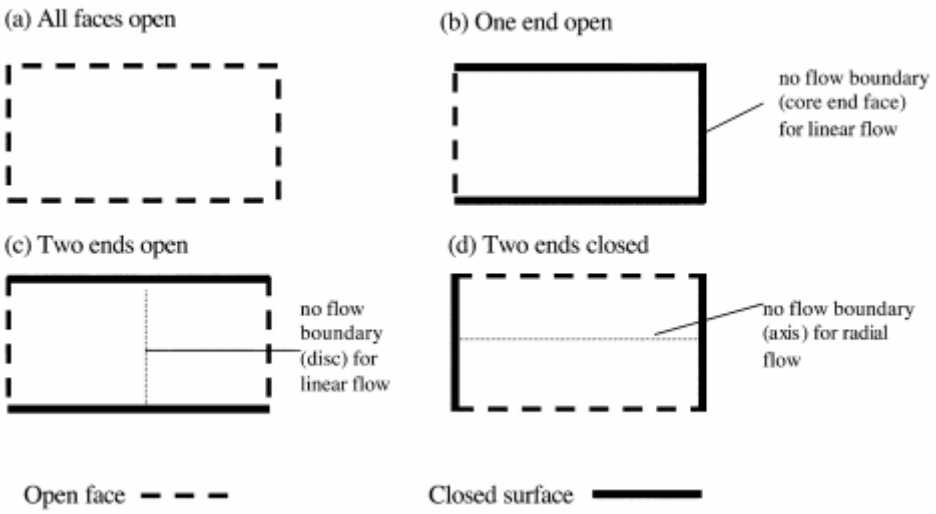

Figure 8 - Four different boundary conditions. a) All-Faces Open, (AFO), b) One-End Open (OEO), c) Two-Ends Open (TEO), d) Two-Ends Closed (TEC) (Morrow and Mason, 2001). During the tests on LRQC, AFO and TEO boundary conditions were used. TEO gave opportunities to separately record the co- and counter current production by imbibition. According to (Mason et al., 2009), AFO (a) is traditionally the most used boundary condition, because it's easy to perform and gives the most reproducible results.

3.4.1 Two Ends Open Free Spontaneous Imbibition test (TEOFSI)

During the use of boundary condition (c) in Figure 8, one end is in contact with the wetting phase, while the other end is in contact with the non-wetting phase. Spontaneous imbibition using this boundary condition is known as *Two-Ends Open Free Spontaneous Imbibition* (TEOFSI) and was studied by (Haugen et al., 2014) after (Dong and Zhou, 1998). To obtain this favourable boundary conditions, the core plugs in this thesis were epoxy coated. During TEOFSI boundary conditions, its possible for co- and counter-current flow to happen simultaneously. With the two ends in contact with different phases, brine can only enter the end in contact with brine, but oil can leave from both. The oil production starts in both ends, but counter-current flow only occurs in the very early stage of imbibition and ends after some time due to its limitations by the action of the capillary back pressure. Oil production continues in the end that is in contact with the non-wetting phase due to zero capillary back pressure.

Capillary back pressure

Capillary back pressure is the pressure difference between the non-wetting phase and the wetting phase of the porous media. For spontaneous imbibition to progress, the imbibition pressure has to exceed the capillary back pressure required for the production of the non-wetting phase out of the largest pores at the open face (Haugen et al., 2014). The capillary back pressure is proportional to the interfacial tension and depends inversely on the size of the large pore throats at the surface and the size of the pores connected with them in the open face region (Li et al., 2006). Pressure distributions during piston-like TEOFSI are shown in Figure 9. The imbibition stops when the pressure at the front of the non-wetting phase ($P_{nw,f}$) gets below the capillary back pressure ($P_{c,o}$).

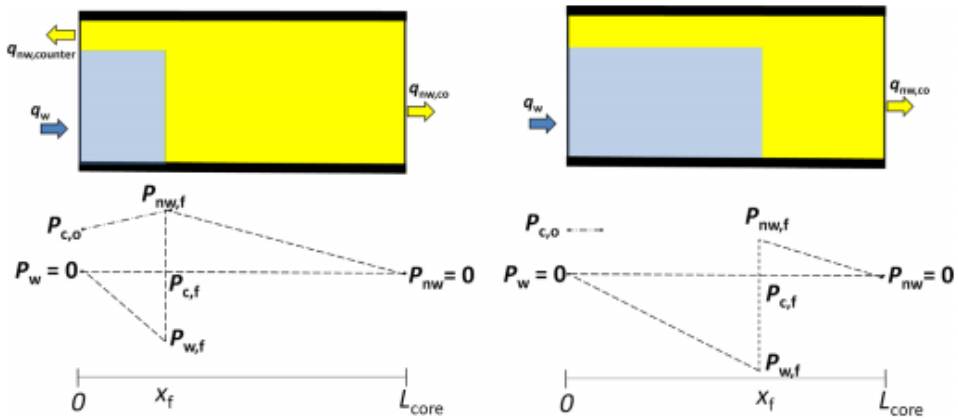

Figure 9 – Pressure distributions during piston-like TEO free spontaneous imbibition. Left: combined co- and counter-current production. Right: pure co-current production. (Haugen et al., 2014)

During the TEOFSI test, production volumes at inlet and outlet are measured. The amount of oil that is produced by counter-current displacement depends on several factors, but viscosity ratio is shown to have a great impact. If oil viscosity is low relative to brine, very little oil is produced counter-currently and it might happen pure co-currently.

3.4.2 Calculations during the TEOFSI test

Assuming saturation front is moving co-currently through the core and that the saturation does not vary with distance behind the front. (Haugen et al., 2014) then explains co-current displacement with TEO free spontaneous imbibition boundary conditions (reproduced in this thesis for completeness) with following equations:

Two assumptions can be made from Darcy's. The flows of the wetting and non-wetting phase like can be expressed as

$$q_w = -\frac{K k_{rw} A}{\mu_w} \frac{(P_{w,f} - 0)}{(x_f - 0)} \tag{15}$$

$$q_{nw} = -\frac{Kk_{rnw}A}{\mu_{nw}}\frac{(0 - P_{w,f})}{(L_{core} - x_f)} \tag{16}$$

where K is the absolute permeability, $k_{r,w}$ and $k_{r,nw}$ are the relative permeability, A is the area, L_{core} is the length of the core and x_f is distance advanced by the front.

The capillary pressure at the imbibition front ($P_{c,f}$) is the difference between the pressure in the non-wetting phase ($P_{nw,f}$) at the front and the pressure in the wetting phase ($P_{w,f}$) at the front:

$$P_{c,f} = P_{nw,f} - P_{w,f} \tag{17}$$

For co-current displacement, the rate of the non-wetting phase (q_{nw}) must be equal and opposite to the rate of the wetting phase (q_w):

$$q_w = -q_{nw} \tag{18}$$

The conservation of volume requirement for the advance of the front gives

$$\frac{dx_f}{dt} = \frac{q_w}{\varphi A(S_{wf} - S_{wi})} \tag{19}$$

Where φ is the porosity, S_{wf} is the saturation of the non-wetting phase behind the front and S_{wi} is the saturation ahead of the front.

Integrating from $x_f = 0$, $t = 0$ to x_f at time t gives

$$\frac{x_f^2}{L_{core}^2} + 2\frac{\mu_{nw}/k_{nw}}{((\mu_w/k_w)-(\mu_{nw}/k_{nw}))}\frac{x_f}{L_{core}} = \frac{2KP_{c,f}}{\varphi L_{core}^2(S_{wf}-S_{wi})}\frac{1}{((\mu_w/k_w)-(\mu_{nw}/k_{nw}))}t \tag{20}$$

The pressure in the non-wetting phase ahead of the front is given by

$$\frac{P_{nw,f}}{P_{c,f}} = \frac{1}{1 + (\mu_w/k_w) - (k_{nw}/(\mu_{nw})(1/((L_{core}/x_f) - 1))} \tag{21}$$

Let

$$\left(\frac{1}{(\mu_w/k_w)(k_{nw}/(\mu_{nw}) - 1}\right) = D \tag{22}$$

For a core saturated with non-wetting phase, the relative permeability ahead of the front ($k_{r,nw}$) is 1. In addition, μ_w and μ_{nw} can be measured separately. Then, if D can be determined, k_w can be calculated. Substituting and adding D^2 to each side of Equation 20 gives

$$\frac{x_f^2}{L_{core}^2} + 2D\frac{x_f}{L_{core}} + D^2 = D^2 + \frac{2KP_{c,f}}{\varphi L_{core}^2(S_{wf} - S_{wi})}\frac{1}{((\mu_w/k_w) - (\mu_{nw}/k_{nw}))}t \tag{23}$$

Equation 23 can be factorized to give

$$(\frac{x_f}{L_{core}})^2 = D^2 + \frac{2KP_{c,f}}{\varphi L_{core}^2(S_{wf} - S_{wi})}\frac{1}{((\mu_w/k_w) - (\mu_{nw}/k_{nw}))}t \quad (24)$$

Let $$\frac{2KP_{c,f}}{\varphi L_{core}^2(S_{wf}-S_{wi})}\frac{1}{((\mu_w/k_w)-(\mu_{nw}/k_{nw}))}t = E \quad (25)$$

Then $$((\frac{x_f}{L_{core}})^2 = D^2 + E \quad (26)$$

During a single displacement with constant fluid and core properties, D and E will be constants, and thus Equation 26 can be solved to give

$$\frac{x_f}{L_{core}} = \sqrt{D^2 + Et - D} \quad (27)$$

Equation 27 calculates the expected position of the front at a given time *t*. The front position can be found from the amount of brine imbibed, which is the same as oil produced. By dividing the brine imbibed at the front by the total amount of brine imbibed at the end, Equation 27 can be used to calculate the front position. If the expected position of the front at a given time *t* is plotted against the experimentally measured position of the front, a value for *D* which makes a plot with a straight line, can be found (Equation 22). After D has been found, a value of E can be determined that gives a gradient of unity. Since the rock is fully oil saturated, the relative permeability to oil ahead of the front is 1. Knowing this together with fluid viscosities, the fitted value of D and Equation 22 can be used to find the relative permeability to brine behind the front, $k_{r,w.}$ Knowing the measured variables in factor E (φ, L_{core}, S_{wf}, S_{wi}, K, μ_w and μ_{nw}) the fitted value of E in Equation 25 is known and can be used to find the capillary pressure at the front, $P_{c,f}$:

$$P_{c,f} = E\frac{\varphi L_{core}^2(S_{wf} - S_{wi})}{2K}\left(\frac{\mu_w}{k_w} - \frac{\mu_w}{k_{nw}}\right) \quad (28)$$

Part II - Experimental Setup and Procedures

4 Experimental procedures

The main objective of this study was in part A to determine porosity, permeability and to study the flow potential and oil storage capacity for the Low Reservoir Quality Chalk core plugs. In a part B, the effect of using the TEOFSI method after (Dong and Zhou, 1998) and (Haugen et al., 2014) was tested on Low Quality Chalk. Relative permeability and capillary pressure were then able to be calculated for successful tests by theory related to this method.

This part gives an overview of the experimental preparations, setups and equipment used. The experimental work was conducted at the University of Bergen, Department of Physics and Technology. Experiments performed are presented in Table 2. Eight spontaneous imbibition tests and four forced imbibition/drainage tests were performed on 12 core plugs that represent different zones and outcrops. All tests were performed in atmospheric temperature, 25 °C. Each method used, is described in detail in the next sections.

Table 2 - Experimental overview. Core ID (see Table 1 for core ID description), saturation fluid and type of experiment conducted.

Core ID	Saturation fluid	Experiment conducted
MM5-6 H5	Water	Primary oil drainage Forced water imbibition Secondary oil drainage
MM5-6 H6	Oil	SI, TEO
MM5-6 H4	Oil	SI, AFO
MM4-5 H1	Water	Primary oil drainage SI, AFO Forced water imbibition Secondary oil drainage Secondary SI, AFO
MM4-5 V1	Oil	SI, TEO
MM3-4 V8	Oil	Forced water imbibition Primary oil drainage
MM3-4 H9	Oil	SI, AFO
BED3 V15	Oil	SI, TEO
ZIGZAG V11B	Oil	SI, TEO
ZIGZAG H11	Oil	SI, TEO
ZIGZAG H12	Oil	SI, TEO
ZIGZAG H13	Water	Primary oil drainage SI, AFO Forced water imbibition Secondary oil drainage Secondary SI, AFO

SI, TEO: Spontaneous imbibition with Two-Ends Open free boundary conditions.
SI, AFO: Spontaneous imbibition with All-Faces Open free boundary conditions.

4.1 Fluids and sample materials

4.1.1 Fluids

Mineral oil (Decane 95%) or synthetic brine (Ekofisk) was used as saturation fluid in all tests. For fluid properties and ion composition, see Table 3. Ekofisk brine was used as the wetting phase for all tests. Here, calcium carbonate ($CaCl_2$) was added to minimize possible dissolution of the core plugs and sodium azide (NaN_3) was added to prevent bacterial growth. In practice, its very difficult to obtain reliable reservoir brine compositions, particularly the divalent ion composition. According to (Scheuerman et al., 1998), these ions may impact significantly on clay swelling and jeopardise any SCAL experimental result.

Table 3 - Liquids properties

Fluid	Composition	Density [g/cm^3]	Viscosity [cP]
Decane 95 %	$C_{10}H_{12}$ Purity – 95 %	0.726±0.001	0.96±0.01
Ekofisk Brine	Distilled water 40 g/l NaCl 34 g/l $CaCl_2$*$2H_2O$ 5.0 g/l $MgCl_2$*$6H_2O$ 0.2 g/l NaN_3	1.05±0.001	1.09±0.01

4.1.2 Core material

Core plugs were drilled from quarried slabs of Upper Cenomanian-Lower Turonian Chalk from Eastbourne, England (Figure 10). Core plugs are considered heterogeneous by CT images, with a porosity ranging from 14% to 26 % and permeability range from 0.002 mD to 0.820 mD. The zones have variable clay content, as described in the geological description in Chapter 2. The outcrops collected is originally above water surface, meaning the core plugs have never been exposed to surface active components or close to crude oil. Their exposure to only water and air therefore argument towards the core plugs being water-wet.

Figure 10 – Core plug H2 drilled from outcrop MM4-5, collected from location Pinapple Steps in Eastbourne England. Core diameter is 4.96 cm (2") and core length is 10.01 cm. Figure shows several fractures visible.

4.2 Core plug preparations

In total, 24 core plugs were cut to size from larger outcrops of six different zones, see Figure 3. A nominal diameter of 2" was drilled for all cores, with variable lengths from 3.38 cm–12.41 cm. Core plugs were drilled by Dr. Marianne Steinsbø, Department of Physics and Technology, UoB and photos from this event is shown in Figure 11. After cutting, core plugs were gently washed and dried in a heating cabinet until constant weight. Further, diameter and length were controlled and measured for bulk volume calculations for each core.

Figure 11 – LRQC core plugs being drilled from outcrops of six different zones described in Figure 5. <u>Right top:</u> Three horizontal cores; H7, H2 and H9 drilled from outcrop MM3-4. The outcrop has visible colour differences. <u>Left top:</u> Outcrop from zone MM5-6 cut in half. Vertical core plugs drilled from the one to the left, while horizontal core plugs are drilled from the one to the right. The outcrop show colour variation and have visible heterogeneities. <u>Right bottom:</u> The bit (in blue) is about to drill a core plug from BED 5. <u>Left bottom:</u> The two core plugs, H10A and H10B drilled from zone BED 5. One is horizontal and one is vertical. Photos are taken by Dr. Marianne Steinsbø, Department of Physics and Technology, UoB.

4.3 Porosity and permeability measurements

4.3.1 Porosity measurement

Porosity is an important reservoir property due to its determination of possible hydrocarbon content within LRQC and its impact on fluid flow and oil storage capacity. Porosity was measured using two methods to evaluate a possible difference between brine and gas porosity. Half of the core plugs were saturated with Ekofisk brine and porosity was measured using the saturation method. The remaining dry core plugs and measured by using Boyles's law.

Saturation method

Porosity of 11 core plugs was measured using the saturation method. The method is based on weight difference before and after the core plug is saturated with brine during vacuum conditions, see Figure 12. The weight difference corresponds to the total volume of brine saturated into the core. Assuming 100 % water saturation and known brine density, pore volume, *Vp*, can be calculated from Equation 1. The Ekofisk brine and the core plug were placed in separated vacuum chambers connected to a vacuum pump. At a low enough vacuum (preferential <170 mTorr), the valve between the brine and the core plug was opened, allowing the core to submerge in brine. The sample was then stored for 24 hours for the brine to imbibe, assuming the sample to be 100% saturation. When obtained, the sample was weighed again.

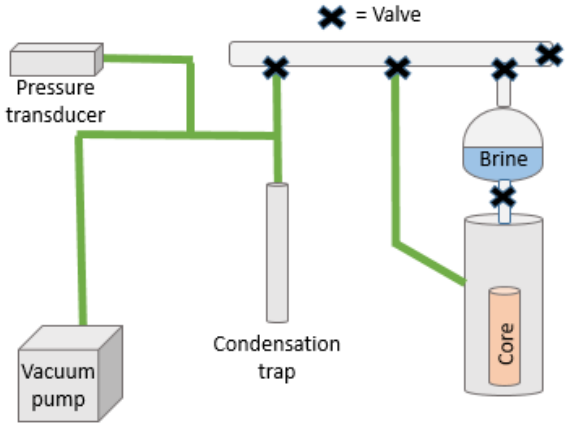

Figure 12 – Saturation method setup showing used equipment and connections. A dry core plug was placed in empty container until favourable vacuumed conditions. When obtained, the valve between the container and brine was opened, allowing the core to submerge in brine in 24 hours until 100% assumed saturation. The condensation trap was placed in liquefied nitrogen to avoid condensation droplets of reaching the pump.

Boyle's law method

Air porosity was measured for 13 core plugs using Boyles Law, see setup in Figure 13. The procedure described below was followed. All valves were opened to atmospheric conditions, and core plug was placed in the Hassler core holder. Then valve 1 and 3 were closed and the pressure was measured in the core plug system (red dashed box) before valve 2 was closed. Using the air pressure regulator, air pressure was set to approximately 1.2 bar and valve 1 was opened, to pressure V_{ref} keeping valve 2 and 3 closed. After stable pressure, valve 2 was opened to record the total system pressure P_{tot}. This procedure was repeated 3 times for 1.2 bar, 1.4 bar and 1.6 bar. The porosity was then calculated by using Equations 1 and 4.

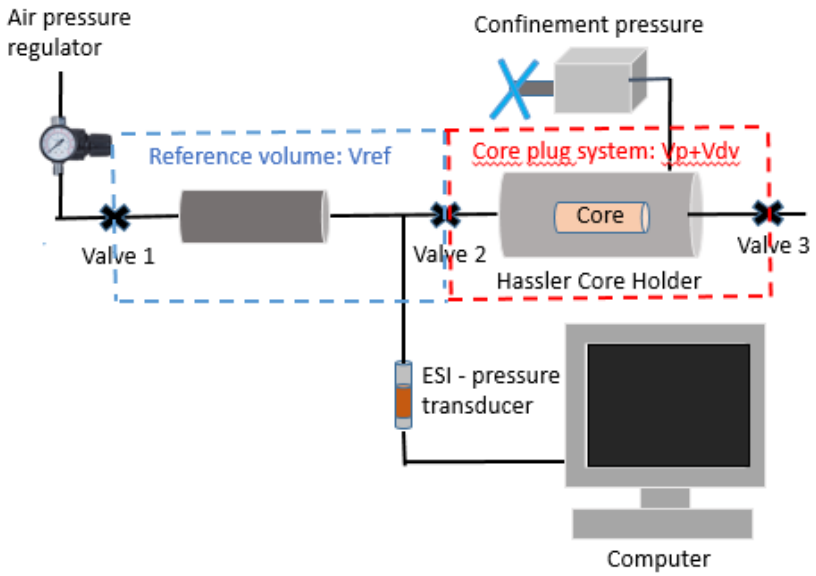

Figure 13 - Sketch of setup to measure porosity with use of Boyle's Law. Blue dashed line represents reference volume, red dashed line represents core plug system volume. The ESI-pressure transducer measures pressure in system depending on which valves that are open/closed. Pressure was always recorded when stable.

4.3.2 Absolute Permeability measurements

Absolute permeability defines a reservoirs capability to transmit fluids through its network of interconnected pores and is therefore important to determine. The Klinkenberg effect is a known impact on gas permeability measurements. To determine how big this effect is on Low Permeable Chalk, absolute permeability was like porosity, measured with brine and gas, for comparison.

The use of both injection fluids involved the core plug to be placed horizontally in the Hassler core holder connected to an ESI-pressure transducer for pressure recording, see Figure 14. A confinement pressure of net 8 bar above the differential pressure was set to ensure that the fluid or the gas actually went through the core. Differential pressure was measured at three different rates in both methods, using the average pressure as the main value. Pressure recordings were registered when both inlet and outlet pressures were stable. Ekofisk brine was injection fluid for saturated cores and the Quizix pump ensured a constant injection rate, Q. Gas, N_2 was injected at a constant rate through the dry core plugs by using a mass flow controller connected to a N_2 tank.

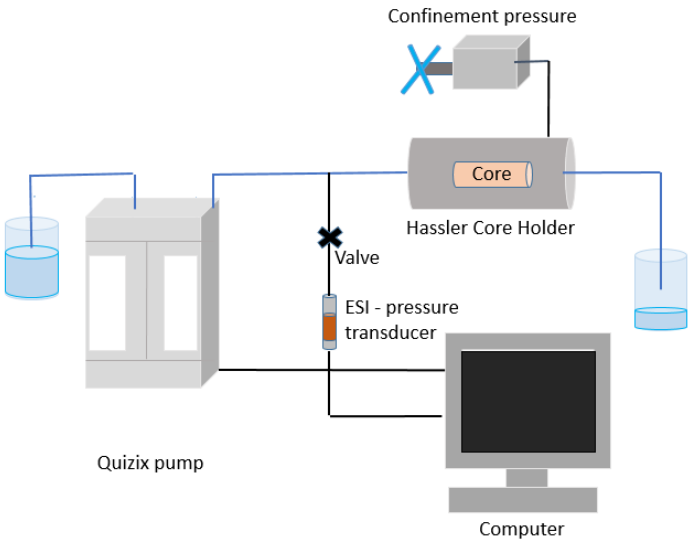

Figure 14 – Illustration of setup for permeability measurements using brine. The Quizix pump ensured constant injection of brine through the core, whereas the ESI-pressure transducer endured pressure recordings. At gas permeability measurements, the Quixix pump was replaced with a mass flow controller connected to a N_2 tank.

Brine permeability measurement for sample MM4-5 H5 was conducted with rates of 2 ml/h, 3.5 ml/h and 5 ml/h. The permeability value was calculated using Darcy's law for uncompressible fluid, Equation 5. Rates and corresponding pressures are plotted in Figure 15. When calculating permeability, if the added trendline through all points is not a straight line then the permeability value needs to be corrected. The correlation is done by subtracting the slope value in a linear equation from the calculated permeability value. A regression line for measured pressures and used rates is illustrated in Figure 15, with associated linear equation for projected points. For a quicker and more frequent recording, the first rate adjustment for every core plug was set as high as possible depending on pressure (not to exceed 35 bar).

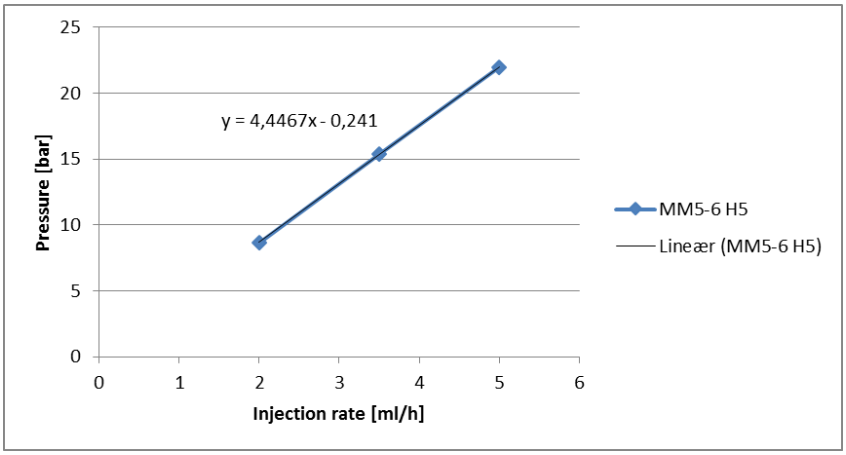

Figure 15 – Pressure versus injection rate for brine permeability measurements. A linear trendline through three measured points with matching equation is illustrated. The slope value in the linear equation, $a = Ak/\mu\Delta l$ and is the point where the line crosses the y-axis. The "a" value helps correlate the calculated permeability value by being subtracted from the calculated permeability value.

Gas is a compressible fluid and have minimum frictional interaction with the walls in a pore channel (slippage effect). Therefore, the Klinkenberg effect need to be taken into account during gas permeability calculations. Value for each core plug was calculated using Equation 5. The Klinkenberg effect is described in Section 1.2.3 and gas permeability values were calculated using Equation 8. Permeability measurements using both gas and oil were conducted for three cores, MM3-4 V8, MM3-4 H9 and MM5-6 H4 for comparison. Gas permeability measurements were conducted with both low and high rates for MM5-6 H4 and MM3-4 V8 to consider how the gas permeability changes with different pore pressures. The results from brine, gas and oil permeability measurements are discussed in Section 5.3.2

4.4 Recovery and flow potential tests by oil and water injections

To examine recovery potential and determine S_{wi}, oil and water floodings were conducted for core plugs described in Table 2. Core plugs were oilflooded by injecting Decane mineral oil and waterflooded by injecting Ekofisk brine. Oil and water floods were conducted interchangeably for the core plugs to check reproducibility. After primary drainage, spontaneous water imbibition was performed for two core plugs, followed by forced water imbibition to check wettability conditions by calculating the Amott-Harvey index. If zero oil was produced during waterflooding after the spontaneous displacement, the core plug was assumed water wet. Both oil and water saturated core plugs were used in these displacement tests.

4.4.1 Setup and Equipment during recovery and flow potential tests

Experimental setup for forced oil- and waterflooding is illustrated in Figure 16. Equipment used is listed below.

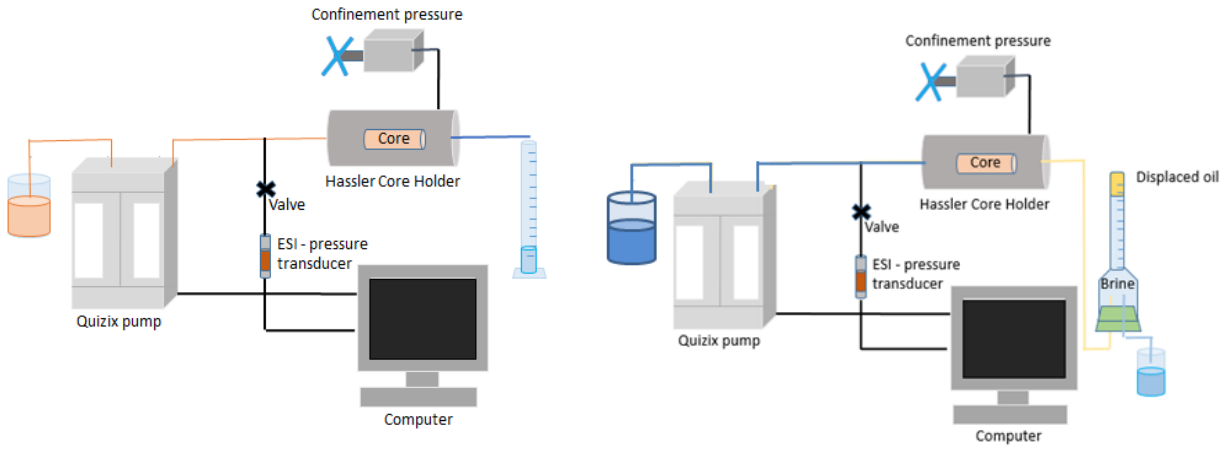

Figure 16 – Illustration of experimental setup for waterflooding (left) and oilflooding (right). A Quizix pump was used for both injections to ensure constant pressure or injection rate. Pressure was frequently recorded using an ESI-pressure transducer. During oilflooding (right) the produced oil could easily be collected in a glass cylinder. The produced water during oilflooding needed to be collected in a closed imbibition cell since the mineral oil is less dense than water.

Equipment used in the setup:

- Quizix QX- 1500 pump for injection of brine or oil.
- Hassler core holder
- ESI-pressure transducer (range 0-40 bar) to measure the differential pressure.
- Plastic tubing, Swagelock fittings, valves and safety valve.
- Computer to control Quizix pump and ESI-pressure transducer logging
- 10 ml graded glass cylinder for measuring produced volume
- Imbibition cell for measuring oil production
- A rack to hold the imbibition cell.

4.4.2 Detailed experimental procedures for recovery and flow potential tests

Primary oil drainage

Initially 100 % water saturated cores plugs were placed in the Hassler core holder and flooded with Decane mineral oil until irreducible water saturation, S_{wi}. Primary drainage was performed at atmospheric outlet pressure and an atmospheric temperature of 25 °C. A higher injection rate results in higher differential pressure through the core plug. Depending on the pressure versus rate ratio, the core was either injected by constant rate between 2.5 ml/h to 17.0 ml/h or constant pressure of 29 bar, until steady state conditions were obtained. If the pressure was assumed to overcome 40 bar using an injection rate lower than 2.5 ml/h, then constant pressure was used due to the risk of destroying the ESI-pressure transducer by exceeding its maximum pressure of 40 bar. Finally, the total volume of produced brine was measured and S_{wi} was calculated. Illustration is shown in Figure 16 (right).

Spontaneous water imbibition

After the primary oil drainage, spontaneous imbibition was performed using All-Faces Open (AFO) boundary conditions on two of the core plugs. In addition, spontaneous imbibition, AFO was performed on two 100% oil saturated core plugs for recovery potential study, see Table 2. Each core plug was placed in an imbibition cell filled with Ekofisk brine, see Figure 17. After end of production, oil recovery was measured and the residual oil saturation, S_{or} was calculated.

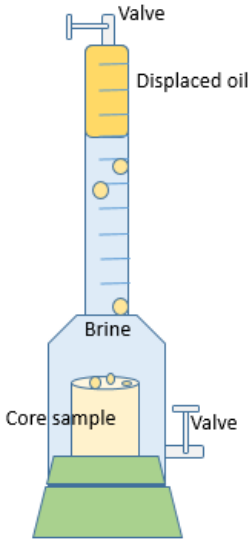

Figure 17 – Illustration of spontaneous water imbibition on oil saturated core plug with AFO boundary condition. Core plug was placed in a closed spontaneous imbibition cell where the up-flowing oil production easily could be recorded on top.

Water flooding

Waterflooding was conducted after spontaneous water imbibition to measure the Amott-Harvey index. The two core samples measured with both spontaneous water imbibition and waterflood had zero additional oil production during the latter test. This indicated that the core plugs were water-wet, as discussed further in Section 8.2. In addition, one initially 100% water saturated core plug was waterflooded direcly after primary drainage and one initially 100% oil saturated core plug was waterflooded to measure residual oil saturation, S_{or} for oil storage potential study, see Table 2. The setup used during waterflood is illustrated in Figure 16 (right).

4.5 Spontaneous imbibition test using epoxy coated core plug

As a part B in this thesis, the Two-Ends Open Free Spontaneous Imbibition (TEOFSI) method was studied on Low Quality Reservoir Chalk. This method had never before been conducted on Low Permeable Chalk and some improvisation needed to be made. However, the same setup as in (Haugen et al., 2014) was used. In total, six dry and clean cores were epoxy coated forming Two-Ends Open (TEO) boundary conditions, ready for oil recovery and fluid flow tests using spontaneous imbibition. By use of this methodology, both co- and counter-current production could be measured and used to calculate relative permeability and capillary pressure by theory of (Haugen et al., 2014).

4.5.1 Preparations and executions using epoxy on core plugs

Two-ends open (TEO) boundary condition was favourable for the spontaneous free imbibition recovery tests. The boundary condition was achieved by using epoxy. Epoxy is a durable glue that provides a high level of bonding properties and can be applied around the cylindrical core plug (not the ends). When epoxy and hardener are mixed, they remain as liquid for some time, making it possible to apply on the outside surface of the core plug. After a few hours, it hardens and become like soft plastic. At first, a thin layer was added around the circumference and left for 24 hours to dry properly.

For pressure recordings during the displacement process, two holes for pressure sensors were drilled, each approximately one cm deep into the core. The inlet pressure sensor were placed 1.0-1.5 cm from the inlet and the outlet pressure sensor 0.5-1.0 cm from the end piece. The sensor distance from inlet and outlet varied due to the differences in core length. Swagelok tubing was fitted into the holes and one end piece was attached making an outlet end, both of them fastened by epoxy and left to dry. Finally, a thicker layer was added around the circumference making sure only the two ends were open. A finished example is shown in Figure 18. The core plugs were saturated with mineral oil one at a time, regarding the undesirable possibility of the core to age, while waiting to be tested. The epoxy coated core plugs were oil saturated the same way as for water saturation, setup in Figure 12. The core plugs were vacuumed for 4 hours, then left to submerge in mineral oil for 24 hours until assumption of 100% saturation. The cores were weighed before and after saturation for pore volume for Oil Originally In Place (OOIP) estimations.

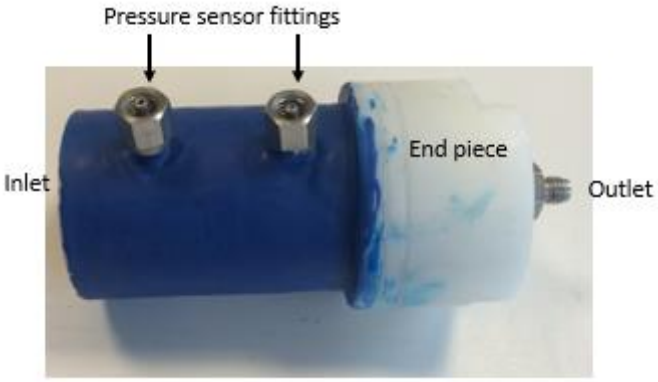

Figure 18 – Example of finished epoxy coated core ready to be oil saturated. Water spontaneously imbibed at the inlet to the left, where some oil was also produced counter-currently (from inlet). Most of the oil was produced co-currently (at outlet through the end piece). No water was injected at outlet due to this ends contact with oil. The two pressure sensors are both drilled approximately 1 cm deep into the matrix and placed at vary distance from the outlet and end piece (depending on core length). Both pressure sensors and the end piece are attached by epoxy.

4.5.2 Setup and equipment used for epoxy on core plugs tests

After 100% oil saturation, the ESI-pressure transducers were attached and an oilfilled short stainless steel tube was connected to the end piece at outlet to make sure of this ends contact with oil. The completed system was placed horizontally in a container filled with brine. Two imbibition cells were placed above both inlet and the outlet end to record oil production versus time. The experimental setup is illustrated in Figure 19.

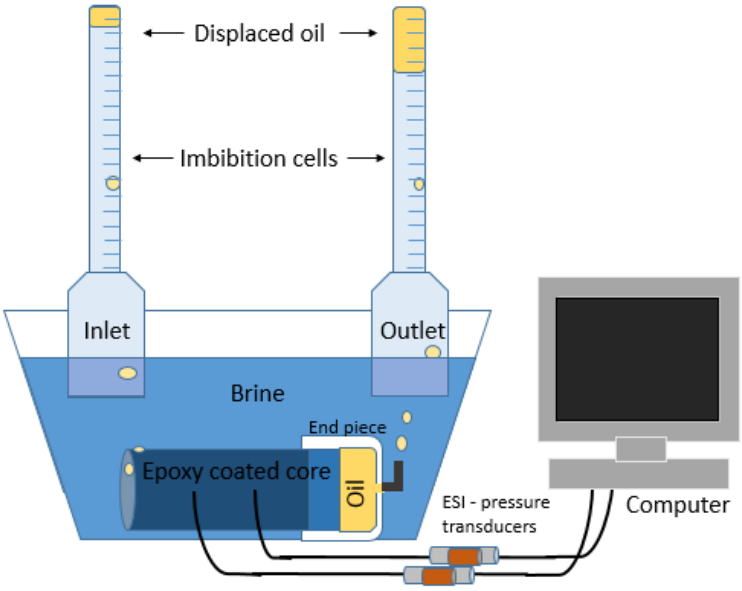

Figure 19 – Schematic diagram of the experimental setup when using epoxy coated core plug for spontaneous imbibition. Two imbibition cells were used to measure co- and counter current production and placed above each core plug end. Two ESI-pressure transducers were connected to a computer to record inlet and outlet pressure during the displacement process.

Part III - Result & Discussion

5 Reservoir characterization of Low Reservoir Quality Chalk

As a part of a bigger project, connected to the Joint Chalk Research Programme, Phase 7 (JCR 7), several tests were performed on Low Reservoir Quality Chalk core plugs, to find more information about its properties as a reservoir rock. The results in this thesis are divided into two main parts; **in part A**, the results related to general reservoir characterization for Low Reservoir Quality Chalk (LRQC), like porosity, permeability and fluid flow, oil storage and recovery potential are presented and discussed together with an evaluation of rock characteristics. **In part B**, the results from the study of the *Two-Ends Open Free Spontaneous Imbibition* (TEOFSI) method, as a first on Low Permeable Chalk are presented together with relative permeability and capillary pressure calculated values.

PART A

5.1 Core plug identification and geometrical properties

Determination of porosity and permeability for LRQC was an important part of this thesis. Porosity and permeability are two of the most important reservoir properties due to their indication of fluid flow, fluid storage- and fluid recovery expectations. Fluid flow through porous media is connected to porosity and permeability with easier flow through high porosity and permeability areas, which is favourable during hydrocarbon production. Porosity and permeability values measured, together with basic geometrical properties like diameter and length are listed in Table 5 for each LRQC core plug. Porosity and permeability measurements were performed using brine, gas or oil, depending on the core sample saturation, described in Section 4.3.1. Different fluids were used for comparisons between oil, brine and gas and to study the Klinkeberg effect on gas permeability measurements on LRQC. The variations in porosity and permeability between core plugs are likely caused by heterogeneities like fractures or free pore space. Basic geometrical properties like diameter, length and weight of the core plugs were measured ahead of experimental work while all core plugs were still dry. The core plugs are from six different zones; MM5-6, MM4-5, MM3-4, BED 5, BED 3 and ZIGZAG, and were collected from two different locations in Eastbourne, England. The geological description of each zone and which location they are from, is described in Section 2.1. Letter H/V in front of the core plug number; indicate if the core plug was drilled horizontally or vertically from the outcrop, i.e. H1 was drilled horizontally.

Table 5 – Core identification, geometrical properties, calculated pore volume and measured porosity and permeability of LRQC obtained from Upper Cenomanian – Lower Turonian Chalk succession at Eastbourne, Sussex in England. Average porosity and each core plugs deviation from the average is in column 6 and 7. The water saturated core plugs measured with brine are marked with "x" in the eight column.

Core ID	Diameter [cm]	Length [cm]	Porosity (φ) [frac]	φ Average	φ Deviation %	Permeability (K) [mD]	Water saturated
MM5-6 V3	4.96	5.32	0.22		0.1	0.022	x
MM5-6 V4	4.96	11.5	0.21		1.4	0.382	
MM5-6 H4	4.96	5.82	0.24	0.22	1.3	0.374	
MM5-6 H5	4.97	7.90	0.21		1.7	0.028	x
MM5-6 H6	4.97	6.38	0.24		1.9	0.410	
MM4-5 V1	4.96	7.12	0.26		0.3	0.531	
MM4-5 V2	4.96	4.41	0.25	0.25	0.6	0.049	x
MM4-5 H1	4.96	4.71	0.25		0.5	0.104	x
MM4-5 H2	4.95	10.0	0.26		0.7	0.820	
MM3-4 V7	4.96	6.40	0.19		2.3	0.016	x
MM3-4 V8	4.97	6.07	0.24		2.3	0.313	
MM3-4 H7	4.97	5.13	0.22	0.21	1.2	0.322	
MM3-4 H8	4.97	4.31	0.17		4.5	0.017	x
MM3-4 H9	4.96	4.80	0.25		3.3	0.306	
BED5 H10A	4.95	4.65	0.15	0.15	0.3	0.003	x
BED5 H10B	4.97	3.83	0.14		0.3	0.002	x
BED3 V14	4.96	7.18	0.19		1.9	0.008	x
BED3 V15	4.96	7.79	0.22	0.21	0.9	0.052	
BED3 H15	4.96	10.3	0.22		1.0	0.108	
ZIGZAG V11A	4.95	6.12	0.23		0.8	0.009	x
ZIGZAG V11B	4.96	6.27	0.22		1.9	0.184	
ZIGZAG H12	4.97	8.23	0.25	0.24	1.8	0.207	
ZIGZAG H13	4.96	6.39	0.23		0.6	0.014	x
ZIGZAG H11	4.97	9.02	0.25		1.5	0.248	

5.2 Porosity measurements

Porosity is an important reservoir property due to its determination of possible hydrocarbon content within LRQC and its impact on fluid flow and oil storage capacity. Porosity was measured using both brine and gas to evaluate a possible difference between the use of two fluids. Porosity was measured by the saturation method for the 11 initially water saturated core plugs and the 13 dry core plugs were measured using Boyles Law, see experimental procedures in Section 4.3.1. Porosity was calculated using Equation 1 and 4 and the value for each core plug are listed in Table 5. To compare porosity values for each zone, and the fluids used, porosity is plotted for each core plug in Figure 20. The zones; BED3, ZIGZAG, MM3-4, MM4-5 and MM5-5 show small variation in porosity and are within the same range, while BED5 was measured to a lower porosity value than the average. The geographical description of BED5 expresses many thin and horizontal lines. In addition, the relative sea-level was at its lowest during the formation of BED5 and both of these factors indicate a higher clay content and lower possible porosity. The previous cold event that ends at the formation of BED5 might have caused fewer animals digging, little excavation and therefore absences of bigger voids within the rock which reflect lower porosity. Density measurement by CT images (Figure 28) proved BED5 to have the highest density value which may be explained by the higher clay content and better lamination for the zone. Lower relative sea-level proved higher clay content and the average porosity values seem to reflect the sea-level changes through time. Porosity decrease during the Lowstand System Track (LST) from ZIGZAG to BED5, when the relative sea-level decreases and then increase from BED5 to MM5-6 during the Highstand System Track (HST) and higher relative sea-level. The Maximum Flooding Surface (MFS) event during the formation of MM4-5 has probably caused this zone to have the highest average porosity value ($\varphi = 0.38$) due to probably lower clay content.

Average porosity was $\varphi = 0.22$ (gas and brine). Porosity measured with Boyles Law was in average $\varphi = 0.04$ higher than by the saturation method. The lower porosity values by saturation method might be caused by gas compressibility or indicate that core plugs were not 100 % water saturated. Core plugs should probably therefore been saturated more than 24 hours until constant weight. The scale of uncertainties within methods could also have an impact on porosity results. Boyle's law has a lower uncertainty due to its use of three different rates, while the porosity measured by saturation method is only based on one weight measurement before and after saturation.

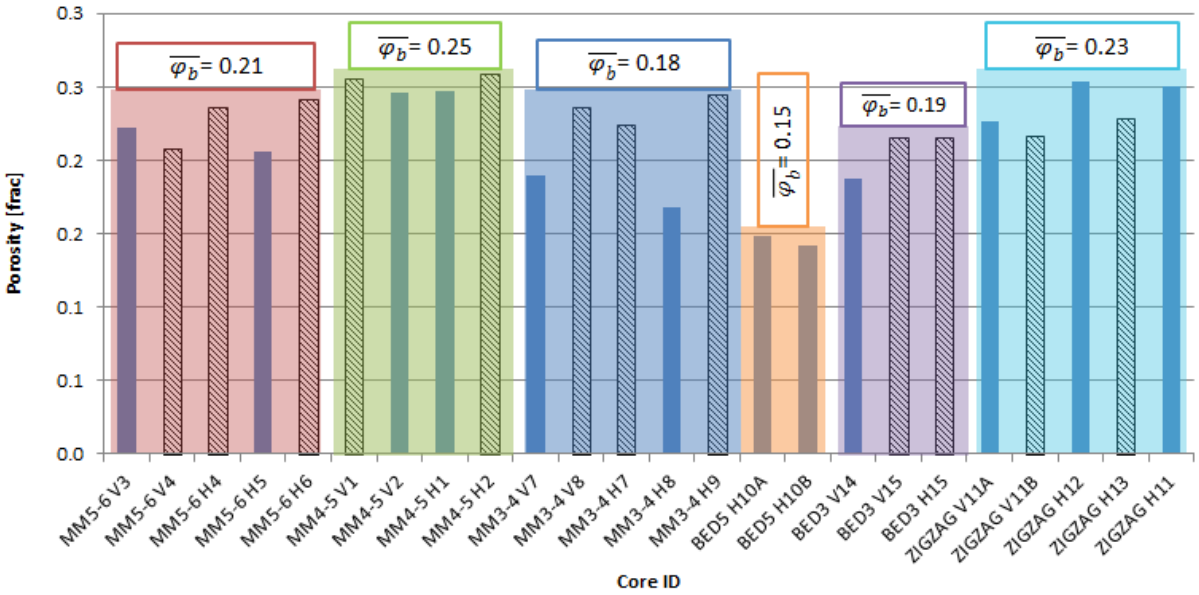

Figure 20 – Bars showing porosity value for each core plug after gas and brine porosity measurements. Core plugs measured with brine are showed in blue bars, while gas porosity values are bars in black stripes. Each zone is shown by different colour and the value above defines the average brine porosity ($\overline{K_b}$). Porosity values measured with brine and gas reflect each other for each zone, meaning if the average brine porosity for one zone is high, then the average gas permeability is also high. MM4-5 was observed as the highest permeable zone and BED 5 as the lowest. Brine porosity was measured using the saturation method and gas porosity was measured using Boyles Law. For zone and core plug description, see Section 2.1.

5.3 Permeability measurement

Permeability is a very important reservoir property to determine because it defines the reservoirs capability to transmit fluids through its network of interconnected pores. Permeability was measured using three different fluids; brine, oil and gas for comparison of values between fluids, see experimental setup in Section 4.3.2. BED3 proved to be difficult measuring with pressure less than 40 bar, due to its long length and apparently low permeability. BED5 represented by sample H10A (K=0.003 mD) and H10B (K=0.002 mD) had the lowest brine permeability, that was 10 times lower than the average for all zones (K_b = 0.030 mD), see Figure 21 for comparison of brine permeability values (blue bars). The geological description of BED5 gives the same arguments for the low permeability values as with porosity. The LST event happening during the formation of BED5 indicate a higher clay content, better lamination and thin horizontal lines, lower porosity (φ=0.15, Section 5.1), higher density (Figure 28) and reflect the lower calculated permeability. The average permeability of each zone reflects the relative sea-level change as porosity. Permeability decrease during the Lowstand System Track (LST) from ZIGZAG to BED5, when the relative sea-level decreases and then increase from BED5 to MM5-6 during the Highstand System Track (HST) and higher relative sea-level. The Maximum Flooding Surface (MFS) event during the formation of MM4-5 has probably caused this zone to have the highest average permeability value (K_{MM4-5}= 0.380 mD) due to probably lower clay content (as with porosity). The average permeability and porosity for each zone also reflect each other, higher porosity equals higher permeability.

Gas, respectively N_2 was used during permeability tests of dry core plugs and calculated values are listed in Table 5. Gas permeability values for each zone show the same result as for brine permeability. The gas permeability increase as the clay content is assumed to decrease, due to change in sea-level. Zone MM4-5 represented by core plug V1 (K=0.531 mD) and H2 (K=0.820 mD) show a much greater permeability than the other zones. This zone increase the average gas permeability significantly, K_a=0.328 mD. The lowest gas permeability value was core plug V15 (K=0.05 mD) in zone BED3. However, no core plugs from BED5 was permeability measured with gas, and might have had a lower value due to lowest brine permeability values due to its assumed higher clay content.

Permeability values for horizontally drilled core plugs are higher than vertically drilled core plugs for respective zones. The higher permeability horizontally is probably caused by sediments being deposited on top of each other. This gives the better lamination and greater connection between pores in horizontally. This argument is uncertain for zone BED5, due to both core plugs from this zone were horizontally drilled.

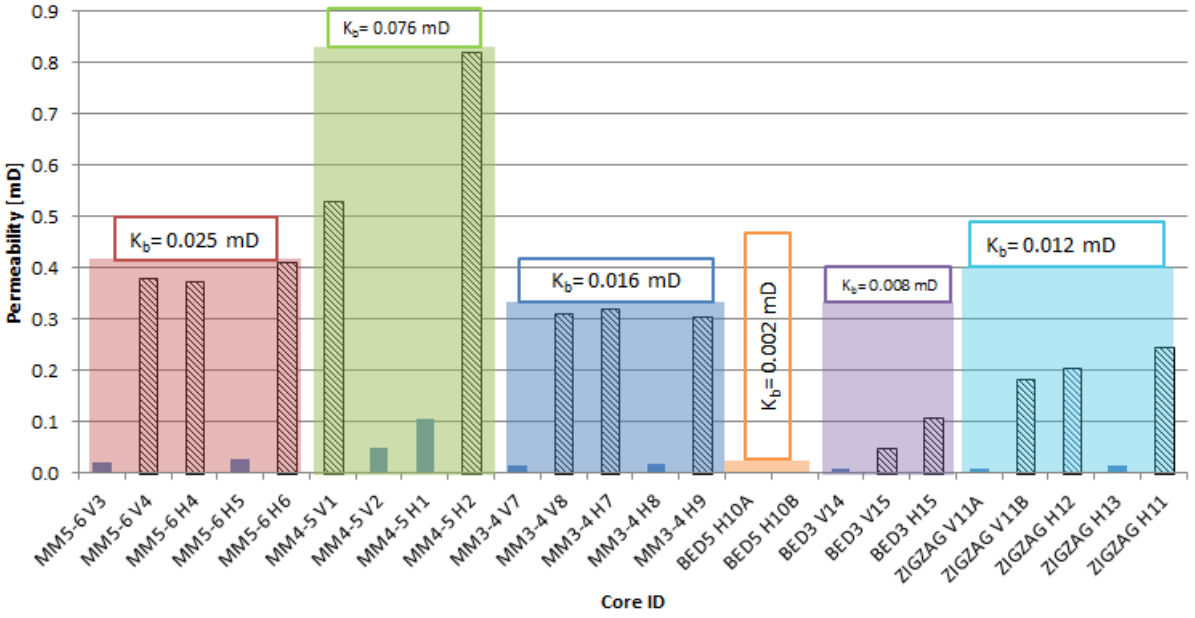

Figure 21 – Bars showing permeability value for each core plug after gas and brine permeability measurements. Core plugs measured with brine are showed in blue bars, while gas permeability values are bars in black stripes. Each zone is shown by different colour and the value above defines the average brine permeability (K_b). Permeability values measured with brine and gas reflect each other for each zone, meaning if the average brine permeability for one zone is high, then the average gas permeability is also high. MM4-5 was observed as the highest permeable zone and BED 5 as the lowest. Values are calculated using Darcy's law with the Klinkenberg effect taken into account when calculating gas permeability. For zone and core plug description, see Section 2.1.

5.3.1 The impact of injection rate on gas permeability measurements

The use of low or high injection rate during gas permeability measurements might have different impact on the Klinkenberg effect. To study this impact on LRQC, gas permeability were examined using four rates in the range of 20-100 ml/h and three rates in the range of 300-400 ml/h on MM5-6 H4. Associated pressures for MM5-6 H4 using low rate was 0.12-0.63 bar and high rate was 1.22-1.63 bar. MM3-4 V8 were measured at five rates in the range of 20-100 ml/h and three rates in the range of 500-600 ml/h. Associated pressures for MM3-4 V8 at low and high rate were 0.15–0.79 bar and 2.53-3.03 bar. Permeability calculations using high rate show higher average permeability values compared to low rate. Respectively, 0.313 mD for high rate versus 0.214 mD for low rate (MM3-4 V8) and 0.374 mD for high rate versus 0.242 mD for low rate (MM5-6 V8). These differences in permeability values reflect that calculated permeability increase with injected rate, as listed in Table 6. Gas permeability of MM3-5 V8 increased a third from lowest to highest injection rate (20 ml/h=0.211 mD, 600ml/h=0.313 mD). The lower permeability values during low injection rate with following low mean pressure through the core, results the mutual collision of gas molecules to be reduced and causing minimum fractional interaction between the gas molecules and the pore wall. This phenomenon is the Klinkenberg Effect. The impact of injection rate on gas permeability is that the Klinkenberg effect becomes more noticeable with decreased injection rate and causes a lower permeability value.

5.3.2 Comparison of brine, gas and oil permeability

To compare permeability measurements for different fluids, oil permeability tests were conducted in addition to gas permeability tests for core plug MM5-6 H4 and MM3-4 V8 and MM3-4 H9. The different fluids were used to study the size of the Klinkenberg effect on gas compared to other fluids on LRQC. Different injection rates and associated pressures are listed in Table 6. Oil permeability (K_o=0.039mD–0.063mD) proved to be 4-5 times lower compared to gas permeability (K_g=0.214mD-0.242mD) calculated with low rates for the two core plugs MM3-4 V8 and MM5-6 H4. Comparing average gas and brine permeability values for all core plugs in Figure 21, gas values are proved to be 13 times higher than brine.

(Li et al., 2009) said high gas permeability compared to liquid was caused due to higher oil and water viscosity, than gas viscosity. The gas slippage phenomenon together with the non-zero velocity layer near the solid wall during gas flow, results in an easier gas flow during injections. This result in an easier flow and higher permeability compared to water and oil. According to (Dong et al., 2012); “For porous materials with low permeability but higher than 1 mD, the Klinkenberg permeability is the same as the liquid permeability. However, for porous materials with permeability lower than 0.1 mD, the Klinkenberg permeability was found to be much higher than the measured liquid permeability”. The permeability values in this thesis matches the theory of (Tanikawa and Shimamoto, 2006), which discovered that gas permeability was ten times larger than water permeability and that the gas and water permeability increase with increasing differential pressure.

Table 6 – Gas permeability values for low and high gas injection rate through core plug MM5-6 H4 and MM3-4 V8 and oil permeability values for MM5-6 H4, MM3-4 V8 and MM3-4 H9. Recordings show differential pressure proportionally increasing with injection rate and calculated higher permeability values for high pressures versus low pressures. In addition, calculations show lower permeability values for when MM5-6 H4, MM3-4 V8 and MM3-4 H9 are measured with oil compared to gas.

Core ID	Injected fluid		Injection rate [ml/h]	Differential pressure [bar]	Permeability [mD]	Permeability (average) [mD]
MM3-4 H9	Oil		10	4.55	0.144	0.087
			14	13.2	0.069	
			17	23.3	0.048	
MM3-4 V8	Oil		5	8.66	0.038	0.039
			10	16.3	0.040	
			15	25.4	0.039	
			20	34.4	0.038	
	Gas	Low rate	20	0.15	0.211	0.214
			40	0.33	0.164	
			60	0.49	0.155	
			80	0.64	0.206	
			100	0.79	0.332	
		High rate	500	2.53	0.314	0.313
			550	2.80	0.311	
			600	3.03	0.313	
MM5-6 H4	Oil		12	12.4	0.063	0.063
			15	15.7	0.062	
			18	18.7	0.063	
	Gas	Low rate	20	0.13	0.245	0.242
			50	0.32	0.239	
			80	0.51	0.241	
			100	0.63	0.242	
		High rate	300	1.22	0.374	0.374
			350	1.43	0.375	
			400	1.63	0.374	

5.4 Rock structure using Computed Tomography (CT)

An X-ray Computed Tomography (CT) scan was performed on all core plugs at Haukeland University Hospital before saturation and further experimental work. The CT imaging was performed by Associate Professor Martin Fernø from the Department of Physics and Technology, UoB. The CT scan was performed to capture several 2D images of each core plug, which were helpful to identify fractures where fluid flow was likely to occur. Figure 22-27 illustrate CT images of each zone represented by one core plug. The image to the left is closest to inlet and the image to the right is closest to outlet. Heterogeneities like fractures, structures with good lamination and low density areas are known as promotors to increase permeability and fluid flow within porous media. None of the zones visualizes a clear lamination, which reflects the low average permeability value in the LRQC core plugs. The higher permeability zones are justified by either having fractures or lower density areas. The images featured are chosen for best representation the core plug as a whole and the distance between the images are dependent on the total length of the core plug. The CT images show distinct differences in the typology of the core plugs and reflect the variation in porosity and permeability measured. Each image needed to be edited and adjusted in ImageJ (a Java based image processing and analysing software) to improve the visualization of the structures. Density values of each core plug was also measured by the CT scan, illustrated in Figure 28 with density difference through and between zones.

Variations in density were illustrated by dark or light areas. Darker colour means less dense while lighter colour means more dense. However, this argument is not valid at the edge of all core plugs in all images, due to the Beam Hardening effect that causes the edge of each core plug to be lighter, which is not usually true for the real density value. X-ray beams are composed of individual protons with a range of energy. Lower energy photons within the proton get absorbed easier than higher energy photons, causing the proton energy to increase when passing through an object. The protons become “harder” and falsely indicate that the edge of each core plug has a higher density than the middle.

MM5-6 is the youngest zone and is represented by core plug V3 (φ=22.2%, K=0.022mD) in Figure 22. Zone MM5-6 shows heterogeneities by fractures in image 22a and 22b, and an area of less density, possible free pore space in image 22c. These observations reflect that the zone had the second highest permeability and could indicate higher flow capacity through the core plug. According to density values in Figure 28, MM5-6 V3 decrease in density from inlet to outlet, confirmed by the images becoming darker towards the outlet and the possible free pore space.

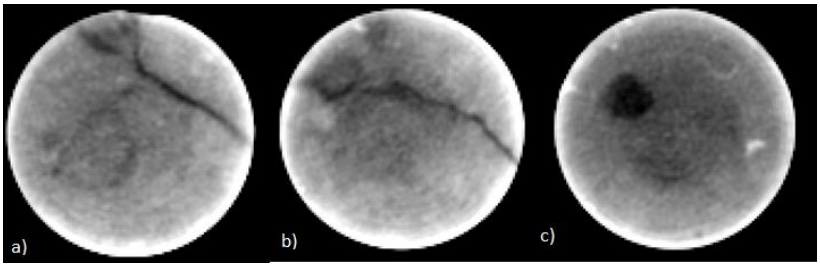

Figure 22 – CT images of core plug MM5-6 V3. The images are taken a) 0.7 cm, b) 1.9 cm and c) 3.7 cm from core inlet (total core length was 5.3 cm). Fractures as visible in image a) and b) and a possible pore space in image c). This indicates higher possible fluid flow. The darker area within the core represent areas of less density, while the whiter parts represent tighter areas with higher density .

CT images of zone MM4-5, represented by core plug V2 (φ=24.6%, K=0.049mD) are shown in Figure 23. The images show no clear fractures, larger pore volumes or lamination through the core plug. Zone MM4-5 had the highest average permeability and porosity values of all zones, but this was not reflected clearly by the images. However, the images show an average darker colour than the other zones, which indicate lower density. The CT scan measured zone MM4-5 to have the lowest average density value of all zones, which then confirms the darker colours in the images and might explain the higher porosity and permeability.

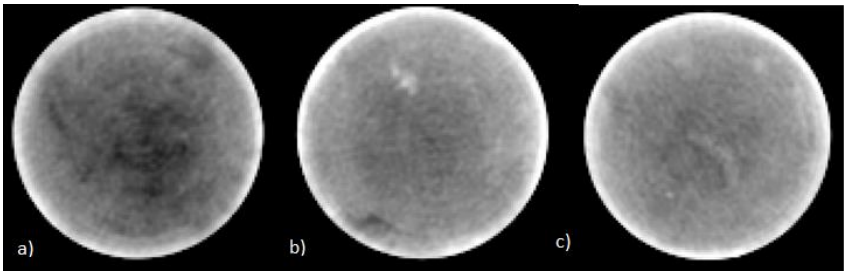

Figure 23 – CT images of core plug MM4-5 V2. The images are taken a) 0.3 cm, b) 2.4 cm and c) 3.6 cm from core inlet (total core length was 4.4 cm). The images show no specific fractures or pore space. However, the images are darker which indicate lower density, possible more pore space and reflects the higher porosity and permeability.

CT images of zone MM3-4, represented with core plug V7 (φ=18.9%, K=0.016mD), are shown in Figure 24. The small lighter patches visible indicate higher density areas and might cause a lower fluid flow potential through the core plug. However, the core plug also has some patches of higher density, which might reflect this zone average porosity and permeability compared to the other zones. The density value measured by the CT scan in Figure 28, indicate a quite homogenous density through the whole core plug, as reflected by the images.

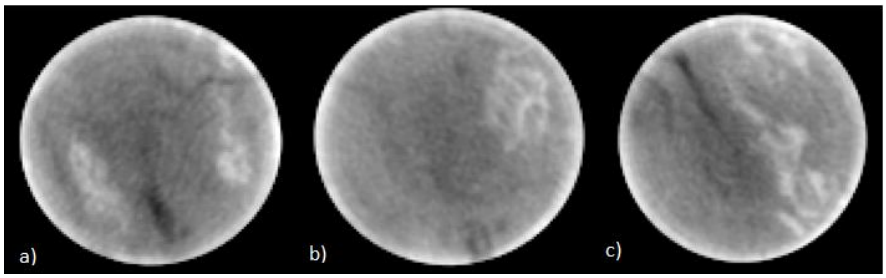

Figure 24 – CT images of core plug MM3-4 V7. The images are taken a) 0.6 cm, b) 2.4 cm and c) 5.2 cm from core inlet (total core length was 6.4 cm). The lighter patches reflect higher density area and might be reducing possible fluid flow through the core plug. Dark spots within the core represent areas of less density, where fluid flow easier can go through.

CT images of zone BED5 are represented by core plug H10B (φ=14.2%, K=0.002mD) in Figure 25. BED 5 has the absolutely lowest porosity and permeability values of all the zones, which are reflected by the images. The images show many small light patches meaning areas of high density, possible lower fluid flow capacity and therefore low permeability. The images are overall light and indicate an average of high density through the core plug. The higher density reflects less pore space and therefore lower porosity in the core plug. The density measurement by the CT scan in Figure 28 defines BED5 to have the highest overall density of all the zones.

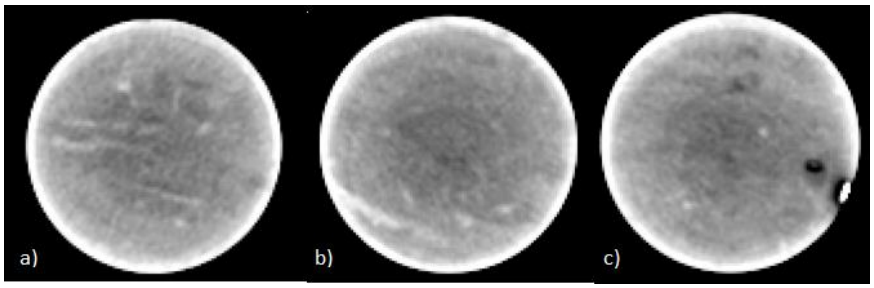

Figure 25 – CT images of core plug BED 5 H10B. The images are taken a) 0.8 cm, b) 1.84 cm and c) 3.2 cm from core inlet (total core length was 3.8 cm). The light patches are areas of higher density and where fluid troubles to flow through. Overall the images are lighter, which indicate a high average density within the core plug.

CT images of BED 3 are represented by core plug V14 (φ=18.8%, K=0.008mD) in Figure 26. The images show darker areas in the middle through the core plug that reflects less denser area. Overall, the images show no visible fractures or larger pore spaces to ensure good fluid flow through the zone. The lightness in the images indicate high average density and these observations reflect that this zone has the second lowest porosity and permeability values compared to the other zones. The density measurement by the CT scan confirms the overall light areas and defines BED3 to have the second highest average density.

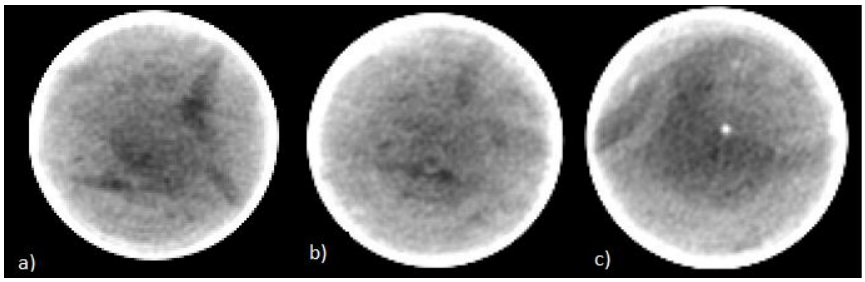

Figure 26 – CT images of core plug BED 3 V14. The images are taken a) 1.2 cm, b) 3.13 cm and c) 5.8 cm from core inlet (total core length was 7.2 cm). The images show no clear light patches of very high density areas that could block fluid flow, but either not fractures or bigger pore spaces to increase fluid flow. The images show average high density, which reflect the low porosity and permeability of the zone.

The ZIGZAG zone is represented by core plug V11B (φ=21.7%, K=0.184mD (K_{air})) in Figure 27. The core plug showed no clear visible fractures or free pore space. In the last image (27c) a lighter area becomes visible which indicate a higher density area where fluid might flow might been blocked. The density measured by the CT scan showed in Figure 28, indicate ZIGZAG V11B to have the next lowest overall density of all zones, and reflect the images of being generally darker than some of the other zones. The lower average density through the zone can then reflect why ZIGZAG had the second highest measured porosity of all zones.

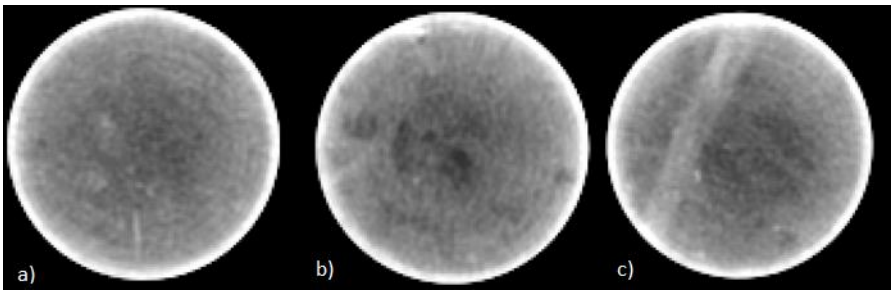

Figure 27 – CT images of core plug ZIGZAG V11B. The images are taken a) 1.6 cm, b) 3.5 cm and c) 4.6 cm from core inlet (total core length was 6.3 cm). The dark areas reflect less density, while the lighter parts represent tighter areas with higher density. The core plug does not show any heterogeneities, however there is a defuse area in image c expressed by higher density.

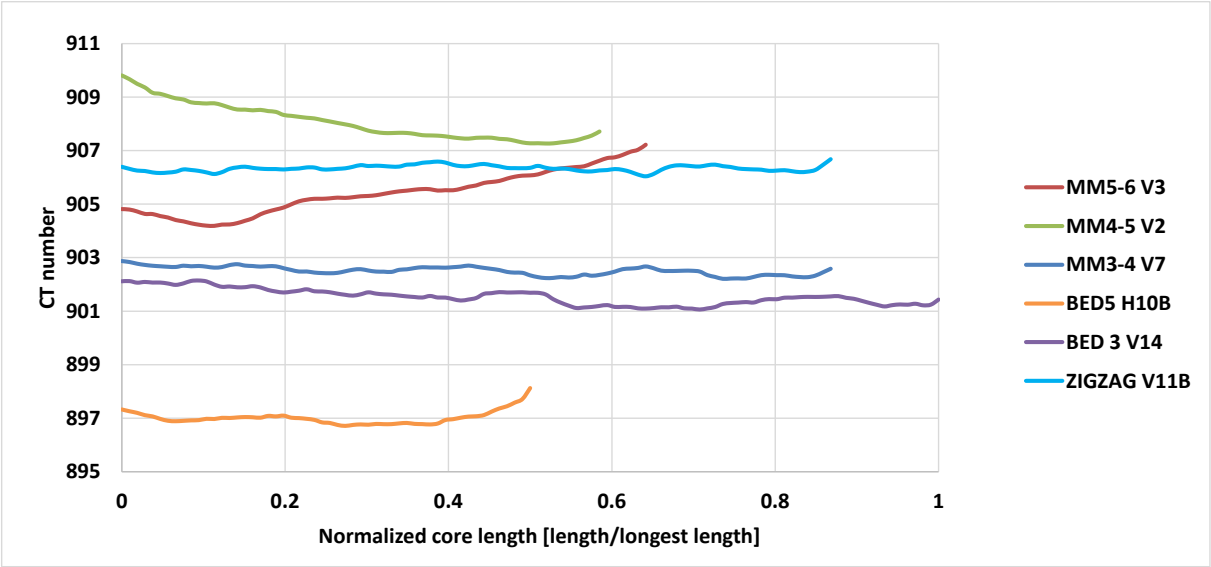

Figure 28 – Density measured by the CT scan. The CT number expresses density through the core shown as a function of normalized length [length/ longest length]. CT numbers are shown in absolute value and lower CT number equals higher density. CT numbers were originally negative because the air around the core plugs was not removed when the density values were collected (black space surrounding the core plugs in Figure 22-27). The air was not removed due to difficulties in precise image cutting around the core plug. The argument for approval of including air is that all the images have the same average of pixels and are the same size. In addition, all core plugs have the same diameter meaning the amount of air is equal in all images. Inlet of each core plug is where the normalized core length equals 0 and outlet is the value closest to 1. Core plug BED 5 H10B shows the highest density values, while MM4-5 V2 shows the lowest density values.

5.5 Porosity and permeability of LRQC compared to other porous material

Porosity and permeability for LRQC were lower than Portland Røldal Chalk, Edward Limestone and Bentheimer Sandstone, see Figure 29. LRQC core plugs measured with gas have relatively similar porosity values to Edward Limestone and Bentheimer Sandstone. The LRQC core plugs measured with brine, especially BED3 show in average lower porosity than the other porous materials. Comparison of permeability values show larger differences between the reservoir rock types (notice the logarithmical scale). Here, the values for LRQC is definitely lowest compared to the other rock types. The average permeability for LRQC is a 1000 times lower than the average value for Bentheimer Sandstone, 20-30 times lower than the Edward limestone and 4 times lower than Portland Røldal Chalk. The results in this thesis prove LRQC to be less favourable as a reservoir rock, which is not surprising according to its name, "Low Reservoir Quality Chalk". The more undesired reservoir properties of LRQC indicate lower fluid flow potential and bigger difficulties during hydrocarbon production. Evaluating porosity and permeability compared to the other reservoir rocks, LRQC would probably have lower oil storage capacity due to lower fluid flow potential and not reach as low residual oil saturation as the other reservoir rocks.

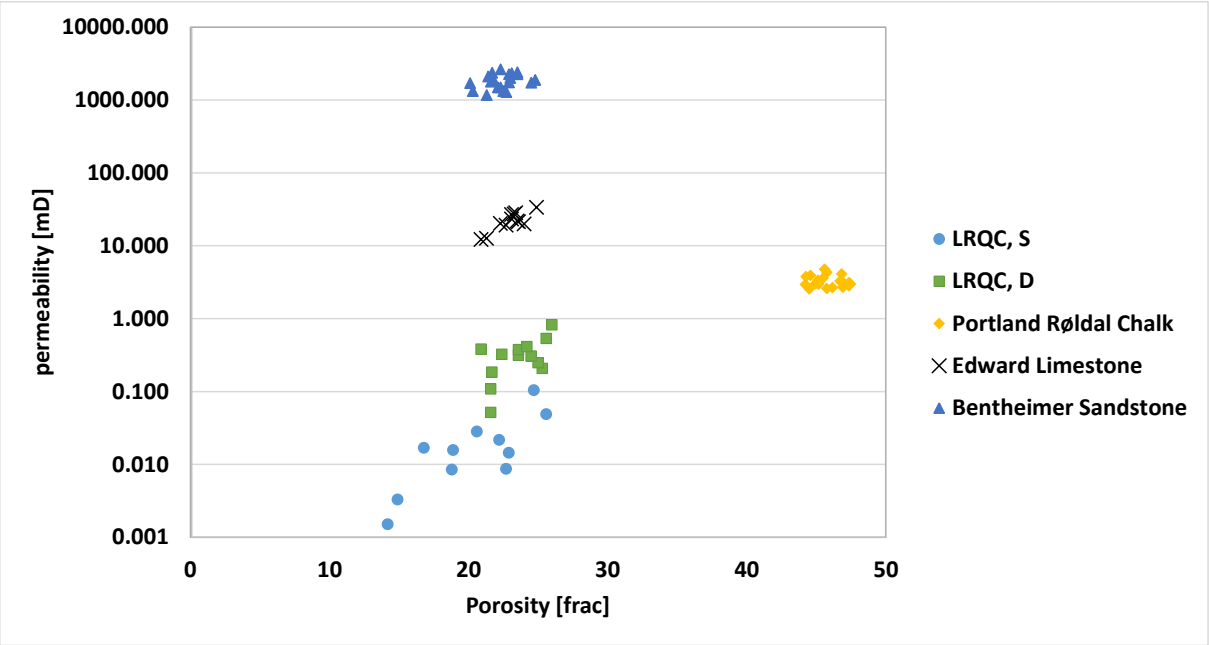

LRQC, S: Low Reservoir Quality Chalk, saturated core plugs – measured with brine
LRQC, D: Low Reservoir Quality Chalk, dry core plugs – measured with gas

Figure 29 – Porosity and permeability values for LRQC (both saturated and dry), Portland Røldal Chalk (Haugen, 2012), Edward Limestone, (Tunli, 2014) and Bentheimer Sandstone (Heldal, 2016). Bentheimer sandstone has the highest permeability values and Portland Røldal Chalk has the highest porosity values. Compared to the other rocks, LRQC has the lowest average permeability and porosity.

6 Flow and storage potential and characterization of LRQC

As a part A, evaluating the reservoir properties and characteristics for LRQC, flow and storage potential tests were conducted by injecting oil into three 100% water saturated core until initial water saturation, S_{wi}. Core plugs from different zones were used for comparison. Geometrical parameters, porosity and permeability for each core plug used, are listed in Table 7.

Table 7 – Geometrical parameters, porosity and permeability values for core plugs used in these oilflooding tests.

Core ID	Diameter [cm]	Length [cm]	Pore Volume [ml]	Porosity (φ) [frac]	Permeability (K) [mD]
MM5-6 H5	4.97	7.90	31.5	0.21	0.028
MM4-5 H1	4.96	4.71	22.5	0.25	0.104
ZIGZAG H13	4.96	6.39	28.2	0.23	0.014

6.1 Oil Storage Capacity

Primary oil drainage was conducted on three initially 100% water saturation core plugs from zone MM5-6, MM4-5 and ZIGZAG using the setup in Figure 16 in Section 4.4.1.

MM5-6 H5

Primary oil drainage of initially 100% water saturated MM5-6 H5 resulted in oil breakthrough after 0.61 PV-injected. Oil breakthrough is illustrated in Figure 30 as where the water recovery curve (blue diamonds) change from a diagonal straight line towards a more horizontal line. After oil breakthrough the water production curve drops significantly. At oil breakthrough, 17±0.2ml water was produced (S_w=0.46) and an additionally 2.5±0.1ml of water was recovered before production end. The Quizix pump stopped in 20 minutes after 0.25 PV injected due to an exceed of the safety pressure at 35 bar. Zero oil was then injected, causing zero water production. This event is illustrated in Figure 30 by a decreased jump in the pressure curve (grey line). A lower constant rate of 2.5ml/h was used the rest of the test and a total of 0.9 pore volumes was injected over 10 hours. Total water recovery ends at 61.9% after primary drainage which gives an initial water saturation of S_{wi}=0.38.

The pressure continued to increase after the Quizix pump was restarted (due to exceeding the safety pressure), and reached peak, 31 bar after 4.9 PV-injected. The pressure started to decrease after 0.61 PV injected because of oil breakthrough. The pressure curve continued to decrease through the rest of the drainage process, due to the non-wetting fluid's location in the middle of each pore and pore channel. The non-wetting fluid therefore need less pressure to flow after breakthrough.

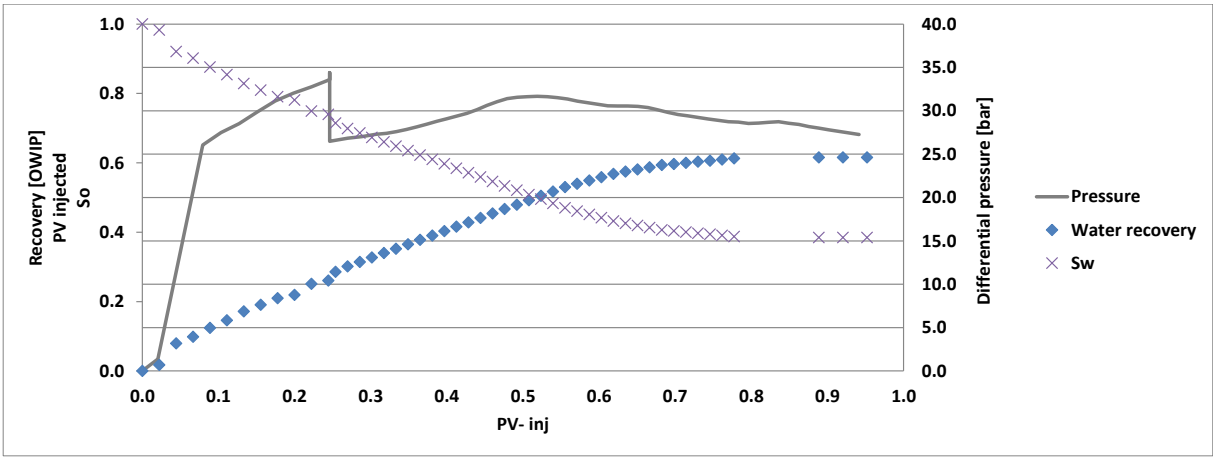

Figure 30 – Core plug MM5-6 H5, primary oil drainage: recovery of Originally Water In Place (OWIP) (blue diamonds), water saturation (purple crosses) and differential pressure (grey line) versus PV-injected. Breakthrough happened after 0.61 PV-injected, illustrated where the water recovery curve change from a diagonal straight line towards a more horizontal line. Pressure decrease after oil breakthrough. The decreased jump in the pressure curve at 0.25 PV injected was caused by a pressure exceed of 35 bar that caused the Quizix pump to stop for 20 minutes.

MM4-5 H1

MM4-5 H1 was that core plug with highest porosity and permeability. Due to permeability and porosity being high, the relative permeability to oil might be assumed higher and causing fluids to be injected at a higher rate. 34 pore volumes were injected during 46 hours and oil breakthrough happened after 0.41 PV-injected, see Figure 31. The oil breakthrough is illustrated where the water production curve breaks from a vertically line to a more horizontal line. After breakthrough, the constant oil injection rate continues the same, while water production curve drops significantly. At breakthrough, 8.4±0.1ml water was produced (S_w=0.64) and additional 6.7±0.1ml of water was produced until injection end. Total water recovery ends at 67.1% after primary drainage and results in an initial water saturation of S_{wi}=0.33. Pressure increased and hits its peak at 28 bar at 0.5 PV-injected. After oil breakthrough the pressure decrease, see grey line in Figure 31. Core plug was assumed water-wet and pressure decreased evenly after breakthrough due to the non-wetting fluid's location in the middle of each pore and pore channel. Oil therefore need less pressure to displace the water. The pressure has an increased jump after 17.4 PV-injected due to an adjustment of the confinement pressure.

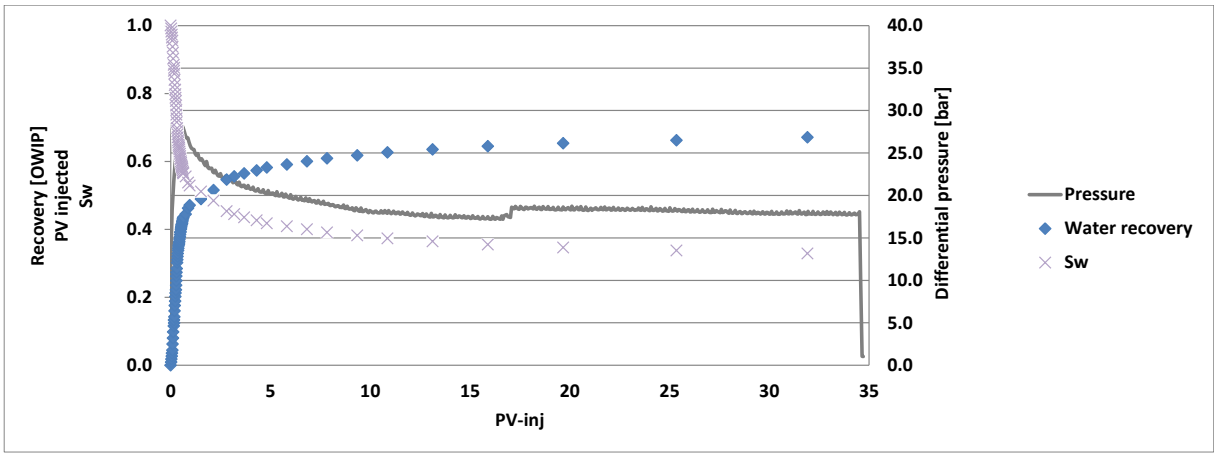

Figure 31 – Core plug MM4-5 H1 during primary oil drainage: recovery of originally water in place (blue diamonds), water saturation (purple crosses) and differential pressure (grey line) versus PV-injected. Breakthrough happened after 0.41 PV-injected, illustrated where the water production curve breaks from a vertically line to a more horizontal line. Pressure decrease through the rest of the drainage process after breakthrough and has an increased jump after 17.4 PV-injected due to an adjustment of confinement pressure.

ZIGZAG H13

During primary drainage of ZIGZAG H13, oil breakthrough happened after 0.37 PV-injected, see Figure 32. Breakthrough is illustrated where the water production line starts to be more horizontal due to a slower production. At breakthrough, 10.3±0.1ml water was produced (S_w=0.64) and an additional 7.8±0.1ml of water was produced until injection end. The water production stopped after 5 days and 9 PV-injected. Total water recovery ended at 64.1% which results in an initial water saturation of S_{wi}=0.36. Due to constant pressure, the injection rate increased after breakthrough. The core plug was assumed water-wet meaning the non-wetting fluid flows in the middle of each pore and pore channel, and the wetting fluid moves along the pore wall. The non-wetting fluid therefore need less pressure to flow after breakthrough.

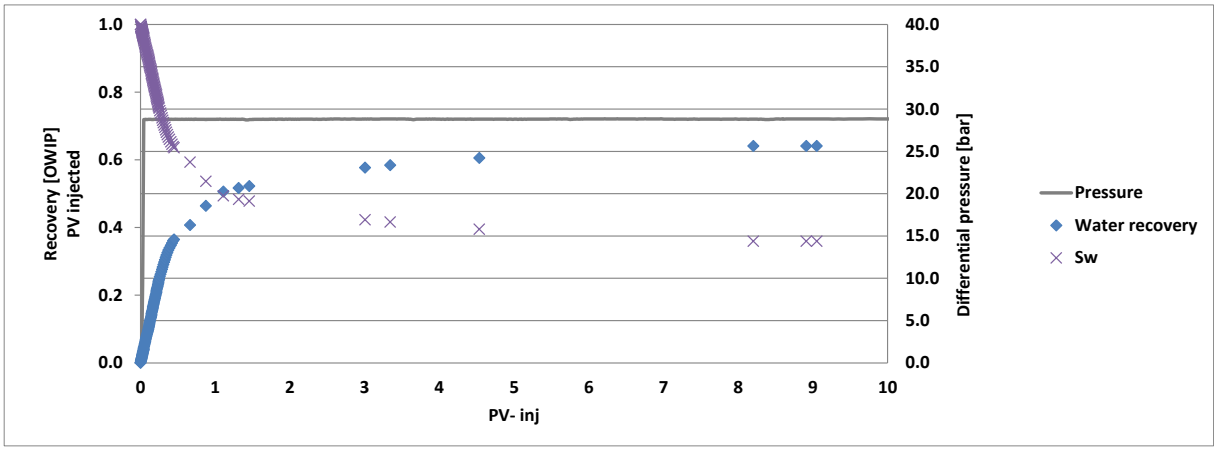

Figure 32 – Core plug ZIGZAG H13: during primary oil drainage: recovery of originally water in place (blue diamonds), water saturation (purple crosses) and differential pressure (grey line) versus PV-injected. Breakthrough happened after 0.37 PV-injected, illustrated where the water production curve starts to be more horizontal. This primary drainage is performed with constant pressure, meaning the injection rate varied.

6.2 Comparison of oil storage capacity for different zones

After primary drainage, S_{wi} was between 32.9%-38.1% for core plug MM5-6 H5, MM4-5 H1 and ZIGZAG H13. During the displacements, oil broke through at 0.37-0.56 PV-inj. for all three zones and the hours until breakthrough varied with many due to difference in injection rate for all core plugs. A short tail production after breakthrough is the optimum during production for less need of injection fluid and possible time saving. Tail production after oil breakthrough had some big variations in pore volume injected from total 0.94 PV-inj. to 34.7 PV-inj. Core plug MM5-6 H5 had the largest total pore volume and longest core length. However, the displacement happened most rapidly in MM5-6 H5, which is interesting due to its porosity being the lowest, and permeability not being the highest of the three samples.

Table 8 lists different recorded and calculated values during the primary drainage displacement. To determine a possible reason for the different oil storage capacities, different parameters were evaluated. A relationship between pore volume injected at breakthrough and time of breakthrough is proven to be inverse and later breakthrough in time gives less pore volume injected at breakthrough. However, there is no relationship between times of breakthrough, pore volume injected and oil storage capacity, according to Table 8. Endpoint relative permeability to oil was calculated using Equation 5, 6 and 7 and the values show a weak relationship between initial water saturation and relative permeability. The result listed in Table 8 show that MM4-5 H1 had the highest oil relative permeability, which is probably caused by the high injection rate that gave a high effective permeability and again a good ratio between the effective and absolute permeability for the core plug. This high relative permeability probably caused MM4-5 H1 to reach the lowest water saturation of the three core plugs. Oil displaced the water in MM5-6 H5 quickly, but the effective permeability proved to be low and gave a lower ratio between the effective and absolute permeability, known as relative permeability. This low relative permeability to oil probably gave the core plug a lower recovery factor which resulted in higher initial water saturation.

Table 8 – Summary of oil storage capacity after primary drainage. Porosity and permeability value from earlier measurements, initial water saturation after primary drainage, number of pore volumes injected at breakthrough and total pore volumes injected before production end.

Core ID	Total PV-inj.	Swi [% frac]	Breakthrough [PV-inj.]	Breakthrough time [hours]	Total time [hours]	Krel, oil
MM5-6 H5	0.94	38.1	0.56	0.6	9.3	0.326
MM4-5 H1	34.7	32.9	0.41	5.6	41	0.564
ZIGZAG H13	9.05	35.9	0.37	6.1	122	0.546

Figure 33 illustrate the relationship between porosity, permeability and PV- injected at breakthrough. The Figure (33) show no relationship between the three properties since MM4-5 H1 has the highest permeability and porosity value and neither have the less or most pore volumes injected at oil breakthrough.

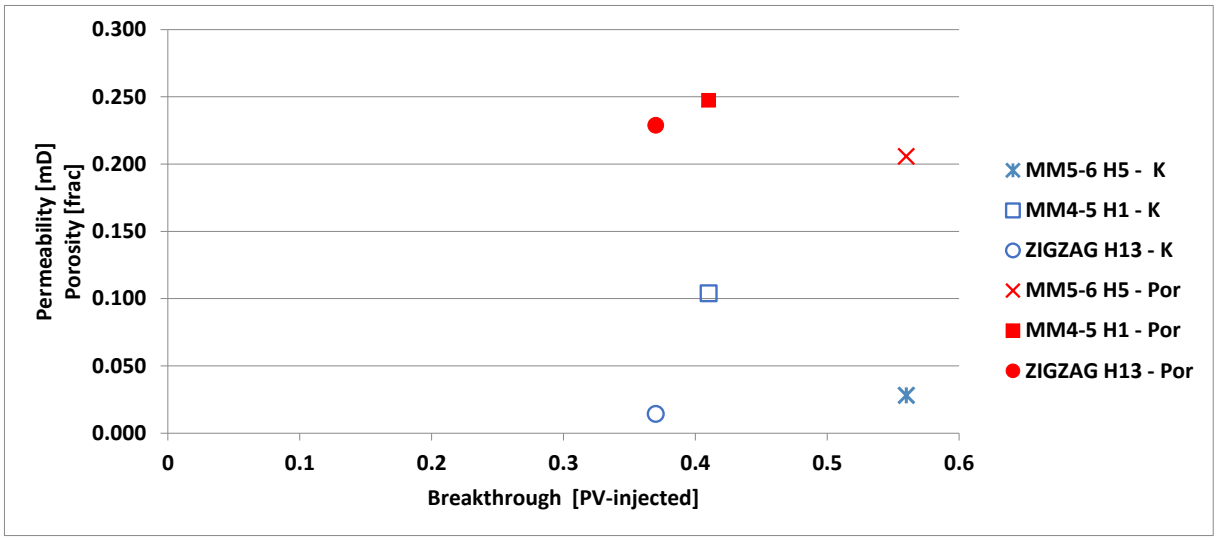

K: Permeability
Por: Porosity

Figure 33 – Permeability (blue) and porosity (red) versus time of breakthrough for different zones. This figure prove that there is no clear relationship between porosity/ permeability and time of breakthrough, due to the oil displacement in the zone with the highest porosity/permeability value either broke through at the earliest of latest.

Since there are no clear relationship between porosity, permeability and pore volume injected at breakthrough, the zones were evaluated through CT images. The differences in total pore volume injected and length of tail production might indicate heterogeneities in the measured zones. Heterogeneities in case of microfractures are observed on the surface of the core plugs, but how do these fractures develop on the inside of the core plugs? X-ray Computed Tomography (CT) performed when the core plugs were dry, gave cross-sectional images of the core sample and showed fractions inside the core plugs that were not visible from the outside. CT images of core plug MM5-6 H5, MM4-5 H1 and ZIGZAG H13 are shown in Figure 34, 35 and 36 and show big differences in heterogeneities between the core plugs. The image to the left is closest to inlet, whereas the image to the right is closest to outlet.

Images of MM5-6 H5 (Figure 34) visualizes a black spot through the core plug. This illustrates an area of a less density and possible free pore space. The low density area became visible after 2.3 cm into the core from inlet and continued through the core until approximately 1.1 cm from the outlet. This pore space might be the reason why the oil got its breakthrough after a short amount of time and why total PV-injected was less than one. If this pore space was filled with water and the oil used it as a main path to displace the water, then the recovery factor in this area would be high due to low capillary pressure and less water attached to the pore wall. The short tail production is also explained by this pore space.

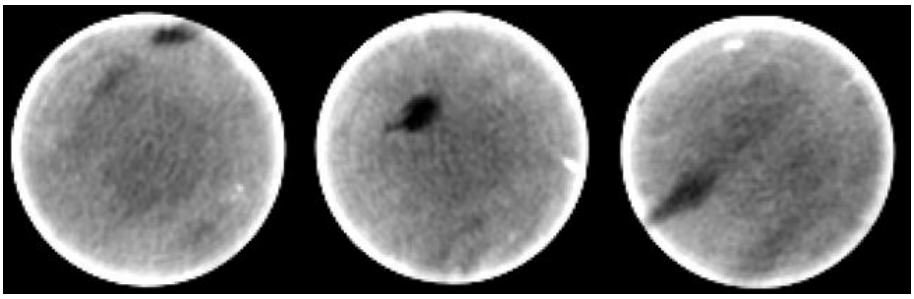

Figure 34 – CT images of core plug MM5-6 H5. The images are taken a) 2.4 cm, b) 4.8 cm and c) 6.2 cm from core inlet (total core length was 7.9 cm). The black spot visible is illustrates an area of less density and is probably a free pore space, which caused the short tail production and short displacement time. The black spot is continuous between 2.3 cm from the inlet to approximately 1.1 cm from the outlet of the core plug.

CT images of MM4-5 H1 are showed in Figure 35. Fractures seem to be visible through the core plug from start till end and obviously the results from the primary drainage were affected by these. In addition, much dark area is visible in the first and last image and this together with big fractures explains the high porosity value for this zone. The fractures explain the high possible injection rate through the core plug and the long tail production might be due to several micro fractures as well.

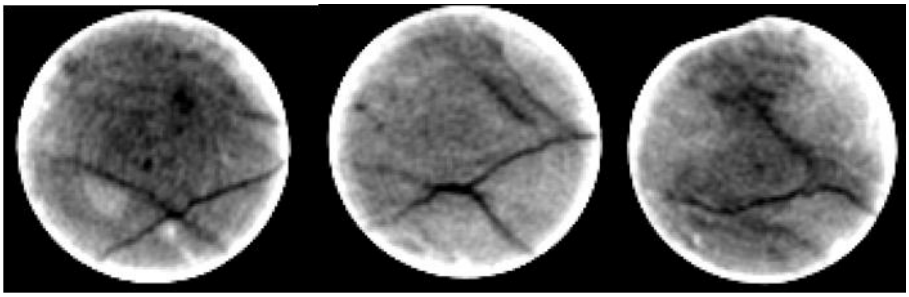

Figure 35 – CT images of core plug MM4-5 H1. The images are taken a) 0.2 cm, b) 1.8 cm and c) 2.9 cm from core inlet (total core length was 4.7 cm). The images show many larger fractures and show big heterogeneity within the core plug. Image a and c are darker as well, which indicate less density in this area. The many fractures explain the long tail production and that many pore volumes needed to be injected before reaching S_{wi}. The long tail production of this core plug might also indicate many micro fractures as well, not visible through these images.

CT images of ZIGZAG H13 are shown in Figure 36. The images do not show any clear fractures or larger pore spaces and the core plug looks homogenous from inlet to outlet. Some small white "dots" are visible which are proved to be very dense. These high dense spots might have blocked the oil path during the displacement, and caused the high pressure and low possible injection rate during the primary oil displacement.

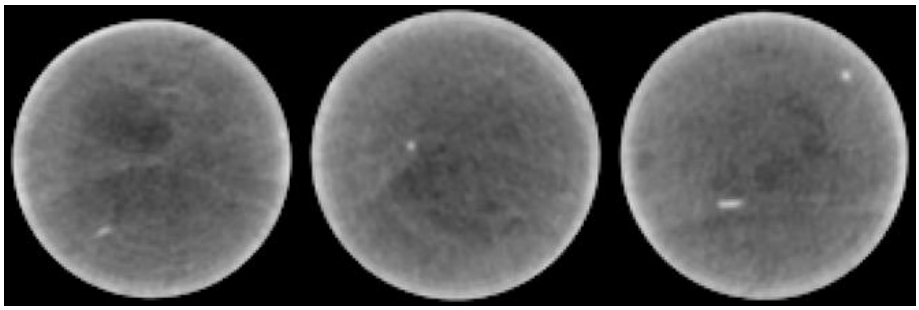

Figure 36 – CT images of core plug ZIGZAG H13. The images are taken a) 0.5 cm, b) 2.7 cm and c) 4.1 cm from core inlet (total core length was 6.4 cm). The images do not show any clear fractures or larger pore spaces and the core plug looks homogenous from inlet to outlet. Some small white "dots" are visible which are proved to be very dense and might block fluid flow, causing the low injection rate and high pressure.

The CT images can indicate density changes through the core plug. Fractures and pore space can decrease the density in a specific area and are illustrated by a darker colour in Figure 34-36. How these density values changes through the core plug is recorded by the CT scanner. The CT numbers that indicate the density values through core plug MM5-6 H5, MM4-5 H1 and ZIGZAG H13 are plotted in Figure 37. MM5-6 H5 shows the overall highest density values. The CT images of this core plug (Figure 34) were light except a visible possible free pore space, and therefore reflect that MM5-6 H5 has the lowest overall density. MM4-5 H1 show less dense values, probably due to its many fractures and overall dark area through the core plug. The CT numbers for MM4-5 H1 increase rapidly at the end due to the core plug not being totally circular at the outlet (measuring more air), (illustrated in Figure 35c).

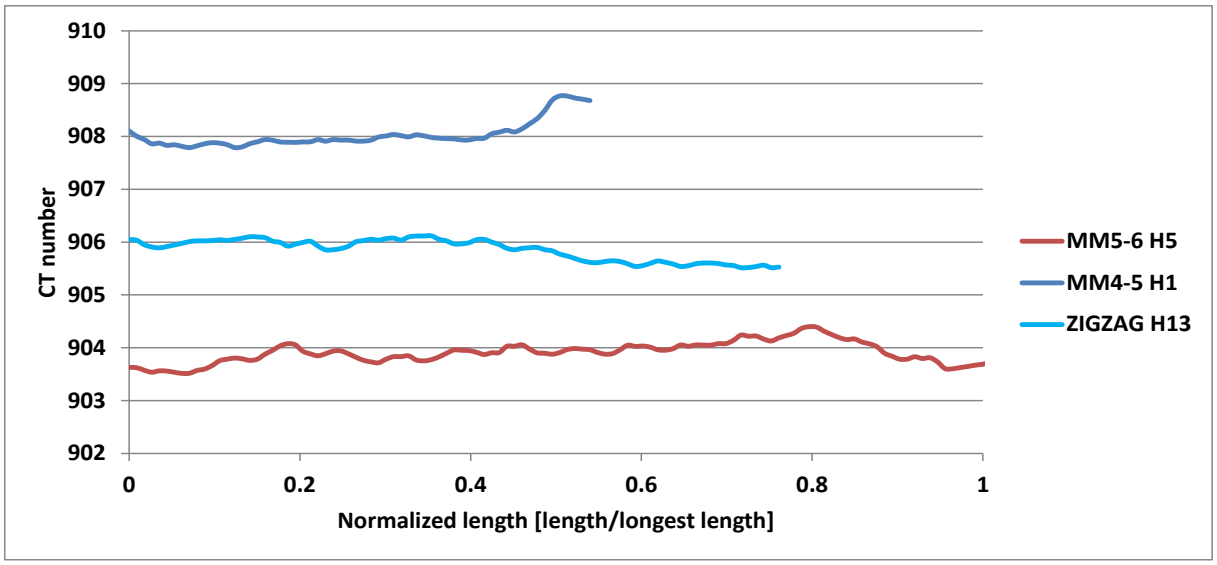

Figure 37 – Density measured by CT scan for core plug MM5-6 H5, MM4-5 H1 and ZIGZAG H13. The CT number expressing density through the core is shown as a function of normalized length [length/ longest length]. CT numbers are shown in absolute value and lower CT number equals higher density. CT numbers were originally negative because the air around the core plugs was not removed when the density values were collected. The air was not removed due to difficulties in precise image cutting around the core plug. The argument for approval of including air is that all the images have the same average of pixels and are the same size. In addition, all core plugs have the same diameter meaning the amount of air is equal in all images. Inlet of each core plug is where the normalized core length equals 0 and outlet is the value closest to 1. Core plug MM5-6 H5 shows the highest density values, while MM4-5 H5 shows the lowest density values.

7 Flow and oil recovery potential for LRQC

As a part A of evaluating the reservoir properties and characteristics for LRQC, oil recovery tests were conducted by injecting and spontaneously imbibing water into initially 100% oil saturated core plugs until reaching residual oil saturation. Core plugs from different zones were used for comparison. In addition was spontaneous water imbibition conducted after primary drainage for core plug MM4-5 H1 and ZIGZAG H13. All core plugs were assumed water-wet and geometrical parameters, porosity and permeability for each core plug used in these flooding and spontaneous imbibition tests, are listed in Table 9.

Table 9 - Geometrical parameters, porosity, permeability and pore volumes for air and oil of core plugs used in recovery tests. Oil permeability was not possible to measure for epoxy coated cores. For geological and core name identification, see Table 1.

Core ID	Diameter [cm]	Length [cm]	Porosity [frac]	Permeability air [mD]	Permeability oil [mD]	Pore volume air [ml]	Pore volume oil [ml]
MM5-6 H4	4.96	5.82	0.24	0.374	0.063	26.6	22.3
MM5-6 H6	4.97	6.38	0.24	0.411		29.9	29.4
MM4-5 V1	4.96	7.12	0.26	0.531		35.2	30.0
MM3-4 H9	4.96	4.80	0.25	0.306	0.087	22.8	16.3
MM3-4 V8	4.97	6.07	0.24	0.313	0.039	27.8	21.0
BED3 V15	4.96	7.79	0.22	0.052		30.0	19.5
ZIGZAG V11B	4.96	6.27	0.22	0.184		25.6	29.2
ZIGZAG H12	4.97	8.23	0.25	0.207		40.4	36.7
ZIGZAG H11	4.97	9.02	0.25	0.248		43.8	40.6

7.1 Recovery mechanisms influence on water imbibition on LRQC

7.1.1 Oil recovery by water flooding of 100% oil saturated core plug

Forced water imbibition was conducted on core plug MM3-4 V8 to test oil recovery potential and evaluate the impact on recovery by forced injection. Brine was injected into the core plug with variable rate and constant pressure ensured by a Quizix pump. The amount of oil produced was the same amount of water injected until breakthrough at 0.44 PV-injected. The core plug had zero oil production after breakthrough illustrated by a clean cut in the oil recovery curve (yellow diamonds) in Figure 38. Total production time was 48 hours and total recovery was 41.4% of Originally Oil In Place (OOIP) after 0.55 PV-inj. Residual oil saturation was S_{or}=0.58 after production end. The calculated endpoint relative permeability to water, K_{rw} was 0.017. Constant pressure was used after 0.03 pore volumes injected to not exceed the maximum pressure of the ESI-pressure transducer of 40 bar and the Hassler core holder overburden pressure at max 40 bar. The variable injection rate after 0.03 PV inj. sinks during the first 0.15 PV inj. and then varies between 0.0-0.3 ml/h the rest of the displacement. The water breakthrough does not show any impact on injection rate, which does not increase after breakthrough. The core plug being water-wet is an argument for this continuous low injection rate through the whole displacement. The clean water breakthrough might indicate one big heterogeneity either as fraction or larger pore space. If so, then the high residual oil

saturation (S_{or}=0.58) might be explained by many larger pores, lower capillary pressure, water flow by the pore wall and possible snap-off.

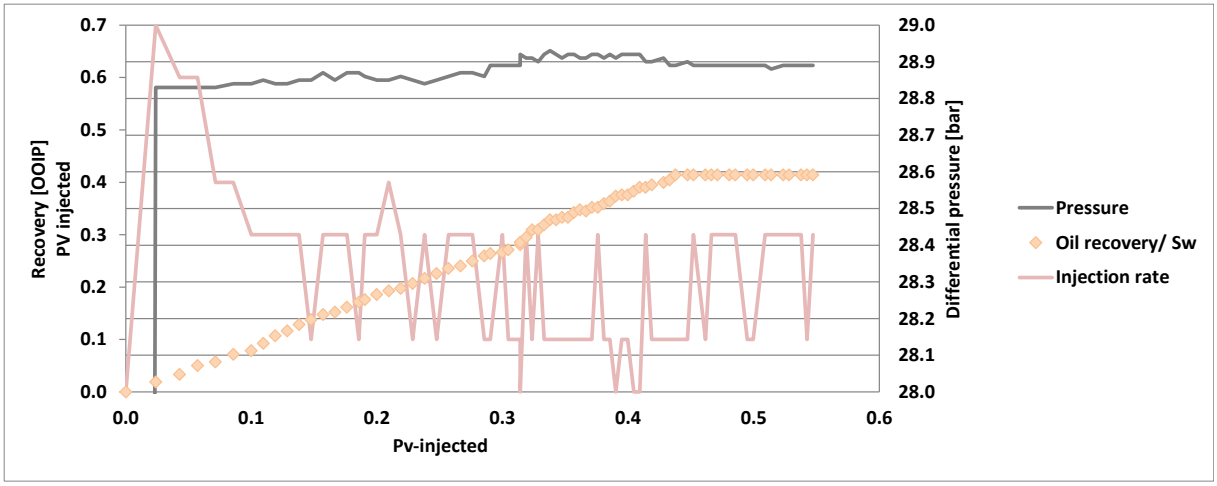

Figure 38 - Forced water imbibition into 100% oil saturated MM3-4 V8 core plug. Figure show oil recovery, brine injection rate and pressure versus PV-Injected. The water saturation value at each PV-injected is the same as oil recovery and a function of Oil Originally In Place (OOIP). Water breakthrough happens after 0.44 PV-injected and 37 hours. Oil production after breakthrough is zero and total recovery ends at 41.4% OOIP.

7.1.2 Oil recovery by spontaneous imbibition of 100% oil saturated core plugs

AFO boundary conditions during spontaneous imbibition

All-Faces Open (AFO) spontaneous imbibition was performed on core plug MM5-6 H4 and MM3-4 H9 to evaluate on recovery by AFO spontaneous imbibition. The two core plugs were 100% oil saturated before placed in each their imbibition cell filled with Ekofisk brine. Water spontaneous imbibed immediately with a rapid oil production at the beginning. Figure 39 show how oil recovery and water saturation increase related to square root of time for the two core plugs during the displacements (blue triangles and red diamonds curves). The core plugs were placed vertically in the imbibition cell, and oil production became first visible at the horizontal top, and then quickly became visible all over the core.

(Austad and Milter, 1997) conducted spontaneous imbibition using AFO on low permeable (2-3 mD) chalk core plugs with both high and low interfacial tension. Without surfactants, oil was observed to take place all over the surface of the core. Rather large oil droplets (≈ 5 mm in diameter) grown before releasing from the core. The same was observed in this work, although oil droplets were not quantified. Comparing oil production, (Austad and Milter, 1997) had a much faster displacement process, which ended after 20 minutes, and the oil production was twice as high as the one on this thesis. The interfacial tension is not known during the experiments on LRQC, and its therefore difficult to draw conclusions regarding the interfacial tensions impact on the low oil production during the tests on LRQC. However, lower production and longer production time in this thesis compared to (Austad and Milter, 1997) is probably caused due to rock properties as lower porosity, permeability and higher density.

Oil recovery happened most rapidly the first 4-5 hours for both core plugs, see blue triangles and red diamonds curves in Figure 39. MM5-6 H5 produces more than MM3-4 H9 the first 6.5 hours and ends at a higher recovery factor. After 4 days, production stops for both core plugs and recovery value ends at 39.0% OOIP for MM5-6 H4 and 33.8% OOIP for MM3-4 H9.

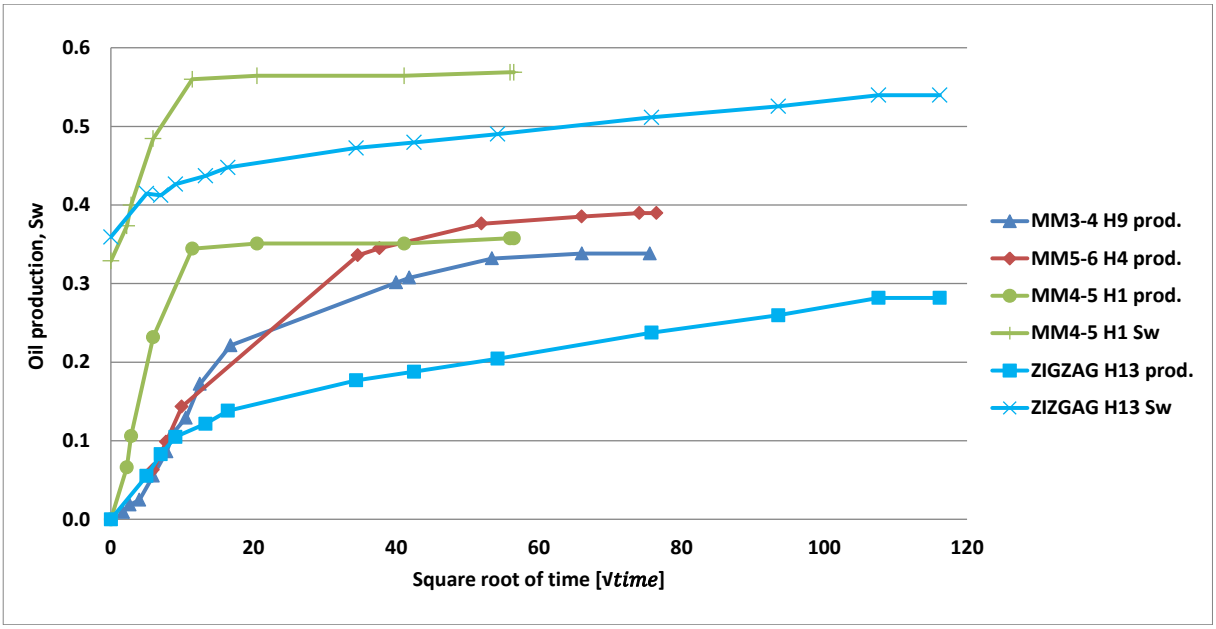

Figure 39 – Oil recovery curve for MM5-6 H4 (red diamonds) and MM3-4 H9 (orange circles) during AFO spontaneous imbibition of initially 100% oil saturated core plugs and oil recovery/water saturation curve for MM4-5 H1 (blue curves) and ZIGZAG H13 (purple curves) during AFO spontaneous imbibition after primary oil drainage. Oil recovery and water saturation are plotted as a function of square root of time for all core plugs. Oil recovery and change in water saturation is equal for MM5-6 H4 and MM3-4 H9. Since MM4-5 H1 and ZIGZAG H13 was initially 100% water saturated and oilflooded during primary drainage, they have a water saturation of S_w=0.32 (MM4-5 H1) and S_w=0.36 (ZIGZAG H13) before spontaneous imbibition start. Recovery factors end at 39.0% OOIP for MM5-6 H4 and 33.8% OOIP for MM3-4 H9 (100% oil saturated). Production during spontaneous imbibition after primary drainage of initially 100% water saturated core plugs was 35.8% OOIP for MM4-5 H1 and 28.2% OOIP for ZIGZAG H13. Note: the lines between the recorded values are just for guidance and are not measured.

Spontaneous imbibition with AFO boundary conditions after primary drainage of initial 100% water saturated core.

Spontaneous imbibition with AFO boundary conditions was performed for core plug MM4-5 H1 and ZIGZAG H13 after primary oil drainage for comparison to spontaneous imbibition on core plugs initially 100% oil saturated. Initial water saturation (S_{wi}) after primary drainage was 32.9 % (MM4-5 V1) and 35.9 % (ZIGZAG H13). The core plugs were placed separately in each imbibition cell filled with Ekofisk brine. Immediately, the water started spontaneously imbibing into the core plugs and oil droplets started to show. Core plug MM4-5 H1 had a visible fracture on the side, where a larger amount of oil was produced from. The changes in oil production and water saturation during the displacements are illustrated in Figure 39. Oil recovery curve for MM4-5 H1 (green circles) show a rapid oil production of 34.4% of oil present in the core after primary within the first 35 minutes. Oil production happens more

slowly in ZIGZAG H13 (turquoise squares) with an oil production of 12.2% of OOIP through a same amount of time. The production ends after 52 hours for MM4-5 H1 with a total oil production of 35.8 % OOIP and after 10 days for ZIGZAG H13 with a total oil production of 28.2 % OOIP.

Compared to the initially 100% oil saturated core plugs, 3.6 % less of OOIP is produced by the initially 100% water saturated core plugs. MM4-5 H1 produces much more rapidly than MM5-6 H4 and MM3-4 H9, which is probably caused by the many fractures and lower density as discussed in Section 6.2 and shown through CT images in Figure 35. The water probably displaced the oil only in the larger fractures, causing the production to end suddenly. ZIGZAG H13 slows down the production earlier than the other core plugs, however, the production lasts twice as long for ZIGZAG H13. The core plug did not show any clear fractures or larger pore spaces in the CT images (Figure 36), and the long tail production during spontaneously imbibition as with primary drainage was probably caused by this.

TEO boundary conditions during spontaneous imbibition (TEOFSI)

As a part B, the TEOFSI method was tested on LRQC core plugs. The results from the total oil recovery values were added in this part of the thesis for comparison of oil recovery methods. *Two-Ends Open* (TEO) spontaneous imbibition was performed on six core plugs; MM5-6 H6, MM4-5 V1, BED3 V15, ZIGZAG V11B, ZIGZAG H11, ZIGZAG H12 All core plugs were epoxy coated as described in Section 4.5.1 and 100% oil saturated as in Section 4.3.1. The core plugs differed in how rapidly the water displaced the oil in the beginning, total oil recovery and total displacement time, illustrated in Figure 40. MM5-6 H5 has the shortest displacement time, and most rapidly production. BED3 V15 had the longest displacement time and the least steep production curve. Total recovery factor vary from 30.4% OOIP to 48.1% OOIP and the recovery factor of each core plug is listed in Table 10. Total displacement time varied from 5-50 days due to a long production time for one core. The average production time was 12 days.

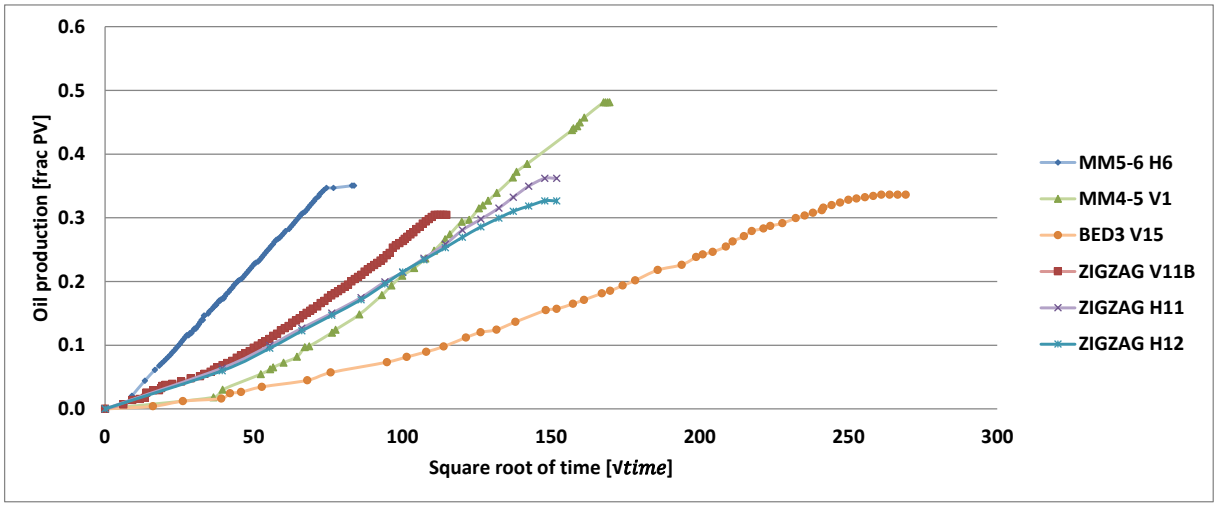

Figure 40 – Oil recovery curve for MM5-6 H6 MM4-5 V1, BED3 V15, ZIGZAG V11B, ZIGZAG H11 and ZIGZAGH12 during spontaneous imbibition with TEO boundary conditions. Oil recovery and water saturation are plotted as a function of square root of time. Total recovery factor vary from 30.4% OOIP to 48.1% OOIP and total time vary from 5-50 days. Note: the lines between the recorded values are just for guidance and are not measured.

7.2 Comparison of oil recovery in different zones and recovery methods

Oil recovery by waterflooding and spontaneous imbibition using AFO and TEO boundary conditions was between 28.2% - 48.1% OOIP. Oil recovery by spontaneous imbibition with TEO boundary conditions varied the most in recovery factor and total time of displacement. Reason for the differences in recovery factor for the TEOFSI displacements was probably caused by heterogeneities and variations in porosity, permeability and density. In addition, MM4-5 V1 produced one third of total oil recovery counter-currently, which increased the recovery factor for this core plug tremendously. Core plug BED3 V15 was stored in oil for 10 days before used for the TEOFSI test, which could have affected the oil production result negatively due to a possible wettability alteration process. The results for the TEOFSI tests are discussed more in detail in Chapter 9. Oil recovery by water flooding on core plug V8 from zone MM3-4 was definitely the fastest displacement process and gave the third highest oil recovery factor 41.4% OOIP. Since only one initially 100% oil saturated core plug was waterflooded, its difficult to compare it to spontaneous imbibition regarding which method that gives the highest recovery factor. Still, the average recovery for AFO spontaneous imbibition was 34.2% OOIP and is lower than the core plug waterflooded. The average of TEO spontaneous imbibition was 36.0% OOIP and are lower than the core plug water flooded, but higher than AFO spontaneous imbibition. However, the average recovery for TEO spontaneous imbibition would have been lower if MM4-5 V1 was not included, due to the tests possibly invalidity, as discussed in Chapter 9. Recovery factors and residual oil saturation for all core plugs used are listed in Table 10.

Table 10 – Summary of oil recovery after water flooding and spontaneous imbibition by boundary conditions. Porosity and permeability values from earlier measurements, oil pore volume before imbibition, residual oil saturation- and oil recovery after imbibition.

Core ID	Pore volume oil [ml]	Sor [% OOIP]	Recovery [% OOIP]	Experiment conducted
MM5-6 H4	22.3	61.0	39.0	SI, AFO
MM5-6 H6	29.4	65.0	35.0	SI, TEO
MM4-5 H1	15.1	64.2	35.8	SI, AFO, after POD
MM4-5 V1	30.0	51.9	48.1	SI, TEO
MM3-4 H9	16.3	66.2	33.8	SI, AFO
MM3-4 V8	21.0	58.6	41.4	Forced water imbibition
BED3 V15	19.5	66.4	33.6	SI, TEO
ZIGZAG H13	18.1	71.8	28.2	SI, AFO, after POD
ZIGZAG V11B	29.2	69.6	30.4	SI, TEO
ZIGZAG H12	36.7	67.3	32.7	SI, TEO
ZIGZAG H11	40.6	63.8	36.2	SI, TEO

SI, TEO: Spontaneous imbibition with Two-Ends Open free boundary conditions.
SI, AFO: Spontaneous imbibition with All- Faces Open free boundary conditions.
SI, AFO after POD: Spontaneous imbibition with All- Faces Open free boundary conditions after Primary Oil Drainage.
FWI: Forced water imbibition

8 Reproducibility, endpoint relative permeability and wettability characterization

To evaluate how LRQC respond to reproducibility, a secondary oil drainage followed by another spontaneous imbibition were performed on MM4-5 H1 and ZIGZAG H13. Endpoint saturations, injection rate and pressure were carefully considered and recorded for relative permeability calculations.

8.1 Change in water saturation during different displacements

Five displacement experiments were conducted on core plug MM4-5 H1 and ZIGZAG H13 for reproducibility study. Change in water saturation, S_w during each displacement was plotted as a function of time for core plug MM4-5 H1, see Figure 41. The orange line represents oil drainage, light blue is spontaneous imbibition and darker blue is forced water imbibition. First, primary oil drainage was conducted, causing the water saturation to decrease to initial water saturation, S_{wi}=0.33. Spontaneous water imbibition then increased the water saturation to S_w=0.57. After spontaneous imbibition, the core was waterflooded in 1000 minutes, without more oil being recovered (dark blue straight line). A secondary oil drainage resulted in S_{wi}=0.35. Finally, a second spontaneous water imbibition increased the water saturation to S_w=0.53. During all experiments, the temperature was 26 degrees Celsius with little vary in day- and night time.

The endpoint saturations of MM4-5 H1 after the two drainages are very similar and only differed in a water saturation of S_w=0.02. The secondary drainage did not reach the same S_{wi} as the primary drainage. The endpoint saturations after the spontaneous imbibition displacements have a difference of S_w=0.04. The two displacements show almost similar reproducibility, which indicate the relative permeability stays approximately the same between the same displacements processes for MM4-5 H1. To compare time for primary and secondary displacement, both secondary- drainage and spontaneous imbibition used approximately 1000 hours less to reach S_{wi}/S_{or} than primary- drainage and imbibition. This might be due to part of the oil and brine paths already were made during the primary drainage and imbibition.

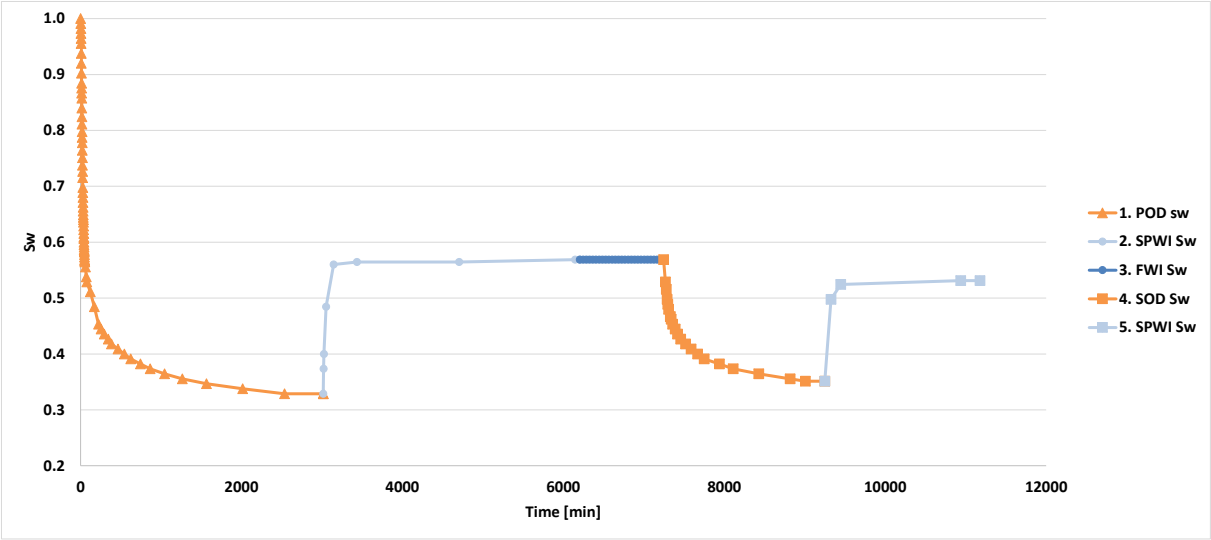

POD, Sw: Primary Oil Drainage, water saturation
SPWI, Sw: Spontanoues Water Imbibition, water saturation
FWI, Sw: Forwced Water Imbibition, water saturation
SOD, Sw: Secondary Oil Drainage, water saturation

Figure 41 – Water saturation profile for displacement processes in MM4-5 H1. Water saturation is plotted against time [min]. Endpoint saturations after the each displacement are listed in Table 11.

Figure 42 illustrated change in water saturation, S_w during different displacements as a function of time for core plug ZIGZAG H13 for reproducibility evaluation. The orange line represent oil drainage, light blue is spontaneous imbibition, while darker blue is forced water imbibition. The same five displacement processes were conducted as for core plug MM4-5 H1. Primary oil drainage decreased the water saturation to initial water saturation, S_{wi}=0.36. Water spontaneous imbibition then increased the water saturation to S_w=0.54. The core plug was waterflooded with 1.1 pore volumes without more oil being recovered (dark blue straight line). A secondary oil drainage resulted in a new decrease in water saturation to S_{wi}=0.32. Finally, a second spontaneous water imbibition increased the water saturation to S_w=0.45. During all experiments, the temperature was 26 degrees Celsius with little vary in day- and night-time.

The endpoint saturations of ZIGZAG H13 after the two drainages differ in 0.04 and the endpoint saturation after spontaneous imbibition differed in 0.09. Both these numbers are higher than MM4-5 H and indicate that ZIGZAG H13 has lower reproducibility than MM4-5 H1. However, ZIGZAG H13 reached a lower Swi during the secondary drainage process compared to primary drainage. In core plug MM4-5 H1, the opposite happened. This difference might be caused by the larger fractures in MM3-4 H1, where oil could be trapped in the middle of larger pores. To compare time difference between displacements for ZIGZAG H13, the secondary drainage used approximately 3000 minutes less to reach S_{or} than the primary drainage and the second imbibition used approximately 11000 minutes less than the first imbibition. The recovery time difference is as with MM4-5 H1 probably caused by the flow paths already were made during the primary displacements. This show a larger difference between displacement times for ZIGZAG H13 compared to MM4-5 H1, and again define ZIGZAG H13 to have lower reproducibility than MM4-5 H1.

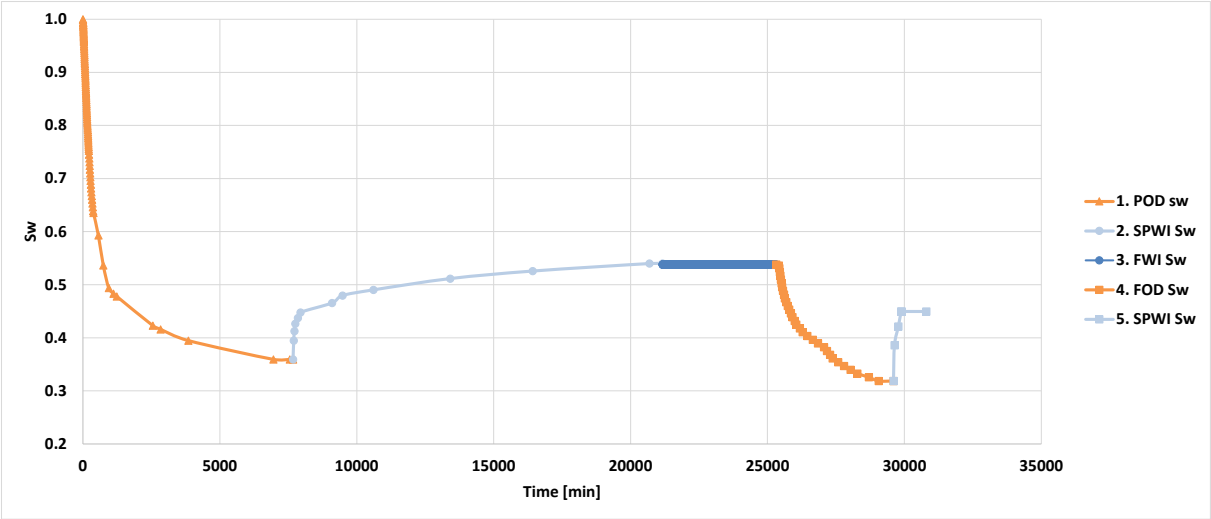

POD, Sw: Primary Oil Drainage, water saturation
SPWI, Sw: Spontanoues Water Imbibition, water saturation
FWI, Sw: Forwced Water Imbibition, water saturation
SOD, Sw: Secondary Oil Drainage, water saturation

Figure 42 – Water saturation profile for displacement processes in ZIGZAG H13. Water saturation is plotted against time [min]. Endpoint saturations after each displacement are listed in Table 11.

Rock characterization for both core plugs are discussed in Section 7.2 and calculated endpoint relative permeability for each displacement is listed in Table 11.

Table 11 – Endpoint water saturation and endpoint relative permeability after each displacement for core plug MM4-5 H1 and ZIGZAG H13. Relative permeability was only possible to calculate for flooding due to the absent of pressure recordings in spontaneous imbibition tests.

		POD	SPWI	FWI	SOD	SPWI
MM4-5 H1	Sw	0.329	0.569	0.569	0.351	0.531
	Kro, Krw	0.564		0.058*	0.276	
ZIGZAG H13	Sw	0.359	0.538	0.538	0.319	0.450
	Kro, Krw	0.546		0.085*	0.310	

POD: Primary Oil Drainage, water saturation
SPWI: Spontaneous Water Imbibition, water saturation
FWI: Forced Water Imbibition, water saturation
SOD: Secondary Oil Drainage, water saturation
Kro: Relative permeability to oil
Krw: Relative permeability to water, marked with *

Imbibition reproducibility was tested in Low Permeable Mantes Chalk by (Cuiec et al., 1994). The coated outcrop chalk bar from Upper Creataceous, Meudon, France had a porosity value of 41.1% and brine permeability of 1.8 mD. Compared to the reproduction by imbibition of LRQC, the experiments did not match. However, the core plugs in this study were not dried between displacements compared to Cuiec et al. (1994). The initial oil saturation before imbibition was quite equal for Mantes Chalk (S_{oi} = 65.1%) compared to LRQC (S_{oi} = 67.1% and 64.1%). However, the oil production (% OOIP) varied a lot between the two chalk types. Mantes chalk's had an excellent reproducibility with oil production of approximately 48.0% to 49.0% OOIP for the two imbibition's and with the same amount of production hours. LRQC had an oil production of 35.8% -18.0% OOIP in MM4-5 H1 and 27.9% - 13.1% OOIP in ZIGZAG H13 after the two imbibition displacements. Compared to Mantes Chalk that had

the same production hours for both imbibition's, LRQC ZIGZAG H13's imbibition displacement differed a lot in hours. First displacement used 10 times longer time than the second imbibition (Figure 42). For potential future work on LRQC, it would have been interesting to dry the core samples before the second imbibition displacements as well, and studied if the LRQC reproduction behaviour equals more to Mantes Chalk.

8.2 Wettability characterization

Water flooding was performed after spontaneous imbibition to determine wettability of the core plugs by the Amott-Harvey method. None of the core plugs had oil production through forced water injection after spontaneous imbibition, which indicate that the zones are water-wet. The wettability was measured by the Amott-Harvey method, using Equation 9, 10 and 11 for core plug MM4-5 H1 and ZIGZAG H13.

For MM4-5 H1 the water index, I_w was 1 and the oil index I_o was 0.67. By subtracting the oil index from the water index it gives an Amott-Harvey index of 0.27 for MM4-5 H1, which according to (Dake, 1983) makes this zone weakly-water-wet. ZIGZAG H13 had a water index, I_w of 1 and an oil index I_o of 0.67, which results in an Amott-Harvey index of 0.58 and defines this core as medium water-wet. The lower residual oil saturation by ZIGZAG H13 compared to MM4-5 H1 was probably caused by their wettability definitions. A statement by (Jadhunandan and Morrow, 1991) says that a reduction in recovery by spontaneous imbibition is observed for weaker water-wet mediums and that viscous forces are proved to have an impact when wettability of a medium moves towards less water-wet conditions.

Since the core plugs are determined to be weakly to middle water-wet, the relative permeability to oil, k_{ro} is higher than the relative permeability to water, k_{rw}. This explains that k_{ro} is 10 times higher than K_{rw} for MM4-5 H1 (listed in Table 11). K_{ro} decrease for both zones in the second primary drainage, due to a smaller mobile area for the oil to flow. CT images of MM4-5 H1 show many fractures and according to (Graue et al., 2001), if a chalk reservoir has high fracture intensity, the wettability becomes more important due to its significantly effect on fractional flow, spontaneous imbibition potential and water flooding production.

PART B

9 Determination of relative permeability and capillary pressure from TEOFSI tests.

As a part B of the experimental study in this thesis, the *Two-Ends Open Free Spontaneous Imbibition* (TEOFSI) method were tested on six LRQC core plugs. The TEOFSI method is after (Dong and Zhou, 1998) and (Haugen et al., 2014) and involve one end in contact with brine and the other end in contact with oil. Brine can then only imbibe from one end of the core plug but oil can be leave from either or both ends. The method has earlier been tested on Portland Chalk by (Haugen et al., 2014), but there is no documentation of the method being tested on Low Permeable Chalk. LRQC is a challenging reservoir rock. Due to its low porosity and permeability, conventional SCAL methods are inadequate and new methods like TEOFSI need to be considered.

Epoxy coating preparations and executions were performed as explained in Section 4.5.1. Core plugs; BED3 V15, ZIGZAG V11B, MM4-5 V1 AND MM5-6 H6 were used due to their differences in permeability, porosity and length, while ZIGZAG H11 and ZIGZAG H12 were chosen due to their similarity in permeability and porosity, although different length. Measured and calculated values for the core plugs are listed in Table 12.

Table 12 – Diameter, length, pore volume, porosity and permeability for the core plugs used in the TEOFSI tests. Core identification is described in Table 1.

Core ID	Diameter [cm]	Length [cm]	Pore Volume [ml]	Porosity [frac]	Permeability [mD]
MM5-6 H6	4.97	6.38	29.94	0.24	0.410
MM4-5 V1	4.96	7.12	35.17	0.26	0.531
BED3 V15	4.96	7.79	29.95	0.22	0.052
ZIGZAG V11B	4.96	6.27	25.61	0.22	0.184
ZIGZAG H12	4.97	8.23	40.41	0.253	0.207
ZIGZAG H11	4.97	9.02	43.82	0.250	0.248

9.1 The behaviour of co- and counter-current production

Oil produced from the inlet end (in contact with brine) is counter-current, whereas oil produced at outlet is co-current. The short core plugs used enable gravity forces to be neglected compared to capillary forces. Depending on the magnitude of capillary to gravity forces in a reservoir, water drive will usually give co- and counter-current flow (Bourbiaux, 2009). According to (Pooladi-Darvish and Firoozabadi, 2000);(Firoozabadi, 2000) most of the flow will be co-currently if the matrix blocks in a reservoir are partially exposed to water. The oil will then prefer to flow against the boundary in contact with oil. (Haugen et al., 2014) conducted TEOFSI experiments in 2014 where they produced approximately 93% of total production co-currently.

The results after TEOFSI of LRQC showed that the average co-current production was 90.2% of total production. Five of the core plugs produced 92-96% of the total oil production co-

currently. However, MM4-5 V1 only produced 67 % of the total oil production co-currently and therefore lowered the average. In a fractured reservoir, both co- and counter-current imbibition may coexist during waterflood (Karpyn et al., 2009), and was proved for LRQC as well. In all tests, the first oil droplet was produced counter-currently, with a visible co-current production shortly thereafter. Co- and counter-current production then coincided shortly, until only co–currently production. Counter-current flow stopped early due to a lower water and oil mobility, which resulted in a lower mobile saturations and relative permeability. Viscous interactions was also higher between the phases for counter-current flow compared to the co-current flow (Bourbiaux and Kalaydjian, 1990), causing a lower production. Oil production at the inlet face in contact with brine was suppressed by the capillary back pressure related to the open end face (Haugen et al., 2014). All LRQC core plugs were initially 100% saturated with the non-wetting phase, and the sharp rise in saturation at the front for all core plugs can be explained by the wetting phase trying to establish continuity through the core plug. This saturation volume at the front is usually equal to half of the produced volume of the non-wetting phase and is also why piston-like displacement can be assumed (Mason et al., 2012).

Figure 43 – Boundary conditions and direction of flow during the TEOFSI test. Inlet end is in contact with brine, while outlet end is in contact with oil. Brine can only imbibe from the end in contact with brine, while oil can be produced from either or both ends (Haugen et al., 2014).

An average of 90.2% of total oil production (OOIP) was produced co-currently, from the outlet face in contact with oil for the LRQC core plugs. The total oil production from each face is summarized in Table 13. Five of the core plugs seem to have same production pattern (production curves in Figure 44), with 1.1% - 2.5% OOIP of total oil production produced from the inlet face, and 28.4% - 35.0% OOIP of total oil production produced from outlet face. Core plug MM4-5 V1 (green curves in Figure 44) produced about the same amount of oil from outlet as the other core plugs, but stand out with an approximately 10 times higher counter-current production (33% of total recovery). Here, co- and counter-current production coexisted through the whole displacement process. Counter-current production slowed down after some time, but never totally ended before both faces ended their production after 22 days. Total recovery factor for all core plugs varied from 30.4% OOIP to 48.1% OOIP and total displacement time varied from 5-50 days due to a long production time for one core. Average production time from start till end was 12 days. Total oil recovery are listed in Table 13 and discussed in detail in Section 7.1.2 during recovery potential for LRQC. Density values from the CT scan for all core plugs are shown in Figure 45. BED3 V15 has the highest average density. However, the core plug did not have the lowest recovery factor. The average recovery factor due to high density and long displacement time, might be caused by many microfractures within the core plug.

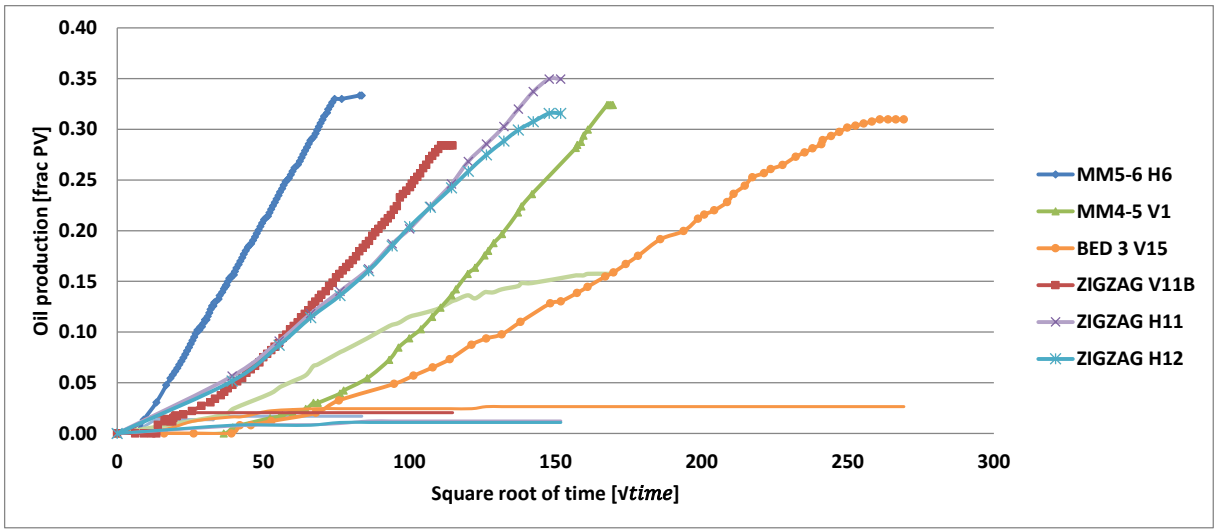

Figure 44 – Cumulative oil production curves from each core end by fraction of pore volume versus square root of time. Inlet production is illustrated in curves without dots, while outlet production is illustrated with dots. Cumulative oil production from inlet varied from 1.1% OOIP to 15.5% OOIP. Cumulative oil production from outlet varied from 28.4% OOIP to 35.0% OOIP.

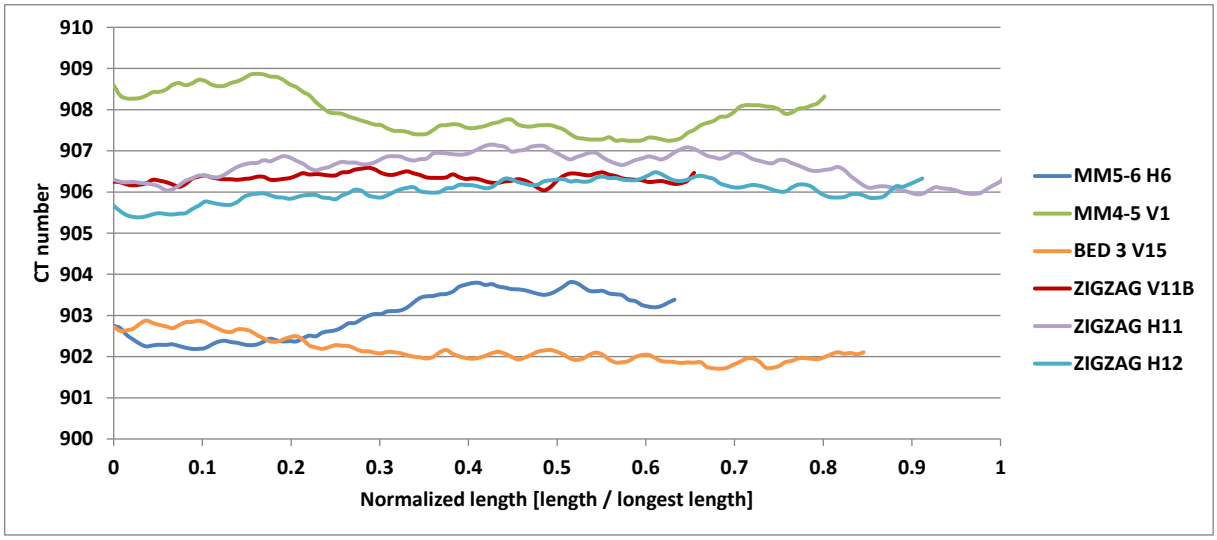

Figure 45 – Density measured by CT scan for core plug MM5-6 H6, MM4-5 V1, BED3 V15, ZIGZAG V11B, ZIGZAG H11 and ZIGZAG H12. The CT number expressing density through the core is shown as a function of normalized length [length/ longest length]. CT numbers are shown in absolute value and lower CT number equals higher density. CT numbers were originally negative because the air around the core plugs was not removed when the density values were collected. The air was not removed due to difficulties in precise image cutting around the core plug. The argument for approval of including air is that all the images have the same average of pixels and are the same size. In addition, all core plugs have the same diameter meaning the amount of air is equal in all images. Inlet of each core plug is where the normalized core length equals 0 and outlet is the value closest to 1. Core plug BED3 V15 shows the highest density value, while MM4-5 V1 shows the lowest density value.

Table 13 – Summarization of total oil recovery and recovery from each face from the TEOFSI tests of LRQC. For core identification, see Table 1.

Low Quality Reservoir Chalk			
Core ID	Recovery [% OOIP]	Oil fraction prod. at inlet [%]	Oil fraction prod. at outlet [%]
MM5-6 H6	35.0	4.90	95.1
MM4-5 V1	48.1	32.7	67.3
BED3 V15	33.6	7.88	92.1
ZIGZAG V11B	30.4	6.74	93.3
ZIGZAG H12	32.7	3.33	96.7
ZIGZAG H11	36.2	3.40	96.6
Average	36.0	9.80	90.2

Five of six tests conducted with the TEOFSI method on LRQC were successful, meaning that the production happened as predicted with above 90% co-current production. One core, MM4-5 V1 behaved differently with approximately 10 times higher counter-current production (15% OOIP) than the other core plugs. Experimental errors might be the cause for this higher counter-current production. After ended production for MM4-5 V1 the inlet pressure sensor fitting was observed loose when being detached, which could possibly have changed the behaviour of the fluid flow within the core. Its a possibility that water has been imbibed around the fitting and changed the pressure distributing compared to the other core plugs and displacing water from the inlet tubing towards the inlet end, causing a larger counter-current production. Another interesting observation on MM4-5 V1 was the behaviour of the counter-current produced oil. Two oil droplets were spotted at the inlet face, one of them 2 cm from inlet, right above the pressure sensor (Figure 46 left). Epoxy is oil-wet, so either the oil has moved from inlet towards outlet on top of the core on the outside along the epoxy, or oil has in addition to outlet been produced from the loose sensor fitting.

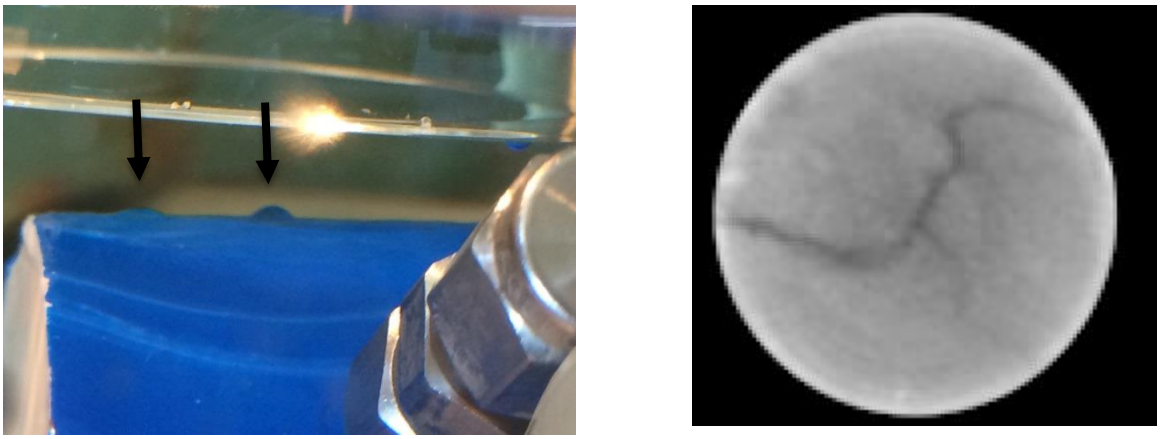

Figure 46 – Right: visible oil droplets 1 cm and 2 cm from the inlet face on MM4-5 V1. The 2 cm droplet is right above the inlet pressure fitting that proved to be loose after the displacement. Right: visible fracture from CT image of MM4-5 V1. The image is taken 1.5 cm from the inlet close to where the hole for the inlet pressure sensor was drilled. It's a possibility that the pressure sensor in the left image is drilled into the fracture in the right image, causing the unpredicted behaviour and a 15% counter-current production for core plug MM4-5 V1.

CT images of MM4-5 V1 showed a fracture between 0.2 cm-1.5 cm from inlet end, see Figure 46 (right). If this fracture was hit while the holes for the sensor fitting was drilled, its a possibility that this might have fractured the core plug more at this point (despite the epoxy covering the circumference). In addition to the other errors causing a higher counter-current production, if the pressure sensor was drilled exactly into the fracture, this might have provoked oil production or water imbibition around the pressure sensor fitting or even caused the looseness of the fitting.

The density value through the MM4-5 V1 is illustrated in Figure 45 (green line). Overall, MM4-5 V1 has the lowest density value. However, the density seem heterogeneous through the core plug due to an increase after approximately 1.5 cm from inlet. This lower density before 1.5 cm from the inlet reflects the fracture within MM4.5 V1, see Figure 46 (right). The fracture and lower density indicate a higher greater fluid flow- and oil storage potential in this area. The increase in density after 1.5 cm indicate less favourable oil recovery conditions compared to before 1.5 cm from inlet. Unfortunately, the computer crashed 12 days into this displacement and the pressure recordings were not to be saved.

9.2 Behaviour of LRQC during free spontaneous imbibition compared to Portland Chalk

The TEOFSI theory was by (Haugen et al., 2014) tested on five Portland Chalk core plugs, with permeability K=4.5-5.6 mD and porosity φ=0.46-0.49. Production values for Haugen et al., 2014 are listed in Table 14 for comparison. Production curves look similar for the two chalk types, but their production hours varied. The production of ZIGZAG H11 lasted for 16 days, while CHP5 lasted for 3 hours. Their huge difference in total production time have most likely exclusively to do with the rock types difference in porosity and permeability. Compared to LRQC, the average oil recovery by Portland Chalk was the twice as high (60% OOIP) as LRQC. Lower production by LRQC is not surprising, due to the unfavourable lower reservoir properties proved to give lower fluid flow- and oil storage potential for the chalk used in this thesis.

Table 14 – Summarization of total oil recovery and recovery from each face from the TEOFSI tests of Portland Chalk (Haugen et al., 2014). The Portland chalk comes from an outcrop chalk from the Røldal quarry at the Portland cement factory in Ålborg.

Portland Chalk (Haugen et al,. 2014)			
Core ID	Recovery [% OOIP]	Oil fraction prod. at inlet [%]	Oil fraction prod. at outlet [%]
CHP2	61.4	6.70	93.3
CHP3	59.2	3.60	96.4
CHP4	57.6	4.20	95.8
CHP5	61.6	4.40	95.6
CHP7	61.4	6.40	93.4
Average	60.2	5.10	94.9

Comparing pressure curves between the two rock types, ZIGZAG H11 has two pressure sensors, one at inlet and outlet. CHP5 had one pressure sensor located in the middle of the core plug. Pressure curves for both tests increase immediately after the core plugs are placed in the brine bath due to the water imbibition start. Maximum pressures for the core plugs were; 0.24 bar at inlet and 0.05 bar at outlet for ZIGZAG H11 and 0.43 bar for CHP5. The maximum pressure for Portland Chalk is twice as high as the maximum pressure for LRQC. The higher pressure is probably caused by a greater fluid flow through CHP5. Inlet and outlet pressures for ZIGZAG H11 decrease faster and have a lower value than the middle pressure for CHP5. At production end, the pressure gets an increase jump for Portland Chalk, which was not visible for LRQC. The reason for the absence of the pressure jump in LRQC might be due to the long and slow displacement process. As described by (Haugen et al., 2014) the rate of oil production at the outlet face, closely tracked the measured pressure with an initial rapid increase and a slow decline. This was true for all TEOFSI tests on LRQC.

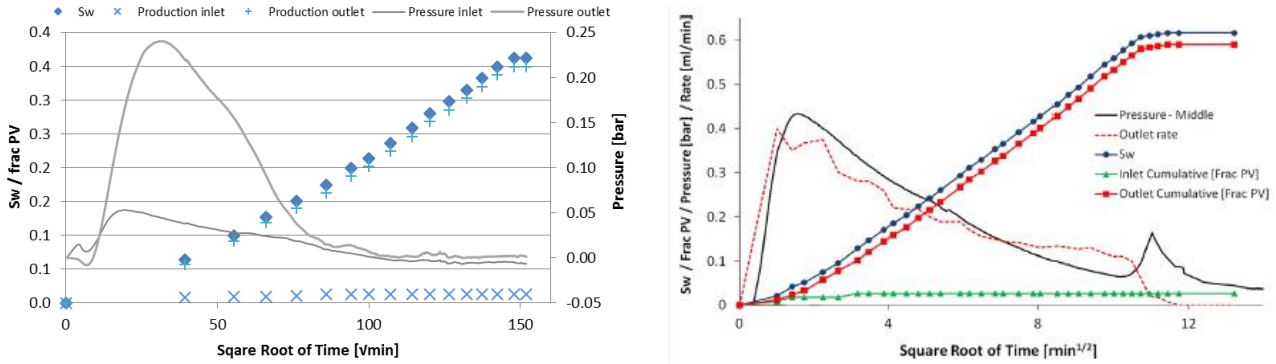

Figure 47 – Production and pressure history all versus square root of time. <u>Left:</u> Core plug ZIGZAG H11 from LRQC. Water saturation (blue diamonds); cumulative production at the inlet face (light blue crosses); cumulative oil production at the outlet face (turquoise plusses); inlet pressure (dark grey line); outlet pressure (light grey line) <u>Right:</u> Core plug CHP5 from Portland Chalk used in (Haugen et al., 2014). "Pressure in the middle of the core (black line); the rate of oil production at the outlet end face (dashed red line); the average water saturation (blue circles); the cumulative oil production at the inlet end face (green triangles) and outlet end face (red squares)"-(Haugen et al., 2014).

9.3 Estimation of relative permeability and capillary pressure

Information about the nature of the front during the TEOFSI displacement can be interpreted by plotting the calculated front position (calculated from Equation 27) versus the measured front position, see Figure 48. The core plugs were covered in epoxy and the "measured" front position was not visible to be measured. Some assumption therefore needed to be made to determine the measured front positions:

- Piston like displacement
- S_{wi}, S_{wf} and φ are uniform along the length of the core.

According to CT numbers (see Figure 45) the last argument is valid for core plug ZIGZAG H11, ZIGZAG H12, ZIGZAG V11B and BED3 that show a relatively homogenous density through the length of the core plug. Core plug MM5-6 H6 show a decrease in small density, while MM4-5 V1 show a small increase in density through the core plug. However, the

argument of uniformity is still used for the two core plugs during calculations. The two assumptions mentioned above together with produced oil [ml], porosity and length of the core plug, gave the measured front position. By adjusting factor D and E, a slope of unity was achieved when plotting the two front positons against each other, see Figure 48. Factor D is defined by Equation 22 and factor E is defined by Equation 25. The calculated front position and the measured front position gave a good match for all valid tests.

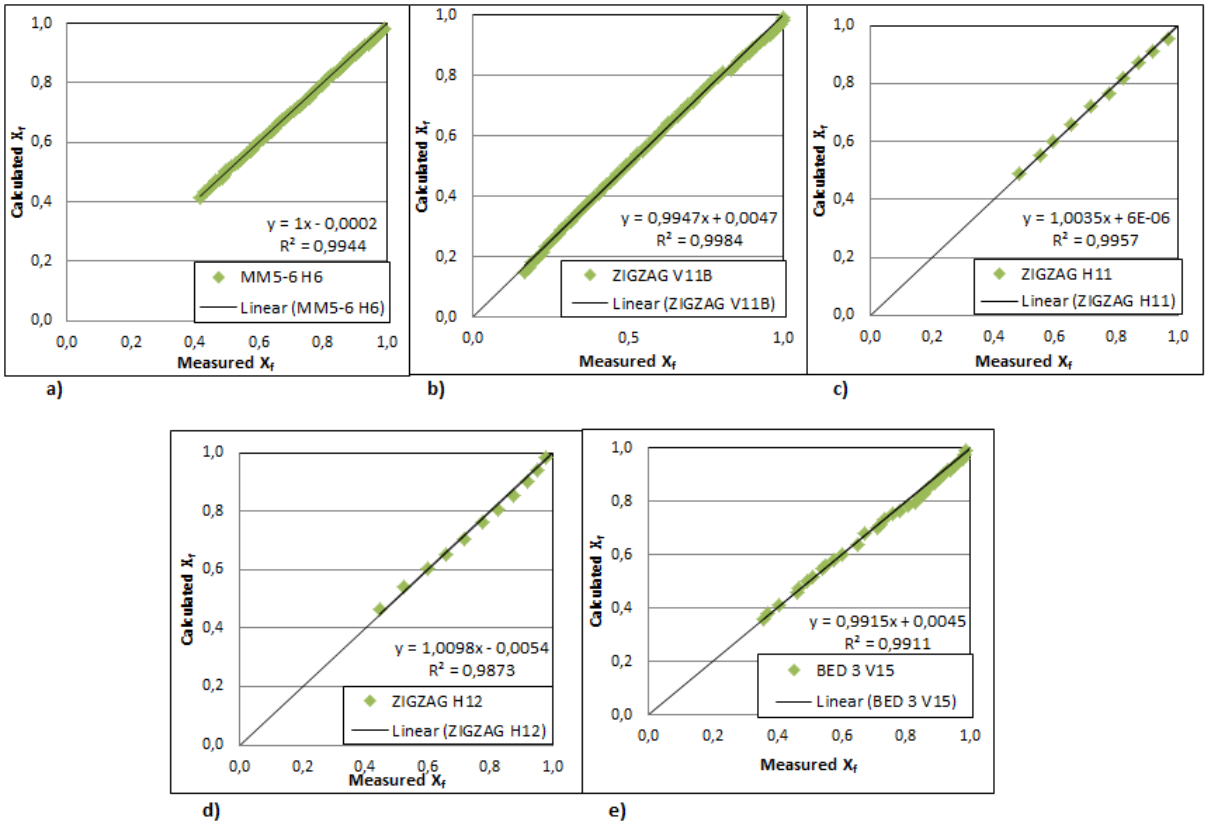

Figure 48 - Plots of calculated front position versus measured front position for a) MM4-5 H6, b) ZIGZAG V11B, c) ZIGZAG H11, d) ZIGZAG H12 and e) BED3 V15. The parameters D and E were adjusted to make the points go in a straight line from point (0.1) to (1.0).

The interpretation of the calculated and measured front position was done with the technique of (Haugen et al., 2014). This method is only valid for the measured production after ended counter-current production. Therefore, only co-current production is included in the plots. Counter-current production lasted until end of total production for MM4-5 V1 and this core plug is therefore not valid and included in the relative permeability and capillary pressure calculations. After achieving a straight line, the values of D and E were used to determine relative permeability to water and capillary pressure for all valid core plugs using Equation 22 and 28. Fluid viscosities were known and the relative permeability to oil was set to 1 ahead of the front, see Table 15 for calculated values. The calculations for Low Reservoir Quality Chalk gave $K_{r,w}$ between 0.055 and 0.366, and $P_{c,f}$ ranging from 8.40 kPa to 47.3 kPa. The results show capillary pressure increase inverse to relative permeability for all core plugs.

Table 15 – List of calculated values for relative permeability to water $K_{r,w}$ and capillary pressure $P_{c,f}$ for core plug MM5-6 H6, BED 3 V15, ZIGZAG V11B, ZIGZAG H11 and ZIGZAG H12. MM4-5 V1 did not have single co-current production and could therefore not the calculated by the technique of (Haugen et al., 2014)

Core ID	$K_{r,w}$ calculated	$P_{c,f}$ calculated [kPa]
MM5-6 H6	0.055	47.3
BED3 V15	0.366	8.40
ZIGZAG V11B	0.330	9.17
ZIGZAG H11	0.294	11.6
ZIGZAG H12	0.157	20.7

The calculated relative permeability value for MM4-5 H6 is low and may not be reliable. Few data points from ZIGZAG H11 and ZIGZAG H12 are also considered as a possible error to the calculations. "The method required quite small adjustments to parameter D and E, and to make these meaningful, a significant number of data point are required" (Haugen et al., 2014). The viscosity ratio between the wetting and non-wetting fluid, $\mu nw/\mu w = 0.88$. The calculated values for relative permeability to water $K_{r,w}$ for LRQC is compared to values for Portland Chalk (Haugen et al., 2014) in Figure 49, where $K_{r,w}$ is plotted against endpoint water saturation. Three out of five calculated $K_{r,w}$ values for LRQC are higher than Portland Chalk, while one is equal and one is lower. These results show that the TEOFSI method works for Low Permeable Chalk core plugs as well as higher permeable chalk. However, the calculated relative permeability and capillary pressure values by this method for LRQC are difficult to evaluate due to zero comparable values for LRQC by other methods.

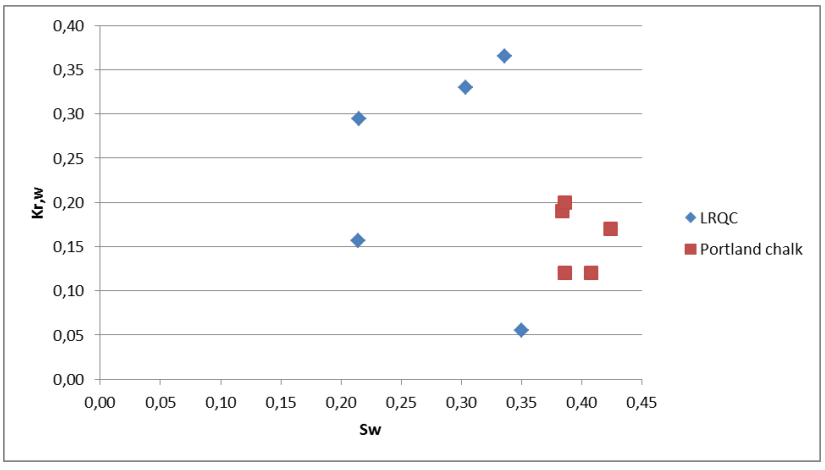

Figure 49 – Relative permeability calculated using equation theory presented by (Haugen et al., 2014). The red square represents Portland chalk from Haugen et al. (2014), while blue diamonds are Low Reservoir Quality Chalk.

Part IX – Conclusions and Future Work

10 Conclusions

This experimental thesis constitute two main parts; **Part A** focus on measurement of porosity, permeability and flow, storage and oil recovery potential for Low Reservoir Quality Chalk (LRQC). **Part B** evaluate the feasibility to apply the *Two-Ends Open Free Spontaneous Imbibition* (TEOFSI) method after (Haugen et al., 2014) in LRQC samples to estimate relative permeability and capillary pressure.

The following key results were identified in Part A

- Porosity was similar for five of six geological zones in the evaluated outcrop, with an average of φ=0.23. One zone (BED5) exhibited significantly lower porosity (φ=0.14-0.15), related to the high clay content in this zone.
- Porosity was measured using air and brine. The results show that the two methods using air (average φ=0.24) or brine (average φ=0.20) produce similar results. In contrast, the average brine permeability (K_b=0.025 mD) and average gas permeability (K_g=0.382 mD) differed with more than a magnitude. Permeability must therefore only be compared using the same fluid. Results show that zone MM4-5 had the highest gas permeability (K_g=0.820 mD), whereas zone BED5 had the lowest permeability (K_g =0.002 mD).
- Core plugs from each zone was evaluated using X-ray Computed Tomography (CT) to visualize internal rock structure and evaluate level of heterogeneity. The images revealed differences between zones and identified features such as large and small fractures, vugs or larger pore spaces, and local areas of lower or higher density. The LRQC zones may therefore be characterized as significantly heterogeneous.
- The variation in measured flow and storage potential for the zones did not directly relate to variation in zone porosity and permeability. However, local heterogeneities proved to have a large impact on water breakthrough during waterflooding, transient, two-phase tail production and initial water saturation. Fractures resulted in higher S_{wi}, earlier breakthrough and a need of several pore volume injected before final oil recovery was reached. Core plugs with few larger voids gave lower S_{wi}, later breakthrough and less than one pore volume was injected before final production was reached.
- Average oil recovery was 41.4 %OOIP for forced water imbibition, 34.2 %OOIP for spontaneous imbibition (AFO) and 36.0 %OOIP for spontaneous imbibition (TEO).

The following key results were identified in Part B

- The TEOFSI method was for the first time implemented on LRQC core plugs, and five out of six tests were successful, with oil produced mainly co-currently for 5 cores: an average of 5.3% of the total oil recovery was produced counter-currently.
- Relative permeability behind the front and capillary pressure at the front was estimated based on a theory assuming piston-like displacement by Haugen et al., 2014. Relative permeability to water, $k_{r,w}$ ranged between 0.055 and 0.366, whereas capillary pressure, $P_{c,f}$ ranged from 8.4 - 47.3 kPa. The mobility ratio between the wetting and non-wetting phase was 0.88 for all tests.

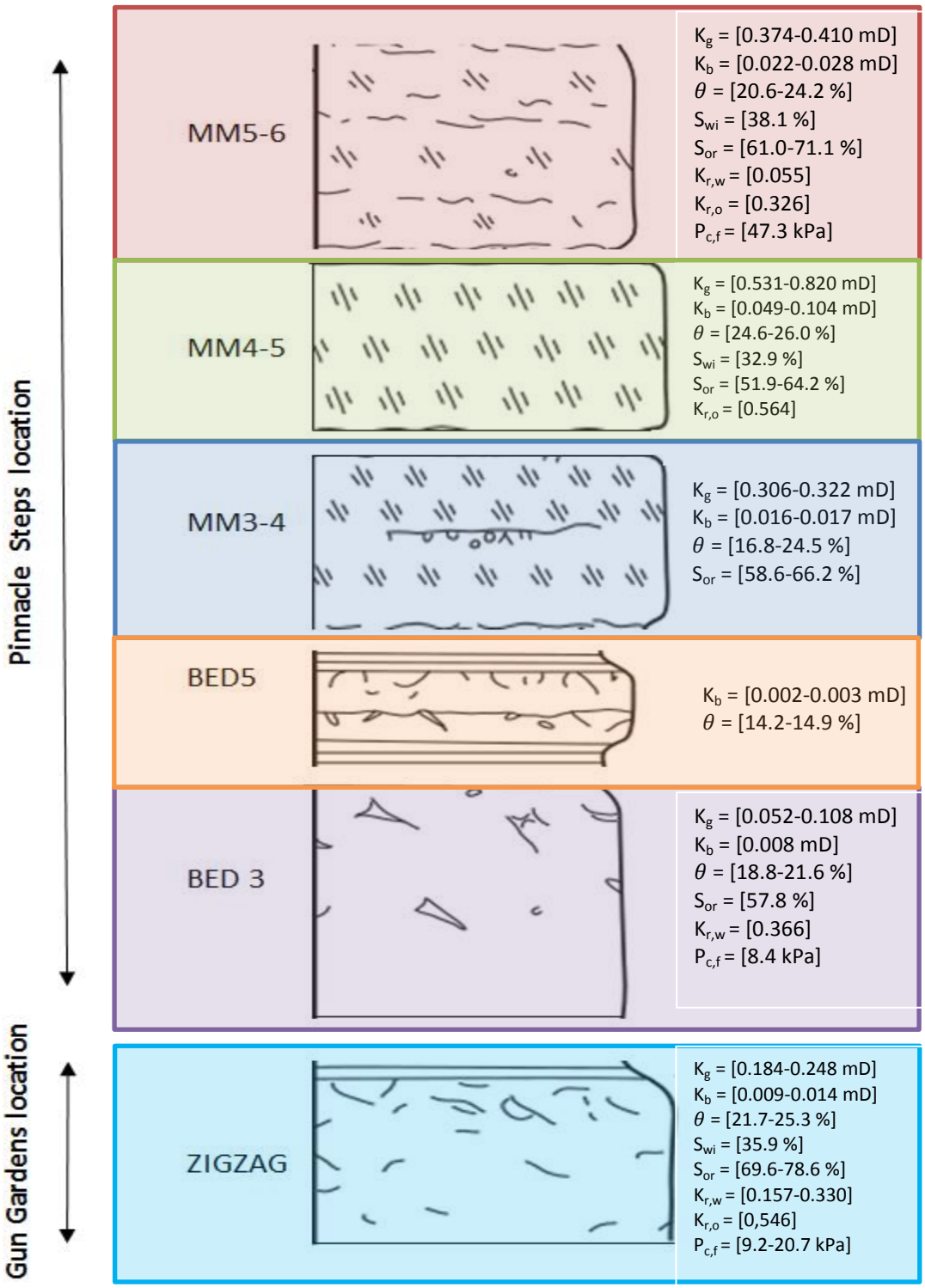

Figure 50 – Properties measured for LRQC through this thesis. Permeability using brine, K_b and porosity, φ were determined for all zones, permeability using gas, K_g were determined for 5/6 zones. Measurements of oil storage potential and initial water saturation, S_{wi} were conducted on 3/6 zones, MM5-6, MM4-5 and ZIGZAG. Oil recovery potential experiments were conducted on 5/6 zones, MM5-6, MM4-5, MM3-4, BED 3 and ZIGZAG to determine the residual oil saturation, S_{or}. Relative permeability to oil, $K_{r,o}$ were determined by oil flooding for zone MM4-5 H1 and ZIGZAG H13, and with the theory of (Haugen et al., 2014), relative permeability to water $K_{r,w}$ and the capillary pressure at the front $P_{c,f}$ were calculated for zone MM5-6, BED 3 and ZIGZAG. In addition, the figure illustrates the geological description for each zone. The short lines represents scattered broken bivalve shells, three parallel lines represents fine grained clean chalk, horizontal lines represents a higher clay content and triangles represents more bioturbation.

11 Future work

The experimental work presented in this thesis was a part of a larger research effort on chalk, named the Joint Chalk Research Programme, Phase 7 (JCR 7). Based on obtained results here are some suggestions for future work:

- The Low Reservoir Quality Chalk core plugs used in this thesis were collected above sea-level, without contact with crude oil. It would therefore been interesting to perform the same experimental work on actual reservoir core plugs, for comparison to the ones in this thesis.

- Relative permeability (K_r) and capillary pressure (P_c) for five Low Reservoir Quality Chalk (LRQC) core plugs were determined experimentally based on a methodology using spontaneous imbibition. Achieved results were difficult to evaluate due to lack of available LRQC Kr and Pc from other studies. Future work should aim to increase statistic related to measurement of relative permeability and capillary pressure, and include standard methods (Steady-state K_r and porous plate) for comparison.

- Using fluids with other viscosities to investigate the effect of viscosity ratio on front behaviour and recovery during the TEOFSI tests. If oil viscosity is low relative to brine, counter-current production is known to decrease. How this affects oil production in LRQC and relative permeability and capillary pressure calculations would be interesting to evaluate.

Part V – Abbreviations, Nomenclature, Appendix & References

Abbreviations

2D	Two dimensional
AFO	All Faces Open
CT	Computed Tomography
HTS	High stand System Track
LRQC	Low Quality Reservoir Chalk
LST	Low stand System Track
MFS	Maximum Flooding Surface
OEO	One End Open
OOIP	Originally Oil In Place
POD	Primary Oil Drainage
SB	Sequence Boundary
SI	Spontaneous Imbibition
SOD	Secondary Oil Drainage
SPWI	Spontaneous Water Imbibition
TEC	Two Ends Closed
TEO	Two Ends Open
TEOFSI	Two Ends Open Free Spontaneous Imbibition
TS	Transgressive Surface
TST	Transgressive System Track
UoB	University of Bergen
VPDB	Vienna Pee Dee Belemnite
OWIP	Originally Water In Place

Nomenclature

φ	porosity
ρ	fluid density
μ	fluid viscosity
μ_w	wetting phase viscosity
μ_{nw}	non-wetting phase viscosity
θ	wetting angle
σ	interfacial tension
A	cross sectional area
b	klinkenberg factor
D	diameter
L	core length
q	flow rate
T	temperature
K	absolute permeability
K_{eff}	effective permeability
k_{rel}	relative permeability
k_{nw}	non wetting phase relative permeability
k_w	wetting phase relative permeability
k_{rw}	relative permeability to water
$k_{rw,or}$	relative permeability to water after waterflooding
$k_{r,o}$	relative permeability to oil
$k_{ro,iw}$	relative permeability to oil after oil drainage
P	pressure
Pc	capillary pressure
$P_{c,o}$	the capillary back pressure
$P_{c,f}$	the capillary pressure at the water front
P_m	mean pressure
P_{ref}	pressure in the reference volume
P_w	pressure wetting phase
P_{nw}	pressure non-wetting phase
S_w	water saturation
S_{iw}	irreducible water saturation
S_{wirr}	irreducible water saturation after oil drainage
S_{spw}	water saturation after spontaneous water imbibition
S_{spo}	water saturation after spontaneous oil drainage
S_o	oil saturation
S_{or}	residual oil saturation
R	ideal gas constant [0.08206 L*atm/(mol*K)]
R_f	total recovery factor
T	temperature
V	volume
V_{DV}	tubing volume
V_{ref}	reference volume
V_p	pore volume
V_b	bulk volume
W_{dry}	weight of dry core [g]
W_{sat}	weight of saturated core [g]
w_t %	weight percent
x_f	waterfront portion

Appendix I – Uncertainty

This appendix contains uncertainty equations used during calculation. Uncertainty is related to input parameters and the values obtained by calculation therefore have a following uncertainty. Uncertainties need to be calculated depending on method. Equations are from (Erdal, 1997).

When a value R is a function of independent variables x, y, z…, the corresponding uncertainty to each variable is given as $S\bar{x}$,,Sz,…,$S\bar{i}$. Using either addition or subtraction the uncertainty $s_{\bar{R}}$ to value R is given by:

$$s_{\bar{R}} = \sqrt{\left(\frac{\partial R}{\partial x} s_{\bar{x}}\right)^2 + \left(\frac{\partial R}{\partial y} s_{\bar{y}}\right)^2 + \left(\frac{\partial R}{\partial z} s_{\bar{z}}\right)^2 + \cdots} \qquad \text{(A1)}$$

Say the independent variables x,,,…, have arithmetical averages of $\bar{x}$,$\bar{y}$,$\bar{z}$,…,$\bar{i}$. If N is the number of values included in the data set, then the measured variables can be calculated from this equation:

$$\bar{x} = \frac{x_1 + x_2 + x_2 + \cdots + x_N}{N} = \frac{1}{N}\sum_{i=1}^{N} x_i \qquad \text{(A2)}$$

Standard deviation is given by:

$$s = \sqrt{\frac{1}{N-1}\sum_{i=1}^{N}(x_i - \bar{x})^2} \qquad \text{(A3)}$$

where N is the number of measurements, x_i is the measured value and $\bar{x}$ is the mean value.

Instruments used in this experimental work have a good accuracy. However, larger uncertainties are connected to readings and the experiment itself. By the experiment itself, meaning changes in temperature, evaporation of liquids or leakage. All measurements have a related uncertainty and all of these contribute to a total uncertainty of the result. Uncertainties associated with instruments used in this work are listed in Table 15.

Table 15: Instrumental uncertainties.

Instrument	Parameter	Uncertainty
Weight (gram)	Mass	±0.01
Caliper (cm)	Length	±0.05
Graded cylinder 5 ml	Volume	±0.05
Graded cylinder 10 ml	Volume	±0.1
Graded cylinder 25 ml	Volume	±0.25
Pressure transducer	Pressure	±0.1 % of full scale
QX Pump	Flow Rate	±0.1 % of setting
	Volume	±0.2 % of volume injected
	Pressure	±0.2 % of full scale

References

ABDALLAH, W., BUCKLEY, J. S., CARNEGIE, A., EDWARDS, J., HEROLD, B., FORDHAM, E., GRAUE, A., HABASHY, T., SELEZNEV, N. & SIGNER, C. 1986. Fundamentals of wettability. *Technology,* 38**,** 268.

ANDERSON, W. 1986a. Wettability Literature Survey- Part 1: Rock/Oil/Brine Interactions and the Effects of Core Handling on Wettability. *Journal of Petroleum Technology,* 38**,** 1125-1144.

ANDERSON, W. 1986b. Wettability literature survey-part 2: Wettability measurement. *Journal of Petroleum Technology,* 38**,** 1,246-1,262.

AUSTAD, T. & MILTER, J. 1997. Spontaneous imbibition of water into low permeable chalk at different wettabilities using surfactants. *International Symposium on Oilfield Chemistry*.

BOURBIAUX, B. J. Understanding the Oil Recovery Challenge of Water Drive Fractured Reservoirs. International Petroleum Technology Conference, 7-9 Desember 2009 Doha, Qatar. International Petroleum Technology Conference.

BOURBIAUX, B. J. & KALAYDJIAN, F. J. 1990. Experimental study of cocurrent and countercurrent flows in natural porous media. *SPE Reservoir Engineering,* 5**,** 361-368.

CRAIG, F. F. 1971. *The reservoir engineering aspects of waterflooding,* New York, Henry L. Doherty Memorial Found of AIME.

CUIEC, L., BOURBIAUX, B. & KALAYDJIAN, F. 1994. Oil recovery by imbibition in low-permeability chalk. *SPE Formation Evaluation (Society of Petroleum Engineers);(United States),* 9**,** 200-208.

DAKE, L. P. 1983. *Fundamentals of reservoir engineering*, Elsevier, Amsterdam.

DONG, M., LI, Z., LI, S. & YAO, J. 2012. Permeabilities of tight reservoir cores determined for gaseous and liquid CO 2 and C 2 H 6 using minimum backpressure method. *Journal of Natural Gas Science and Engineering,* 5**,** 1-5.

DONG, M. & ZHOU, J. 1998. Characterization of waterflood saturation profile histories by the 'complete'capillary number. *Transport in porous media,* 31**,** 213-237.

ERDAL, A. 1997. *Elementær innføring i sannsynlighetsregning og problemløsninger ved analyse av måleresultater,* Bergen, Alma mater.

EWY, R., HAGIN, P., BOVBERG, C. & SHALZ, M. Permeability change under different stress and fluid pressure conditions. International Symposium of the Society of Core Analysts 16-19 September 2013 Napa Valley, California, USA.

EXXONMOBILCORPORATION 2014. The Outlook for Energy: A View to 2040. Exxon Mobil Corporation Irving, TX.

FIROOZABADI, A. 2000. Recovery mechanisms in fractured reservoirs and field performance. *Journal of Canadian Petroleum Technology,* 39.

GALE, A. S., KENNEDY, W. J., VOIGT, S. & WALASZCZYK, I. 2005. Stratigraphy of the Upper Cenomanian–Lower Turonian Chalk succession at Eastbourne, Sussex, UK: ammonites, inoceramid bivalves and stable carbon isotopes. *Cretaceous Research,* 26**,** 460-487.

GRAUE, A. Nuclear Tracer Saturation Imaging of Fluid Displacement in Low-Permeability Chalk. Low Permeability Reservoirs Symposium, 26-28 April 1993 Denver, CO.

GRAUE, A., ASPENES, E., MOE, R., BALDWIN, B., MORADI, A., STEVENS, J. & TOBOLA, D. MRI tomography of saturation development in fractures during waterfloods at various wettability conditions. SPE Annual Technical Conference and Exhibition, 3. Sept.-3. Oct 2001 New Orleans, Louisiana.

GUO, X., MA, J., LI, J., HAO, Y. & WANG, H. Effect of reservoir temperature and pressure on relative permeability. SPETT 2012 Energy Conference and Exhibition, 2012.

HARDMAN, R. 1982. Chalk reservoirs of the North Sea. *Bulletin of the Geological Society of Denmark,* 30**,** 119-137.

HAUGEN, M. 2012. CO2 Injection in Fractured Chalk for Enhanced Oil Recovery. *Master.* University of Bergen: Department of Physics and Technology

HAUGEN, Å., FERNØ, M., MASON, G. & MORROW, N. 2014. Capillary pressure and relative permeability estimated from a single spontaneous imbibition test. *Journal of Petroleum Science and Engineering,* 115**,** 66-77.

HELDAL, S. 2016. An Experimental Study Using Nanoparticle Stabilized CO_2 -Foam for EOR in Sandstone. *Master.* University of Bergen: Department of Physics and Technology

HONARPOUR, M. & MAHMOOD, S. 1988. Relative-permeability measurements: An overview. *Journal of Petroleum Technology,* 40**,** 963-966.

JADHUNANDAN, P. & MORROW, N. 1991. Spontaneous imbibition of water by crude oil/brine/rock systems. *In Situ;(United States),* 15, No. 4, 319.

JADHUNANDAN, P. & MORROW, N. R. 1995. Effect of wettability on waterflood recovery for crude-oil/brine/rock systems. *SPE reservoir engineering,* 10**,** 40-46.

JOS MAAS, N. S. 2014. JCR 7 - Advanced Core Measurements “Best Practices” for Low Reservoir Quality Chalk.

KARPYN, Z., HALLECK, P. & GRADER, A. 2009. An experimental study of spontaneous imbibition in fractured sandstone with contrasting sedimentary layers. *Journal of Petroleum Science and Engineering,* 67**,** 48-56.

KIRBY, B. J. 2010. *Micro-and nanoscale fluid mechanics: transport in microfluidic devices*, Cambridge University Press.

KLINKENBERG, L. The permeability of porous media to liquids and gases. Drilling and production practice, 1941. American Petroleum Institute.

LENORMAND, R., ZARCONE, C. & SARR, A. 1983. Mechanisms of the displacement of one fluid by another in a network of capillary ducts. *Journal of Fluid Mechanics,* 135**,** 337-353.

LEWIS, A. M. & BOOSE, E. R. 1995. Estimating volume flow rates through xylem conduits. *American Journal of Botany*, 1112-1116.

LI, S., DONG, M. & LI, Z. 2009. Measurement and revised interpretation of gas flow behavior in tight reservoir cores. *Journal of Petroleum Science and Engineering,* 65, 81-88.

LI, Y., MORROW, N. R. & RUTH, D. 2003. Similarity solution for linear counter-current spontaneous imbibition. *Journal of Petroleum Science and Engineering,* 39, 309-326.

LI, Y., RUTH, D., MASON, G. & MORROW, N. R. 2006. Pressures acting in counter-current spontaneous imbibition. *Journal of Petroleum Science and Engineering,* 52, 87-99.

LIEN, J. R. 2004. PTEK 211, Grunnleggende reservoarfysikk.

LIEN, J. R. 2011. PTEK 212, Reservoarteknikk I. *Uni. of Bergen, Bergen*.

MASON, G., FERNØ, M., HAUGEN, Å., MORROW, N. & RUTH, D. 2012. Spontaneous counter-current imbibition outwards from a hemi-spherical depression. *Journal of Petroleum Science and Engineering,* 90, 131-138.

MASON, G., FISCHER, H., MORROW, N. R. & RUTH, D. W. 2009. Spontaneous counter-current imbibition into core samples with all faces open. *Transport in porous media,* 78, 199-216.

MASON, G. & MORROW, N. R. 2013. Developments in spontaneous imbibition and possibilities for future work. *Journal of Petroleum Science and Engineering,* 110, 268-293.

MEURANT, G. 1972. *Carbonate sediments and their diagenesis*, Elsevier.

MORROW, N. R. 1990. Wettability and its effect on oil recovery. *Journal of Petroleum Technology,* 42, 1,476-1,484.

MORROW, N. R. & MASON, G. 2001. Recovery of oil by spontaneous imbibition. *Current Opinion in Colloid & Interface Science,* 6, 321-337.

PEARCE, M. A., JARVIS, I. & TOCHER, B. A. 2009. The Cenomanian–Turonian boundary event, OAE2 and palaeoenvironmental change in epicontinental seas: New insights from the dinocyst and geochemical records. *Palaeogeography, Palaeoclimatology, Palaeoecology,* 280, 207-234.

POOLADI-DARVISH, M. & FIROOZABADI, A. 2000. Cocurrent and countercurrent imbibition in a water-wet matrix block. *Spe Journal,* 5, 3-11.

SCHEUERMAN, T. R., CAMPER, A. K. & HAMILTON, M. A. 1998. Effects of substratum topography on bacterial adhesion. *Journal of colloid and interface science,* 208, 23-33.

SCHLANGER, S. O. & JENKYNS, H. 2007. Cretaceous oceanic anoxic events: causes and consequences. *Netherlands Journal of Geosciences/Geologie en Mijnbouw*.

SELLEY, R. C. & SONNENBERG, S. A. 2014. *Elements of petroleum geology*, Academic Press.

TANIKAWA, W. & SHIMAMOTO, T. 2006. Klinkenberg effect for gas permeability and its comparison to water permeability for porous sedimentary rocks. *Hydrology and Earth System Sciences Discussions,* 3, 1315-1338.

THOMAS, L. K., DIXON, T., PIERSON, R. & HERMANSEN, H. 1991. Ekofisk nitrogen injection. *SPE Formation Evaluation,* 6**,** 151-160.

TUNLI, R. 2014. An Experimental Study of CO2 and CO2 foam Injection in Carbonate Rocks. *Master.* University of Bergen: Department of Physics and Technology.

VOGEL, S. 1994. *Life in moving fluids: the physical biology of flow*, Princeton University Press.

ZOLOTUKHIN, A. & URSIN, J. 2000. Introduction to Petroleum Reservoir Engineering. 2000. *Høyskoleforlaget AS-Norwegian Academic Press: Kristiansand*.